NASA CR-135104



# AN EXPERIMENTAL STUDY OF A SELF-CONFINED FLOW WITH RING-VORTICITY DISTRIBUTION

by Kon-Mang Lin and Franklin K. Moore

Cornell University
Ithaca, New York


Prepared for

NATIONAL AERONAUTICS AND SPACE ADMINISTRATION
Lewis Research Center
Cleveland, Ohio 44135

August 1976

Grant NGL-33-010-042

| 1. Report No. | 2. Government Accession No. | 3. Recipient's Catalog No. |
|---|---|---|
| NASA CR-135104 | | |

| 4. Title and Subtitle | 5. Report Date |
|---|---|
| AN EXPERIMENTAL STUDY OF A SELF-CONFINED FLOW WITH RING-VORTICITY DISTRIBUTION | 6. Performing Organization Code |

| 7. Author(s) | 8. Performing Organization Report No. |
|---|---|
| Kon-Mang Lin and Franklin K. Moore | None |

| 9. Performing Organization Name and Address | 10. Work Unit No. |
|---|---|
| Cornell University<br>Ithaca, New York 14850 | 11. Contract or Grant No.<br>NGL-33-010-042 |

| 12. Sponsoring Agency Name and Address | 13. Type of Report and Period Covered |
|---|---|
| National Aeronautics and Space Administration<br>Washington, D.C. 20546 | Contractor Report |
| | 14. Sponsoring Agency Code |

15. Supplementary Notes

Final report. Project Manager, Cecil J. Marek, Airbreathing Engines Division, NASA Lewis Research Center, Cleveland, Ohio. Report was submitted as a thesis by the first author in partial fulfillment of the requirements for the degree Doctor of Philosophy at Cornell University, Ithaca, New York, in August 1976.

16. Abstract

A new form of self-confined flow was investigated where a recirculation zone forms away from any solid boundary. An inviscid-flow analysis indicated that in a purely meridional axisymmetric flow a stationary, spherical, self-confined region should occur in the center of a streamlined divergent-convergent enlargement zone. The spherical confinement region would be at rest and at constant pressure. Experimental investigations were carried out in a specially built test apparatus to establish the desired confined flow. The streamlined divergent-convergent interior shape of the test section was fabricated according to the theoretical calculation for a particular streamline. The required inlet vorticity distribution was generated by producing a velocity profile with a shaped gauze screen in the straight pipe upstream of the test section. Fluid speed and turbulence intensity were measured with a constant-temperature hot-wire anemometer system. The measured results indicated a very orderly and stable flow field. There was no flow separation anywhere in the flow, not even at the sharply divergent wall of the front test section. The experimental results confirmed for the first time the existence of such a unique self-confined region in a high Reynolds number flow field with the ring-vorticity distribution as prescribed by the theory.

| 17. Key Words (Suggested by Author(s)) | 18. Distribution Statement |
|---|---|
| Recirculation zone<br>Stable confined flow | Unclassified - unlimited |

| 19. Security Classif. (of this report) | 20. Security Classif. (of this page) | 21. No. of Pages | 22. Price* |
|---|---|---|---|
| Unclassified | Unclassified | 159 | |

* For sale by the National Technical Information Service, Springfield, Virginia 22161

CONTENTS

## LIST OF ILLUSTRATIONS

LIST OF TABLES

## NOMENCLATURE

| | |
|---|---|
| $\rho$ | Fluid density |
| $\vec{q}$ | Velocity vector |
| $\vec{\omega}$ | Vorticity vector |
| $P$ | Static pressure |
| $\vec{f}$ | Volume force vector |
| $\sigma_{ij}$ | Viscous stress tensor |
| $r, \theta, \chi$ | Coordinates of a cylindrical coordinate system |
| $R, \varphi, \xi$ | Coordinates of a spherical polar coordinate system |
| $\vec{e}_r, \vec{e}_\theta, \vec{e}_\chi$ <br> $\vec{e}_R, \vec{e}_\varphi, \vec{e}_\xi$ | Unit vectors in the cylindrical coordinate $(r, \theta, \chi)$ and the spherical polar coordinate $(R, \varphi, \xi)$ systems, respectively |
| $u, v, w$ <br> $u_s, v_s$ | Components of the velocity, $\vec{q}$, in $\vec{e}_\chi, \vec{e}_r$ & $\vec{e}_\theta, \vec{e}_R$ & $\vec{e}_\varphi$ directions respectively, i.e. $\vec{q} = u\vec{e}_\chi + v\vec{e}_r = u_s\vec{e}_R + v_s\vec{e}_\varphi$, $w=0$ |
| $\omega_\theta$ | $\theta$ -component of the vorticity, $\vec{\omega}$ |
| $\psi, \psi_r, \psi_\chi$ | The stream function in the cylindrical coordinate system and its derivatives with respect to $r$ and $\chi$ |
| $F(\psi)$ | $= -\frac{\omega_\theta}{r} = a$ , a constant |
| $a, M, N$ | Constants |
| $r_s$ | The radius of the spherical confined region |
| $R$ | The spherical radius, $R = \sqrt{\chi^2 + r^2}$ |
| $V_r$ | The reference velocity at $r' = 1.4$ |
| $\zeta$ | A dummy variable of integration |
| $u_o$ | The axial velocity on the axis of symmetry at the test chamber entrance |
| $\beta$ | The angle between the normal to the gauze screen and the flow direction |
| $\psi'$ | The non-dimensionalized stream function, $\psi' = \psi / a r_s^4$ |

| | |
|---|---|
| $f(t)$ | An arbitrary time dependent function |
| $\overline{f(t)}$ | Time average of $f(t)$ |
| $t$ | Time |
| $E$ | The bridge output voltage of the anemometer |
| $A, B$ | Hot wire calibration constants |
| $n$ | The exponent in the hot wire calibration relationship |
| $T_s$ | The hot wire sensor operating temperature (hot) |
| $T_e$ | The fluid or environment temperature |
| $R_H$ | The hot sensor resistance (at operating temperature) |
| $R_c$ | The cold sensor resistance (unheated) |
| $\alpha_c$ | The temperature coefficient of resistance of the sensor |
| $\overline{u}, \overline{v}, \overline{w}$ | Velocity components of the basic, steady flow in the pipe in $\vec{e}_x$, $\vec{e}_r$ & $\vec{e}_\theta$ directions |
| $\overline{u}(r)$ | $\overline{u}$ as an arbitrary function of $r$ |
| $u_m$ | The maximum generated velocity at the edge of the boundary layer |
| $\eta$ | Normalized radial dimension $\eta = (R_p - r)/\delta$ |
| $R_p$ | The inside radius of the pipe |
| $\delta$ | The boundary layer thickness |
| $R_e$ | Reynolds number based on pipe diameter D, Re $= uD/\nu$ |
| D | Diameter of the pipe, D = 4.144 inches |
| $\nu$ | Kinematic viscosity of the fluid (of room air) |
| $q'$ | Local fluctuating component of $\vec{q}$ |
| Q | Local average fluid speed |
| | $\left.\begin{array}{l}\\ \\ \end{array}\right\} \vec{q} = \vec{Q} + \vec{q}'$ |
| $Q_r$ | The average speed of twelve Q values at the same radius $r$ |
| $Q_{ref}$ | The reference speed at the chamber entrance $x$ = +5.2 inches and on the axis $r$ = 0.0 inch |

# CHAPTER I

# INTRODUCTION

Fluid flows with regions of closed streamlines or stream-surfaces away from the solid boundaries may be called self-confined flows. These phenomena can occur either naturally or by design. A particular example of this is the "vortex breakdown" in a spiraling flow (Figure 1-1). It has been observed to occur over delta wings (Refs. 1 to 7) at large incidences and in axisymmetric flows in tubes (Ref. 8). And it has been the subject of extensive theoretical and experimental studies for more than a decade (Refs. 9 to 15). The difficulties, both mathematical and experimental, involved in describing the nature, predicting the location, and identifying the occurrence of the phenomenon have been well documented (Cf. Hall in Ref. 16, P. 53 et seq.).

## 1. Motivation of the present study

For these self-confined flows, like that of the axisymmetric mode of the vortex breakdown consisting of a nearly self-confined recirculation zone, there could be useful applications in the fields of combustion, chemical or general fluid mechanical processes where a region of fluid or fuel must be contained within a flowing medium. In a gas turbine combustor, for example, with the help of turbulence across the region interface, diffusion as well as containment, and as a consequence, combustion of the fuel could be better controlled.

In the recent past, there had been considerable interest in

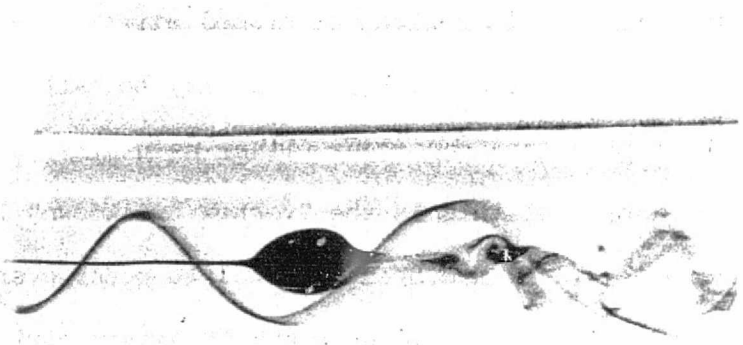

Figure 1-1. Axisymmetric vortex breakdown in a spiraling flow. Flow enters the pipe from the left througth a series of vanes in order to acquire swirling velocity. As indicated by the dye lines, an axisymmetric bubble is formed on the centerline and the outer flow rotates in a spiral form (From Ref. 15).

harnessing the nuclear energy by using a concept of the gas-core power reactor. But it was clear that this energy could not be efficiently or effectively utilized without drastic improvement of the thermal efficiency. This meant that the maximum power cycle temperatures would have to be increased far above the 1000°F level of today's nuclear power plants. Therefore, the entire energy-conversion process would have to be rather independent of material limitations. One of the conceptual design of the gas-core power reactor was that a gaseous uranium cloud would undergo fission, became extremely hot, and transfered heat by

thermal radiation to a working fluid introduced between the cloud and the reactor vessel wall. If the cloud could be contained without touching the walls, its temperature might be permitted to rise to tens of thousands of degrees, and presumably a magnetohydrodynamic generator could be used to derive electrical energy directly from the working-fluid plasma in a closed circuit. This arrangement would provide a power-generation system of very high efficiency without undue damages to the environment. In order to meet today's challenges of a rising energy demand and minimum pollution into the environment, with more extended developmental work, this gas-core power reactor may yet be a possible method for future usage of the nuclear energy.

Above are just a couple of examples where self-confined flows could play an important role. These enclosed regions of fluids can be confined relatively independent of the chamber walls. The confining mechanism is provided by the resistance of the vortex lines, because of rotational inertia, to the stretching process involved. This is analogous to the resistance to lateral deflection of magnetic field lines in a conducting fluid. Conceivably, these two resistance forces could be combined to provide a powerful mechanism for fluid containment. Interest in such fundamental fluid mechanical phenomena motivated us to investigate another possible form of self-confined flows.

## 2. The problem

The heretofore mentioned axisymmetric vortex breakdown in swirling flow occurs only when the swirl to axial velocity ratio reaches a certain magnitude. An analytical study based on inviscid-flow theory

indicated that another form of self-confined region, different from the vortex breakdown, should occur in a purely meridional, swirl free flow field with a certain prescribed ring-vorticity distribution (see Moore and Leibovich, Ref. 17). By ring-vorticity distribution is meant an axisymmetric distribution of azimuthal vorticity in the fashion of a bundle of coaxial smoke-rings in axial motion. This vorticity induces an axisymmetric velocity field with no swirl component about the axis of symmetry. According to the analysis, when the vorticity in each ring is simply proportional to the distance from the axis in an inviscid, incompressible, steady flow field, a self-confined region of spherical shape should occur on the axis. One may think, in this regard, of Hill's spherical vortex (A description of Hill's spherical vortex can be found in Refs. 18 and 19) in which vorticity is continuously distributed in a sphere and there is no vorticity at all beyond the sphere.

Then the question may rise, is this flow unique? Given the above initial distribution of outer vorticity, the sphere is perhaps the only shape within which fluid can be confined. A different vorticity distribution might well yield another shape, provided the duct walls were also modified in the proper way. There seems to be no flow of this character in two dimensions, nor should it be expected; a straight vortex line can pass around a cylinder without stretching and hence without exerting a containing force. Therefore, the plane-flow experiment by Ragsdale and Lanzo (Ref. 20) is probably only superficially comparable to the flow we have just proposed to study. We feel that the axisymmetric geometry may be fundamental to the success of the approach.

Another question may rise very naturally. One may ask, can this

kind of confined region exist in a real situation? Turbulence and separation characteristics of the flow may undermine its existence. And then even if these problems can be brought under control, would the self-confined region be stable? Can a region of fluid be confined by the resistance of smoke-rings in the outer flow to the stretching process involved in passing around this region? In fact, the Hill's spherical vortex flow is not statically stable without the interposition of, for example, surface tension at the sphere.

Theoretical analysis of the existence and stability questions is difficult for the proposed self-confined flow in a real situation. It is obscured by factors like turbulence, viscous effect, separation, flow symmetry, etc. Examples of such flows are scarce. Most closely related example occurs in the physiological phenomenon of peristaltic pumping actions of the ureter, the gastro-intestinal tract, the bile duct or other glandular ducts. In their paper (Refs. 21 and 22) Shapiro, Jaffrin and Weinberg described the discovery of a surprising phenomenon called "trapping" in the peristaltic pumping process. In their theoretical model, they assumed an inertia-free flow of constant density and viscosity fluid, and that the wall motion consisted of an infinite sinusoidal wave train of infinite wave length. In the wave frame of reference, the velocity had a parabolic profile --- similar to our test condition in the incoming pipe (see Chapter III for further details); and under certain pumping range, the center streamline split to enclose a bolus of fluid particles describing closed streamlines or the so called "trapping" phenomenon. In the laboratory frame of reference, this bolus moved as a whole at the wave speed as if trapped by the wave. Accordingly,

the fluid particles contained in the bolus moved at a mean speed of advance exactly equal to the wave speed. This trapping phenomenon does have some similarity to the self-confined flow we have proposed to study here.

More recently, Hung and Brown (Ref. 23) have reported the finding of a trapping region in their experimental study of solid-particle motion in two-dimensional peristaltic flows. This trapping region formed a pair of vortices as viewed in the moving frame of reference. Again, this finding has some similarity, though maybe only superficially, to the flow pattern in our self-confined region as indicated by the tuft probe (see Chapter IV). Both examples of the peristaltic flows mentioned above were for the low Reynolds number cases. The present study, however, has shown that a self-confined region (described in later chapters) exists in a flow of very high Reynolds number (about 150,000).

Attempting to answer some of , if not all, the questions raised, this experimental study was undertaken. The main effort has been made on trying to produce this flow in the laboratory, if possible, and to map out the flow field after it had been successfully produced. Then based on the measured flow data, attempts are made to clear up some aspects of the important question about the flow stability.

## 3. Outline

In the second chapter, a prior theoretical analysis based on inviscid-flow theory for an assumed inviscid, incompressible, steady flow in a conservative force field is reviewed. Pertinent equations are obtained; and proper solutions are found.

In the third chapter, experimental methods and the description of the apparatus are presented to establish an experiment which will represent the theoretical model. The method of generating that crucial ring-vorticity distribution by the "vorticity generator" is delineated. The stability of the generated velocity profile is analysed. Furthermore, flow measurement equipments for both the mean speed and turbulence intensity are described in some detail. They consist of the constant-temperature hot wire anemoneter system and its associated equipments, the traversing mechanism, pitot-static probes and micromanometers. An visualization scheme using a piece of short, soft tuft at the end of a small hypodermic tubing is employed in the whole test chamber to give an approximate visual indication of the flow field. The rough picture thus obtained is then compared with the hot wire measurements to form an idea of the flow.

Visualization results from the tuft probe as well as the quantitative results of the speed and turbulence intensity from hot wire measurements are given in the fourth chapter. Situations inside the incoming pipe, both with and without the vorticity generator, and in the test section are included. Important information summarized in the form of graphs is presented. Samples of measured data are included in the Appendix. Furthermore, a flow rate calculation is performed to verify the existence of the self-confined region in the test section.

Finally, some discussions and conclusions on this experimental study are presented in the fifth chapter. Its potential applications and the direction for future studies are suggested.

# CHAPTER II

# THEORY

In this chapter, we investigate the confining mechanism of the flow provided by the resistance of the vortex lines to the stretehing process involved, and also find the necessary conditions required of the flow field such that general criteria can be established for the realization of an experiment in the laboratory.

## 1. The governing equations

Vorticity is the key element in this problem. Therefore, mathematical equations can be more conveniently analysed by starting with the vorticity equation rather than the usual momentum equation. Continuity and vorticity equations may be written in the form of Cauchy's equations of motion as follows.

$$\begin{cases} \dfrac{D\rho}{Dt} + \rho \nabla \cdot \vec{q} = 0 & (2\text{-}1) \\ \dfrac{D\vec{\omega}}{Dt} = (\vec{\omega}\cdot\nabla)\vec{q} - \vec{\omega}(\nabla\cdot\vec{q}) + \nabla P \times \nabla\left(\dfrac{1}{\rho}\right) \\ \qquad\qquad + \nabla\times\vec{f} + \nabla\times\left(\dfrac{1}{\rho}\sigma_{ij,j}\right) & (2\text{-}2) \end{cases}$$

Where $\rho$, $\vec{q}$, $\vec{\omega}$, $P$, $\vec{f}$, and $\sigma_{ij}$ represent the fluid density, velocity, vorticity, static pressure, volume force and viscous stress tensors respectively.

In order to make things simple, we now assume that the fluid is

inviscid and incompressible. Furthermore, the flow is steady, and in a conservative force field. Then the following relationships hold:

$$\begin{cases} \sigma_{ij} = 0 \\ \nabla P \times \nabla\left(\frac{1}{\rho}\right) = 0 \\ \frac{\partial}{\partial t} = 0 \\ \nabla \times \vec{f} = 0 \end{cases}$$

Equations (2-1) and (2-2) can thus be simplified to:

$$\begin{cases} \nabla \cdot \vec{q} = 0 & (2\text{-}3) \\ (\vec{q} \cdot \nabla)\vec{\omega} = (\vec{\omega} \cdot \nabla)\vec{q} & (2\text{-}4) \end{cases}$$

Since we are looking for the solutions of a confinement region in a vorticity field without swirling component, an axisymmetric geometry will be assumed. For this case, a cylindrical coordinate system $(r, \theta, \chi)$ is most convenient (Figure 2-1A). In this figure, $e_r$, $e_\theta$, $e_\chi$ are the unit vectors in the direction of their respective coordinates. As a consequence, all derivatives with respect to $\theta$ will vanish, i.e., $\frac{\partial}{\partial \theta} = 0$, Velocity has only two components in the $r$ and $\chi$ directions and the vorticity has only one component in the azimuthal direction. They may be written as:

$$\begin{cases} \vec{q} = u\vec{e}_x + v\vec{e}_r & (2\text{-}5) \\ \vec{\omega} = \nabla \times \vec{q} = \omega_\theta \vec{e}_\theta & (2\text{-}6) \end{cases}$$

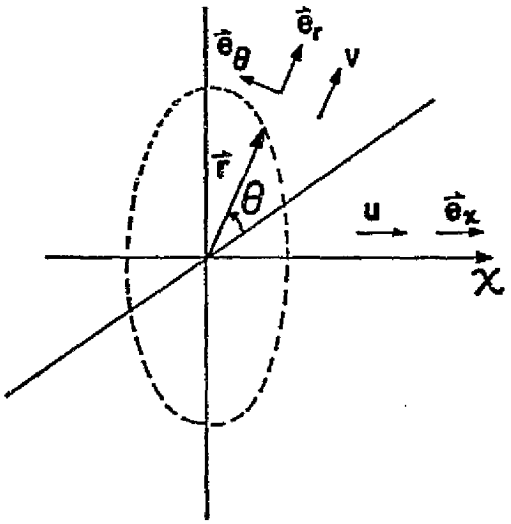


Figure 2-1A. Cylindrical coordinate system.

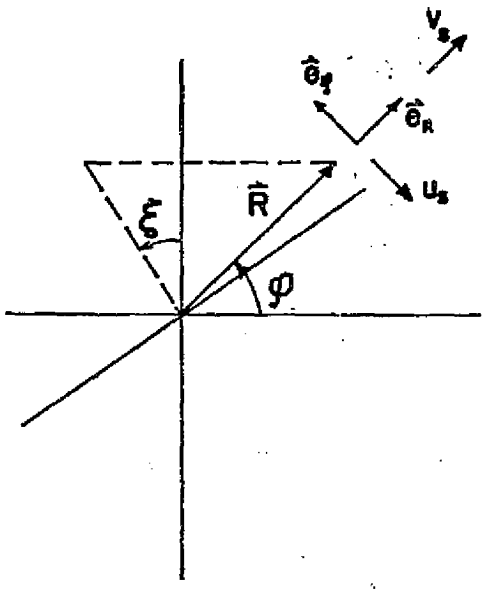


Figure 2-1B. Spherical polar coordinate system.

Equations (2-3) and (2-4) are then reduced to the following form:

$$\begin{cases} \frac{\partial}{\partial r}(rv) + \frac{\partial}{\partial x}(ru) = 0 & (2\text{-}7) \\ u\frac{\partial}{\partial x}\left(\frac{\omega_\theta}{r}\right) + v\frac{\partial}{\partial r}\left(\frac{\omega_\theta}{r}\right) = 0 & (2\text{-}8) \end{cases}$$

Equation (2-7) suggests a stream function which will satisfy the continuity equation identically. Hence we define a stream function $\psi$ such that:

$$\begin{cases} ru = \dfrac{\partial \psi}{\partial r} = \psi_r & (2\text{-}9) \\ rv = -\dfrac{\partial \psi}{\partial x} = -\psi_x & (2\text{-}10) \end{cases}$$

Substituting equations (2-9) and (2-10) into $\left[ r \times (2\text{-}8) \right]$, we obtain:

$$\psi_r \frac{\partial}{\partial x}\left(\frac{\omega_\theta}{r}\right) - \psi_x \frac{\partial}{\partial r}\left(\frac{\omega_\theta}{r}\right) = 0 \qquad (2\text{-}11)$$

It is obvious that if we let $(\omega_\theta / r) = -F(\psi)$, it would satisfy this equation identically. Therefore, from equation (2-6), an expression can be derived for $\omega_\theta$, the $\theta$-component of the vorticity, in terms of the stream function $\psi$. It is:

$$\begin{aligned} \omega_\theta &= \nabla \times \vec{q} \\ &= -\frac{\partial u}{\partial r} + \frac{\partial v}{\partial x} \\ &= -\frac{1}{r}\left(\psi_{rr} + \psi_{xx} - \frac{\psi_r}{r}\right) \end{aligned} \qquad (2\text{-}12)$$

By substituting $\omega_\theta = -rF(\psi)$ into equation (2-12), we can arrive at the following relations in terms of the stream function $\psi$ and an unknown function $F(\psi)$ as:

$$\begin{cases} \psi_{xx} + \psi_{rr} - \dfrac{1}{r}\psi_r = r^2 F(\psi) & (2\text{-}13) \\ F(\psi) = -\dfrac{\omega_\theta}{r} & (2\text{-}14) \end{cases}$$

This then becomes the set of governing equations for the flow problem we seek to explore.

2. Solutions

The set of equations shown above involves an unknown function $F(\psi)$. Once a certain value of $F(\psi)$ is specified, a solution to equation (2-13) can then be attempted. Such a solution has been found by Moore and Leibovich (Ref. 17), and is presented below. The simplest case is when $F(\psi)$ vanishes everywhere in the flow. This would represent an irrotational flow field and the stream function is simply that of a potential flow. However, this is not the case we are interested in.

Now if we assume that $F(\psi)$ is a constant, i.e., the vorticity is simply proportional to the radial distance from the axis of symmetry, $r$, not just along each stream surface, but throughout the flow; that $\omega_\theta = -ar$. Then the right-hand side of equation (2-13) becomes just $ar^2$. A suitable solution for our purpose can then be constructed as follows:

$$\psi = Kr^2(\chi^2+r^2) + Mr^2 + \frac{N r^2}{(\chi^2+r^2)^{3/2}} \qquad (2\text{-}15)$$

Substituting (2-15) in to (2-13) and matching the coefficients, we can determine K. By differentiating equation (2-15), following relations are found:

$$\psi_\chi = 2Kr^2\chi - 3N\frac{r^2\chi}{(\chi^2+r^2)^{5/2}}$$

$$\psi_{xx} = 2Kr^2 - 3N\frac{r^2}{(x^2+r^2)^{5/2}} + 15\frac{r^2x^2}{(x^2+r^2)^{7/2}}$$

$$\psi_r = 2Krx^2 + 4Kr^3 + 2Mr + 2N\frac{r}{(x^2+r^2)^{3/2}} - 3N\frac{r^3}{(x^2+r^2)^{5/2}}$$

$$\frac{1}{r}\psi_r = 2Kx^2 + 4Kr^2 + 2M + \frac{2N}{(x^2+r^2)^{3/2}} - \frac{3Nr^2}{(x^2+r^2)^{5/2}}$$

$$r\left(\frac{1}{r}\psi_r\right)_r = 8Kr^2 - \frac{12Nr^2}{(x^2+r^2)^{5/2}} + \frac{15Nr^4}{(x^2+r^2)^{7/2}}$$

The value of K is then found to be $a/10$. Hence equation (2-15) takes the form:

$$\psi = \frac{a}{10}r^2(x^2+r^2) + Mr^2 + N\frac{r^2}{(x^2+r^2)^{3/2}} \qquad (2\text{-}16)$$

This solution involves the sum of a particular solution, a free stream, and a potential doublet. For Hill's spherical vortex (Refs. 18 and 19), one uses the first and second terms inside the sphere, and the second and third terms outside. The values of the constants M and N can be appropriately chosen to make a sphere of radius $r_s$ a stream surface. A different set of choices was made by Lighthill (Ref. 24) who was concerned with the rotational flow behind a curved bow shock washing over the forward part of a sphere. Thus, he determined M and N by applying a shock condition and a requirement that the sphere be a stream surface. In his case, the vorticity was outside the sphere.

In a similar manner, we will find the values of M and N by

applying equation (2-16) outside the sphere and requiring that both components of the velocity vanish on the sphere. So that the sphere, or the boundary of the confined region will become a stream surface. Recall from equation (2-9) and (2-10), we have the following relations:

$$u = \frac{1}{r}\psi_r = \frac{a}{5}(x^2+2r^2) + 2M - N\frac{(2x^2-r^2)}{(x^2+r^2)^{5/2}} \qquad (2\text{-}17)$$

$$v = -\frac{1}{r}\psi_x = -\frac{a}{5}xr + \frac{3Nxr}{(x^2+r^2)^{5/2}} \qquad (2\text{-}18)$$

If we let $u_s$ and $v_s$ be the components of velocity, $\vec{q}$, in the directions of $-\vec{e}_\varphi$ and $\vec{e}_R$ of a spherical polar coordinate system $(R, \varphi, \xi)$ (Figure 2-1B); then $R = \sqrt{x^2+r^2}$ is the spherical radius. By a simple transformation, expressions for $u_s$ and $v_s$ can easily be found in terms of quantities in cylindrical coordinates.

$$u_s = u\,\mathrm{Sin}\,\varphi - v\,\mathrm{Cos}\,\varphi$$

$$= u\frac{r}{R} - v\frac{x}{R}$$

$$= \frac{a}{5}\left(\frac{x^2r}{R} + \frac{2r^3}{R} + \frac{x^2r}{R}\right) + \frac{2Mr}{R} + \frac{N}{R^5}\left(\frac{2x^2r - r^3 - 2x^2r}{R}\right)$$

$$= \frac{2}{5}arR + 2M\frac{r}{R} - N\frac{r}{R^4}$$

$$= \frac{r}{R}\left(\frac{2}{5}aR^2 + 2M - \frac{r}{R^4}\right)$$

$$v_s = u\,\mathrm{Cos}\,\varphi + v\,\mathrm{Sin}\,\varphi$$

$$= u\frac{x}{R} + v\frac{r}{R}$$

$$= \frac{a}{5}\left(\frac{x^3}{R} + \frac{2xR^2}{r} - \frac{xr^2}{r}\right) + \frac{2Mx}{R} + \frac{N}{R^5}\left(\frac{2x^3 - xR^2 + 3xr^2}{R}\right)$$

$$= \frac{a}{5}xR + \frac{2Mx}{R} + \frac{2Nx}{R}$$

$$= \frac{x}{R}\left(\frac{1}{5}aR^2 + 2M + \frac{2N}{R^3}\right) \qquad (2\text{-}20)$$

Now we apply the required boundary conditions to $u_s$ and $v_s$, i.e., $u_s$ and $v_s$ both vanish on the sphere of radius $r_s$. Then, at $R = r_s$ the following conditions hold:

$$\begin{cases} \frac{2}{5}ar_s^2 + 2M - \frac{N}{r_s^2} = 0 \\ \frac{1}{5}ar_s^3 + 2M + \frac{2N}{r_s^3} = 0 \end{cases}$$

$$\begin{cases} M = -\frac{1}{6}ar_s^2 & (2\text{-}21) \\ N = \frac{1}{15}ar_s^5 & (2\text{-}22) \end{cases}$$

Substitute the values of M and N in equations (2-21) and (2-22) into (2-16), (2-17), (2-18), (2-19) and (2-20), final solutions are found.

$$\psi = ar_s^4 (r')^2 \left[\frac{1}{10}(R')^2 - \frac{1}{6} + \frac{1}{15}\frac{1}{(R')^3}\right] \qquad (2\text{-}23)$$

$$u = \frac{ar_s^2}{15}\left\{3\left[(x')^2 + 2(r')^2\right] - 5 + \frac{2(x')^2 - (r')^2}{(R')^5}\right\} \qquad (2\text{-}24)$$

$$v = \frac{a r_s^2}{15}(3r'x')\left[\frac{1}{(R')^5} - 1\right] \tag{2-25}$$

$$u_s = \frac{a r_s^2}{15} r' \left[6(R')^2 - 5 + 2\left(\frac{1}{R'}\right)^3\right] \tag{2-26}$$

$$v_s = \frac{a r_s'}{15} x' \left[3(R')^2 - 5 + 2\left(\frac{1}{R'}\right)^3\right] \tag{2-27}$$

Where primed quantities are non-dimensionalized with reference to $r_s$ .

$$x' = \frac{x}{r_s}\ ,\quad r' = \frac{r}{r_s}\ ,\quad R' = \frac{R}{r_s} = \frac{\sqrt{x^2+r^2}}{r_s} = \sqrt{(x')^2 + (r')^2}$$

3. Evaluation of the solution

The solutions obtained above are for the specific conditions that we have previously established. Clearly, both $u$ and $v$ or $u_s$ and $v_s$ vanish on the surface of the sphere $R' = 1$. Now, for given values of the constants $a$ and $r_s$, the solutions can be evaluated for velocity and pressure distributions. Stream surfaces can also be found. Figure 2-2 from Ref. 17 shows the essential features of this flow. Streamlines are curves in the upper half of the figure. The velocity at $r' = 1.4$, $x' = 0$ is denoted as $V_r$ , and all other resultant velocities are indicated at various positions on the streamlines as the ratio $u/V_r$ . Pressure distribution is given by curves in the lower half of the figure. The axial velocity at $x' = 1.8$ is indicated.

Figure 2-2 shows that the streamlines are reasonably shaped for flow over a sphere. But it should be noted that there is no free stream in this flow; velocities approach infinity far upstream and far downstream. Thus, there is no characteristic velocity for this problem.

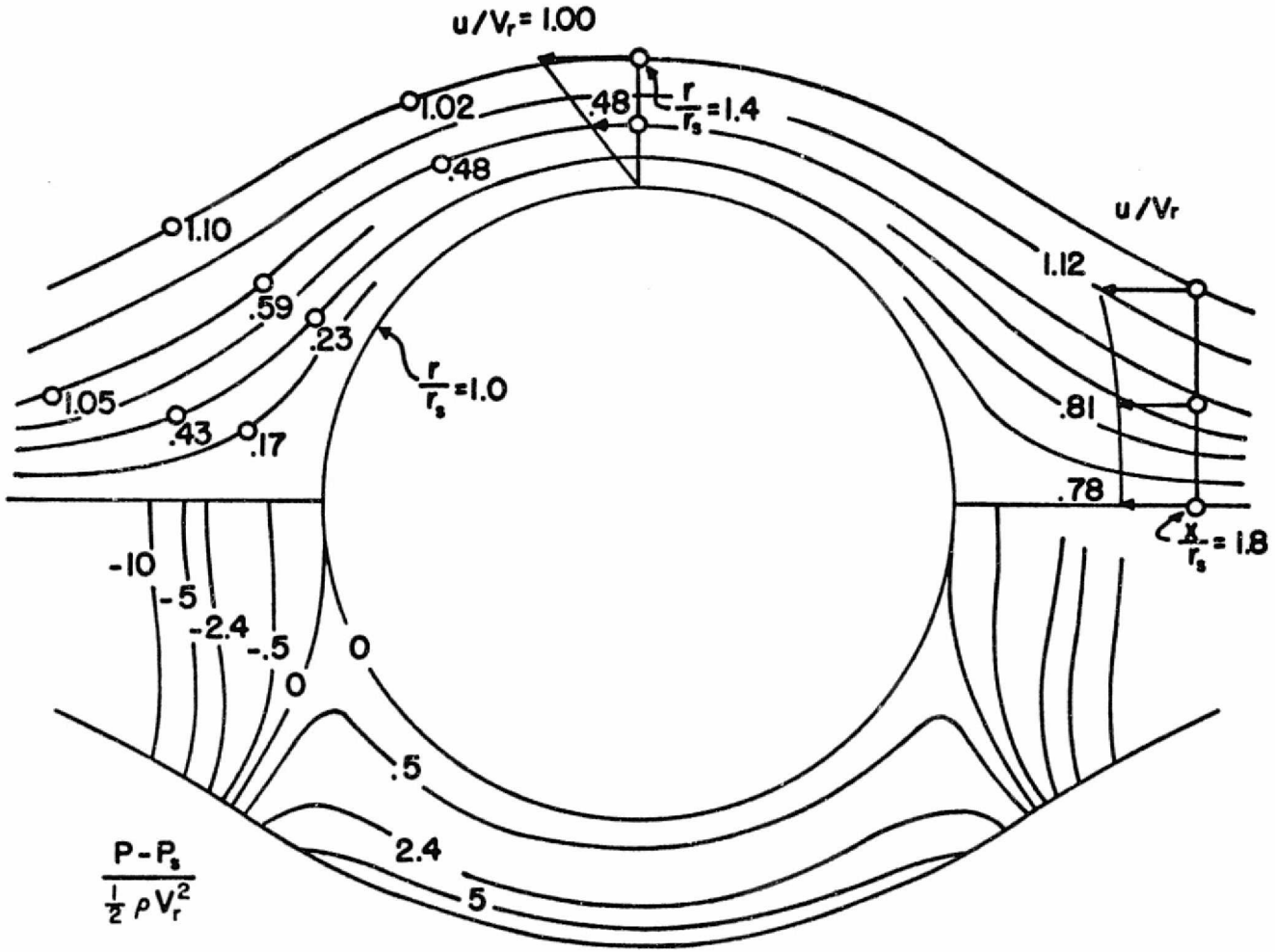


gure 2-2. Streamlines, velocities, and pressure distribution in the smoke-ring solution (From Ref. 17).

Also note that, since velocities vanish on the sphere, the confined region at the center is at rest and at constant pressure $P_s$.

It is quite remarkable that the velocity remains nearly constant over the central portion of each streamline path. This is reflected in the pressure contours as well. In the region $50^\circ$ to either side of the central vertical, where pressure is higher than $P_s$, pressure is nearly constant along streamlines.

Now one may ask, is the flow unique? Given an initial ring-vorticity distribution, linear with $r$, the sphere is perhaps the only shape within which fluid can be confined. A different vorticity distribution might well yield another shape, provided the duct walls were also modified in the proper way. There seems to be no flow of this character in two dimensions, nor should it be expected; a straight vortex line can pass around a cylinder without stretching and hence without exerting a containing force. Therefore the plane-flow experiment by Ragsdale and Lanzo (Ref. 20) is probably only superficially comparable to the flow phenomenon just described. It is felt that the axisymmetric geometry is fundamental to the success of the approach.

As for the stability of the flow just mentioned, we will try to answer some aspects of this question by the following experimental study. Obviously, the quiescent center is favorable, as is the positive outward pressure gradient. The weak streamwise pressure gradient is no doubt helpful for boundary layer stability. As shown in Figure 2-2, pressure is nearly constant along streamlines. This circumstance should be helpful in maintaining an attached boundary layer along the duct walls.

# CHAPTER III

# EXPERIMENTS

As stated in the introduction, the primary objective of this study is to find out whether the self-confined flow described in the previous chapters does exist in a real situation; whether the flow turbulence and separation characteristics would undermine the existence of the confined region. Also, if the flow does exist, we hope at least some aspects of the stability question can be answered by the information obtained from mapping out the entire flow field.

First, and experimental apparatus was designed and developed in the laboratory in accordance with the theory formulated in the last chapter. The flow medium was air, and the initial assumptions of an inviscid, incompressible, and steady flow were closely met. Then a visualization method using a piece of short, soft tuft was used to identify the self-confined region and its surrounding flow field. Finally, quantitative measurements of flow mean velocity and turbulence data were taken with a constant temperature hot wire anemometer system. Analysis of these quantitative results are presented in the next chapter.

## 1. The flow apparatus

In order to conform to the initial assumptions made for the theoretical model of being an inviscid, incompressible and steady flow, a low speed (maximum Mach number was less than 0.07) flow apparatus was designed using air as the flow medium. Room air was drawn into an inlet chamber through high efficiency filters, then went through a turbulence-

manipulating section--consisting of a honeycomb and a flat screen--into a straight pipe. Thus the turbulence of the stream was reduced to an acceptable level. A vorticity generator was placed in the stream, at an appropriate distance behind the turbulence manipulator to shape the velocity profile and to produce the desired vorticity distribution. When the generated velocity profile was well established, a boundary layer removal section peeled off the boundary layer of the flow before it entered the test chamber. Combined with the low turbulence level in the flow, the effect of viscosity could thus be minimized.

The test chamber was machined out of Plexiglas. Its interior wall was shaped to be one of the stream surfaces obtained from the theoretical solution without any boundary layer correction because the estimated boundary layer thickness was small and its effect would be negligible. Attached to the downstream side of the test chamber was a four-way traversing mechanism; it could make axial and radial traverses, azimuthal rotation as well as tilting in any meridional plane. Then the flow went into a settling chamber through a slowly diverging diffuser, and exited at the blower outlet into the room. A schematic diagram of the flow apparatus is shown in Figure 3-1, and two photographs of the actual experimental set up are shown in Figures 3-2A & 3-2B.

1.1. Entrance section

The room air was drawn into the flow apparatus and then exited at the blower outlet into the room in an open return circuit. During the initial hot wire calibration stage, a severe dust problem was encountered. Both the wire and its supports were coated with a thin layer of fine,

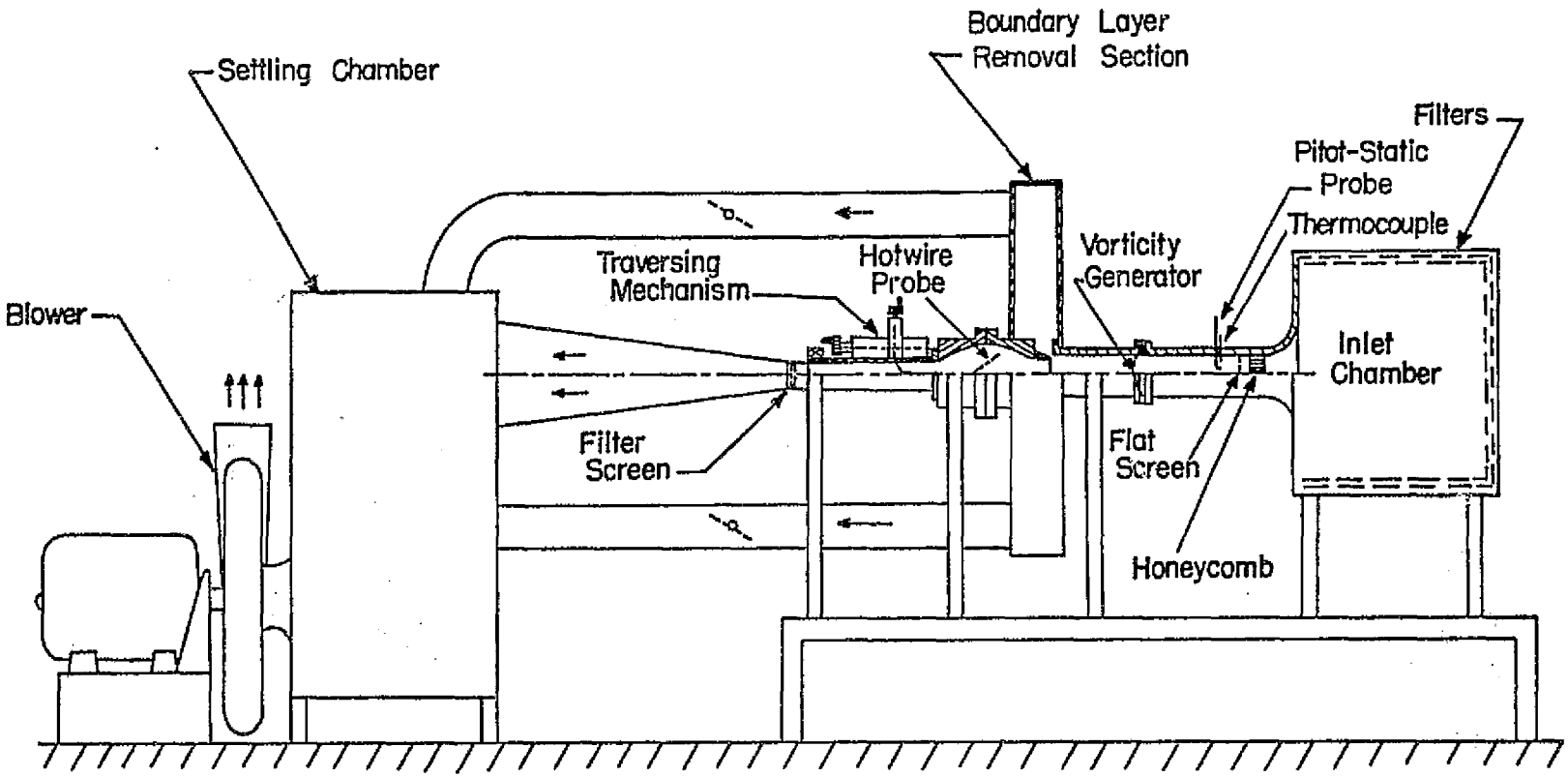


Figure 3-1. Schematic of the flow apparatus.

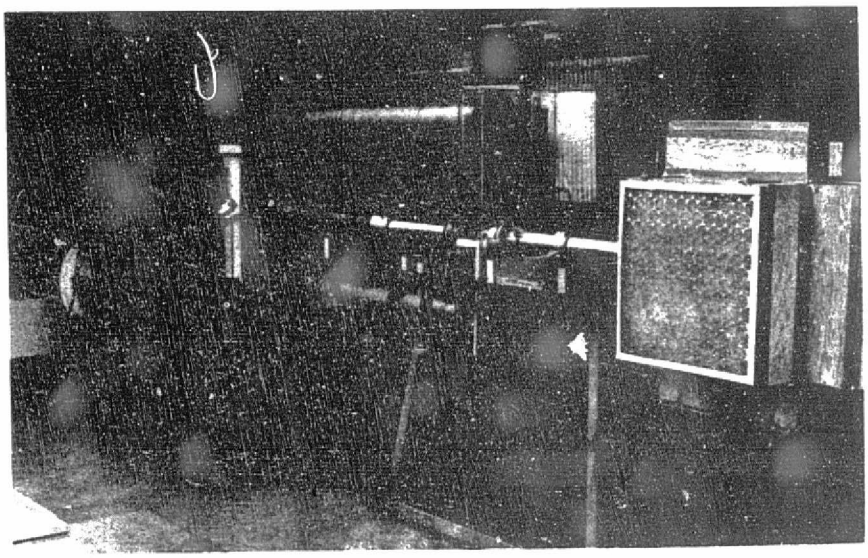

Figure 3-2A. Flow apparatus

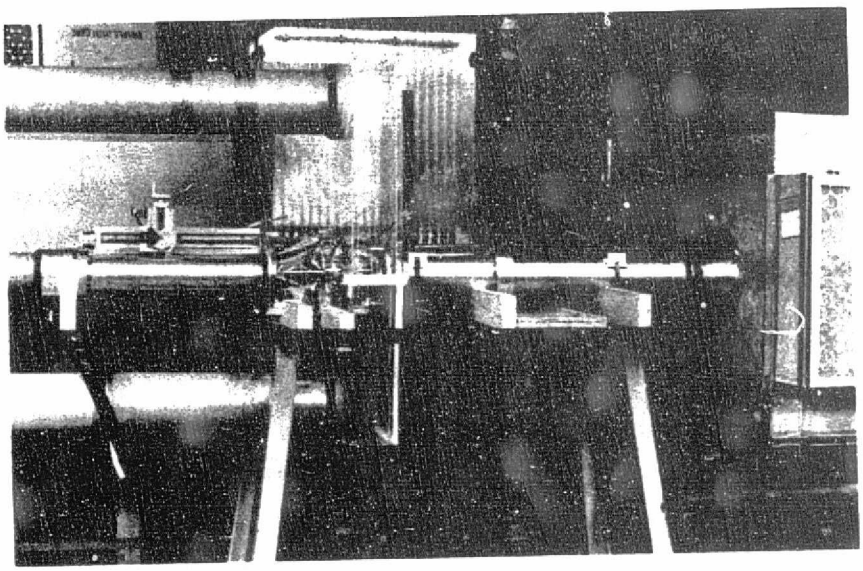

Figure 3-2B. Flow apparatus

brownish dust powder causing the calibration curve to continously drift with the running time. Therefore, air filters of very high efficiency were used to solve this problem.

Two layers of filters were used on all five sides of a cubical inlet chamber; the remaining side was the inlet bellmouth. The first layer was a common furnace filter (24" x 24" size). It was used as a pre-filter to remove the larger sizes of particulate matter, lint and other contaminants. The second layer was a Model 7A10-L Flanders Airpure Absolute Filter, made by the Flanders Filter Inc., Washington, North Carolina. The overall filter dimensions were 24" x 24" x $5\frac{7}{8}$" with a flow capacity rated at 775 CFM. This was a very high efficiency air filter; the minimum efficiency was 99.97% by the DOP (Dioctyl Phthalate) test for a homogeneous smoke of 0.3 microns in diameter (Ref. 25). At the maximum test capacity of approximately 150CFM, pressure drop across each filter was about 0.05" of water gage. After these air filters were properly installed and sealed, a very clean air flow was achieved inside the flow apparatus and the problem of hot wire drift due to dust was completely eliminated.

An aluminum bellmouth was installed at the center of the remaining side of the inlet chamber and connected to a straight aluminum pipe of 4.144" inside diameter. At the entrance section, flow straighteners and "turbulence manipulators" were used to eliminate any swirling velocity component and to manage the turbulence level such that a low turbulence, axial flow was established in the straight pipe. A section of a precision, hexagonal, aluminum honeycomb (0.25" cell size x 1.45" long), manufactured by the Aerospace Technology Corporation, New York, N. Y.,

was used both as a flow straightener and as a part of the turbulence manipulator. The turbulence manipulator mentioned here consisted of a honeycomb section and a flat gauze screen (30 mesh/inch, 0.012" wire dia.) 1.04 inches downstream of the honeycomb. The choice of the honeycomb, the flat gauze screen and their relative spacings were experimentally found in order to achieve the desirable flow characteristics. These manipulators suppressed the level of the incoming turbulence and generated new turbulence with scales characteristic of the device and its shear layer. As pointed out by Loehrke and Nagib (Ref. 26) that the process of turbulence generation might be due to instabilities of wakes caused by the device or to boundary layers generated within the device (as in honeycombs at high Reynolds numbers), or to the action of the Reynolds stress on the mean shear. And the ultimate effect of these generation processes might at times be an overall reduction in the turbulence level. Hence, they could be used to control, manage and modify the incoming flow of high turbulence level to a low turbulence flow for practical applications.

The level, structure and decay of the generated turbulence depended, in part, on the instabilities and therefore could be modified by passive devices acting on the shear layers immediately downstream of the manipulators. For honeycombs, the suppression of the incoming turbulence appeared to mostly due to the inhibition of lateral components of the fluctuating velocity. It was conjectured by Loehrke and Nagib that part of the energy in the undesirable larger scales of motion drains away through the action of the Reynolds stresses of the smaller scale laminar and turbulent motions (including the instabilities). An

experimental study on the management of free-stream turbulence had been carried out by them and a quite extensive bibliography, on theoretical and experimental information of the effect of screens, honeycombs and other devices on turbulence, were included in their AGARD report.

The resulting flow in the pipe downstream of the turbulence manipulators were checked with both pitot-static probe and hot wire measurements. A swirl-free low turbulence stream (turbulence intensity about 1% of local velocity -- see Chapter 4 for detailed results) were established three to four pipe diameters downstream of the flat gauze screen.

1.2. Vorticity generator

It has been shown in the last chapter that one of the key features of this self-confined flow is the ring-vorticity distribution. Vorticity is axisymmetrically distributed throughout the flow in the fashion of a bundle of coaxial smoke-rings in axial motion; and the vorticity in each ring is simply proportional to the radial distance, $r$, from the axis of symmetry ( i.e. $F(\psi) = -\omega_\theta/r = a$).

One of the main problems we faced at the beginning of the experiment was how to generate the required vorticity distribution in the flow apparatus conveniently. It should be noted that there was no free stream in the theoretical flow model; velocities approached infinity far upstream and far downstream (Cf. Figure 2-2). Ideally, the wall of the flow apparatus should correspond to a particular streamline such that the field velocity would have both axial and radial components as shown by equations (2-24) and (2-25). However, in order to simplify the construction, two separate sections were designed for the flow apparatus

---- a test section and a straight-pipe section. The test section was centered around the self-confined region, and its wall was machined in accordance with a particular streamline shape calculated from equation (2-23) (see Section III.1.1.4.). A straight-pipe section was used upstream of the test section in order to avoid difficult contour machining in a pipe. In doing this, it had been assumed that even the proper radial velocity component was not generated in the incoming pipe, the general confinement characteristics would not be affected to any significant extent as long as the proper vorticity distribution could be produced at the entrance of the test section. It was expected that once the flow entered the test chamber, due to the divergence of the wall, radial velocity components would be developed to provide the suitable flow field for confinement without any flow separation.

In a straight pipe flow, velocity had an axial but not a radial component. Therefore, the axial velocity profile had to be modified so that a prescribed vorticity distribution was established. If $F(\psi) = -\omega_\theta/r = a$, a constant, the corresponding axial velocity profile could be found. Recall that:

$$\omega_\theta = -ar = -\frac{\partial u}{\partial r} + \frac{\partial v}{\partial x} = -\frac{\partial u}{\partial r}$$

There was no $v$ component in the pipe. Integrating once with respect to $r$, we get:

$$u = \int_0^r a\zeta\, d\zeta + u_0 = \frac{1}{2}ar^2 + u_0 \qquad (3\text{-}1)$$

Where $\zeta$ is a dummy variable, and $u_o$ is the velocity on the axis of symmetry. When the dimension of the test chamber was specified, $u_o$ could be chosen as the axial velocity at the chamber entrance according to the calculation of equation (2-24). This parabolic velocity profile would provide the proper vorticity distribution as well as the correct axial velocity on the axis of symmetry at the entrance of the test chamber.

In order to generate the parabolic velocity shown above for the proper vorticity distribution, a vorticity generator was used. The straight-pipe section was divided intc two parts. The first part constituted the entrance section with flow straightener and turbulence manipulators. The second part was just a straight pipe. These two parts were joined together with flanges and the vorticity generator was installed between these two flanges in a holder. Both parts of the pipe were made of aluminum pipes of 4.144" inside diameter and 18" & 12" in length respectively. Along the centerline of both pipes, 1/8" diameter probing holes were drilled at 1/2 of a pipe diameter intervals starting from the flat gauze screen so that probes (both pitot-static & hot wire) could be inserted for measurements. The downstream end of the second pipe was also flanged to provide convenient joint to the test section through spacers. The length of each pipe was selected for the best results in velocity profile and turbulence intensity.

Various devices were tried as the vorticity generator. All these devices were designed to have variable resistance across the pipe diameter in order to produce a parabolic velocity profile with larger velocity at larger radius. Some of the devices which were able to produce

this kind of velocity profile are described below.

The first device tried was a non-uniform shear screen (Figure 3-3A). It consisted of concentric rings of various diameters suitably spaced to give the desired solidity. The entire shear screen assembly was bounded to a metal honeycomb and mounted in a metal frame. The honeycomb served to stiffen the assembly structurally and to prevent flow instabilities. This non-uniform shear screen redistributed the energy of the incoming stream by selectively introducing losses. The static pressure immediately downstream of the sereen was not constant over the screen because the screen losses were not uniform. Far downstream, the flow readjusted to a condition of uniform static pressure. Consequently it was not possible to simply extrapolate the desired velocity distribution back to the screen to determine the required distibution of screen losses. A theory for such a screen design and calculation was provided by Vidal and Curtis in their report (Ref. 27) along with some experimental results. This non-uniform shear screen was tested in the present experiment; the velocity profile generated, while generally conformed to the required form, did not have good axisymmetry. It was difficult to fabricate a series of good quality concentric rings and mount them accurately on the honeycomb support in our machine shop. For this reason, other methods were tested.

The second device tried was a shaped foam screen (Figure 3-3B). A piece of Scott industrial foam (fully reticulated polyurethane foam), made by Scott Paper Company, Philadelphia, Pa., was first soaked in a liquid epoxy, then cleaned with compressed air and hardened in room temperature so that a thin, hard coating was applied to the entire foam

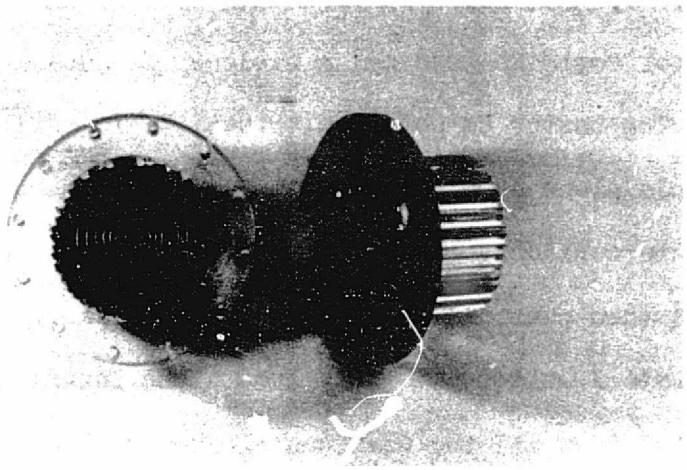

A. Non-uniform shear screen

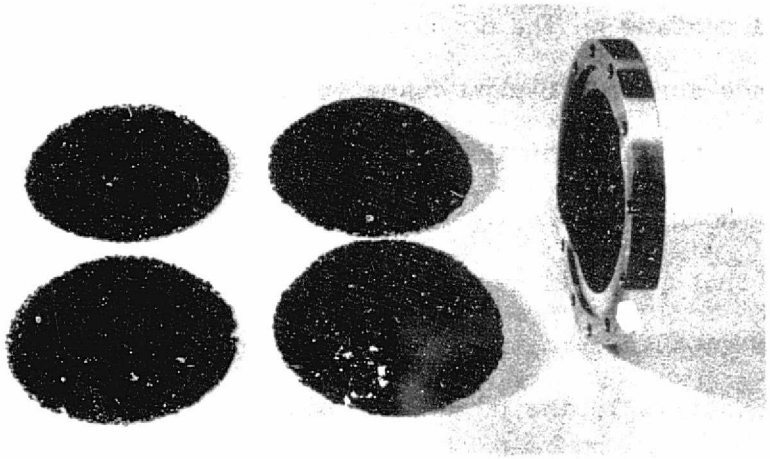

B. Shaped foam screen and holder

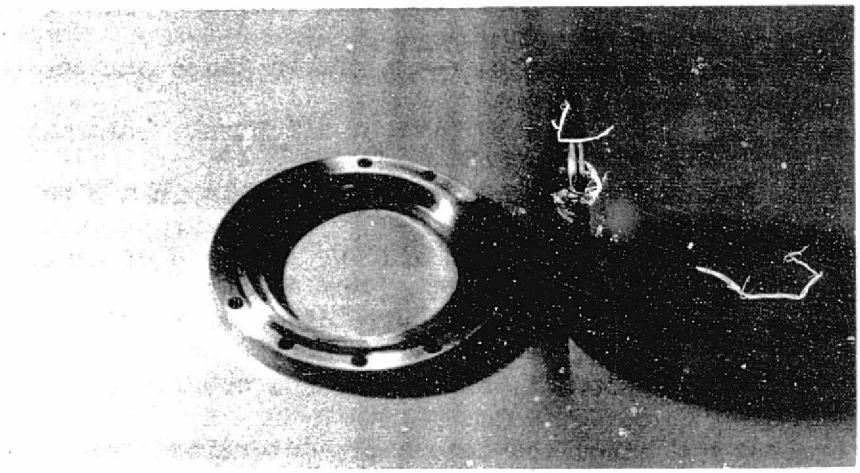

C. Shaped gauze screen and holder

Figure 3-3

structure without any hole blockage. The liquid epoxy used was composed of a Hysol resin R8-2038 and a hardener H2-3404 made by the Hysol Division of The Dexter Corporation, Olean, N. Y. After 24 hours of curing time, this piece of hardened foam was then soaked in liquid wax and allowed to cool down till a solid piece of mold was formed. The wax mold was then machined on a lathe to a desirable shape which could be fitted into a holder and installed in the incoming pipe. Then the wax was melted down and the foam was cleaned with appropriate wax solvent. The finished foam screen had a flat surface on the upstream side and a curved surface on the downstream side. It also provided variable resistance across the pipe diameter and produced the required velocity profile. The shape of the curved surface could be obtained with a few trials. However, like that of the first device, although the velocity profile thus produced generally agreed with the shape required, it did not have good axisymmetry. The created velocity profile appeared to be quite sensitive to the pore uniformity of the curved surface. It was difficult to get a good pore uniformity on any surface of a porous foam. Therefore, this foam screen was not used for our experiment.

The third device tested was a shaped gauze screen, (Figure 3-3C) and (Figure 3-4), furnished by Livesey and Laws. This method of producing a required axisymmetric velocity profile in a pipe was worked out by them and reported in Refs. 23 and 29. A piece of gauze screen of known mesh size (20 mesh/in.) and wire diameter (0.016 inch dia.) -- thus of known gauze porosity and resistance coefficient -- was successively pressed and annealled into a pre-determined shape. A specially made steel punch and hard rubber die arrangement was used to form the

shape of the gauze screen, and it was necessary to anneal the gauze between each press to prevent the screen from tearing. The edge of the finished gauze screen was then rigidly sandwiched between two metal rings which in turn could fit into a holder. The whole gauze screen and holder assembly was then tightly bolted between the flanges of the upstream and downstream sections of the incoming straight pipe. The velocity profile produced by this shaped gauze screen agreed generally well with the required form, and it was reasonably axisymmetric (maximum velocity deviation from the corresponding averaged value was about 5% in the azimuthal distribution --- see detailed results presented in the next chapter). Among the various devices tried, the shaped gauze screen provided the best velocity distribution and was finally used as the vorticity generator for this experimental study.

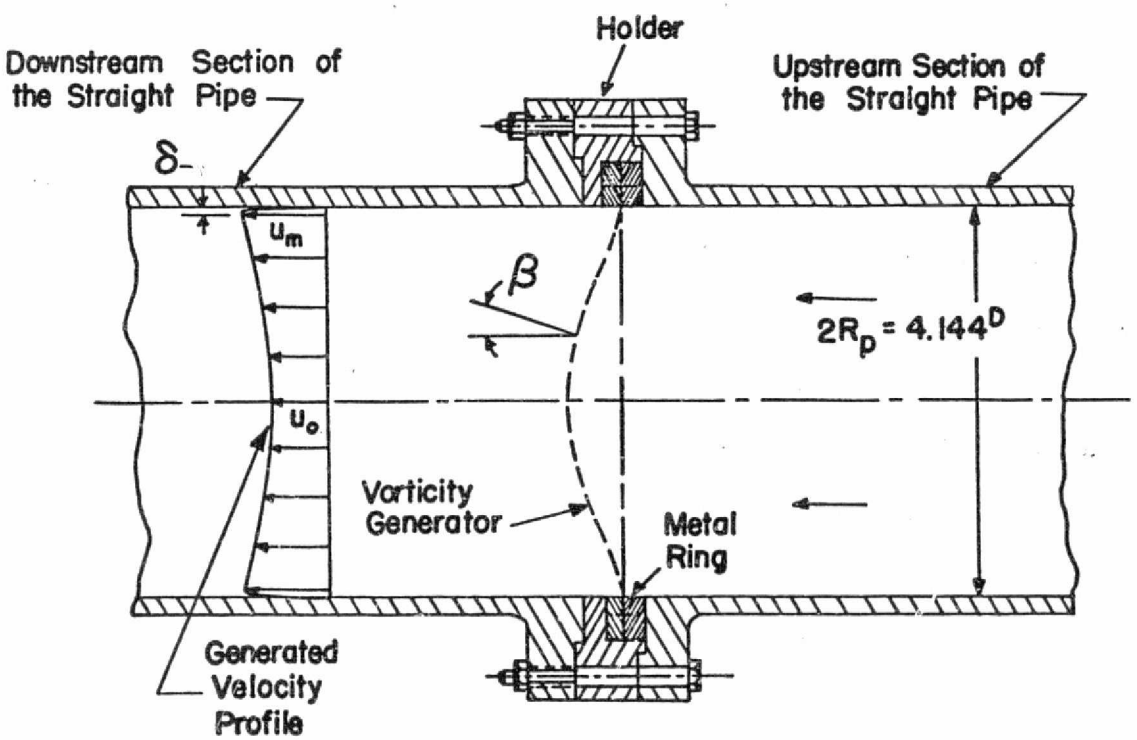


Figure 3-4. Gauze screen installation.

For a given velocity profile, the required gauze screen shape could be found with the method outlined as the "Indirect Problem" in the papers by Livesey and Laws. The solution, in this case, employed an iterative numerical technique with the local screen angle, $\beta$, as an unknown. Gauzes with the same resistance and deflection coefficients would produce the same downstream velocity profiles. By varying the gauze mesh size and wire diameter so that the screen porosity remained constant, the effect was to vary the turbulence characteristics (e.g. intensity and scale) of the downstream profile. In such a way, it was possible to vary the profile shape and initial turbulence structure of the profile independently. The analysis also provided the method of calculation for the "Direct Problem" -- i.e. for a given gauze screen shape, the downstream velocity distribution could be calculated. Some experimental results were also presented in these papers.

There was another work by Sajben, Kroutil, Hoffman and Sedrick (Ref. 30) on generation of arbitrary axisymmetric velocity profiles. It used plane screens of variable solidity, fabricated by electroplating a uniform screen in a rotating apparatus. A wide range of screen mesh sizes could be used, permitting control of the overall turbulent intensity as well as velocity profiles. Good results had been found for relatively fine screens (24 mesh/in.). This method was not tried in our experiment.

1.3. Boundary layer removal section

In order to minimize the effect of the viscous boundary layer, a boundary layer removal section was built at the junction of straight

pipe and test section (Cf. Figures 3-1, 3-2 & 3-5). Immediately before the established flow, with the prescribed velocity profile, entered the test chamber, fluid in an annulus of 3 inches inside diameter and 4.144 inches outside diameter were peeled off into the boundary layer removal section. Thus the flow entering the test chamber were free from any previous boundary layer build-up. Of course, new boundary layers would build up again in the test chamber; nevertheless, the effect of this new layer would be kept to a minimum by the removal procedure.

The incoming straight pipe had an inside diameter of 4.144 inches and was bolted to the test section, with an entrance scoop of 3 inches of inside diameter, through six spacers. A chamber, made of Plexiglas, was built around the gap bridging the downstream section of the straight pipe and the test section. It was sealed on both sides so no outside air could leak into the chamber. Two furnace pipes, 6 inches in diameter, connected the boundary layer removal chamber to the rear settling chamber as shown in Figure 3-1. In each of these pipes, a butterfly valve was installed to allow controls on removal rate.

In the original design, the entrance scoop of the test section had a rather sharp leading edge. Very turbulent and unsteady flow conditions were found in the test chamber which was later traced to having been caused by the leading edge separation at the sharp leading edge. This problem was corrected by blunting out the sharp edge to a semicircular shape.

1.4. Test section

The test section was just a hollowed chamber in which the self-

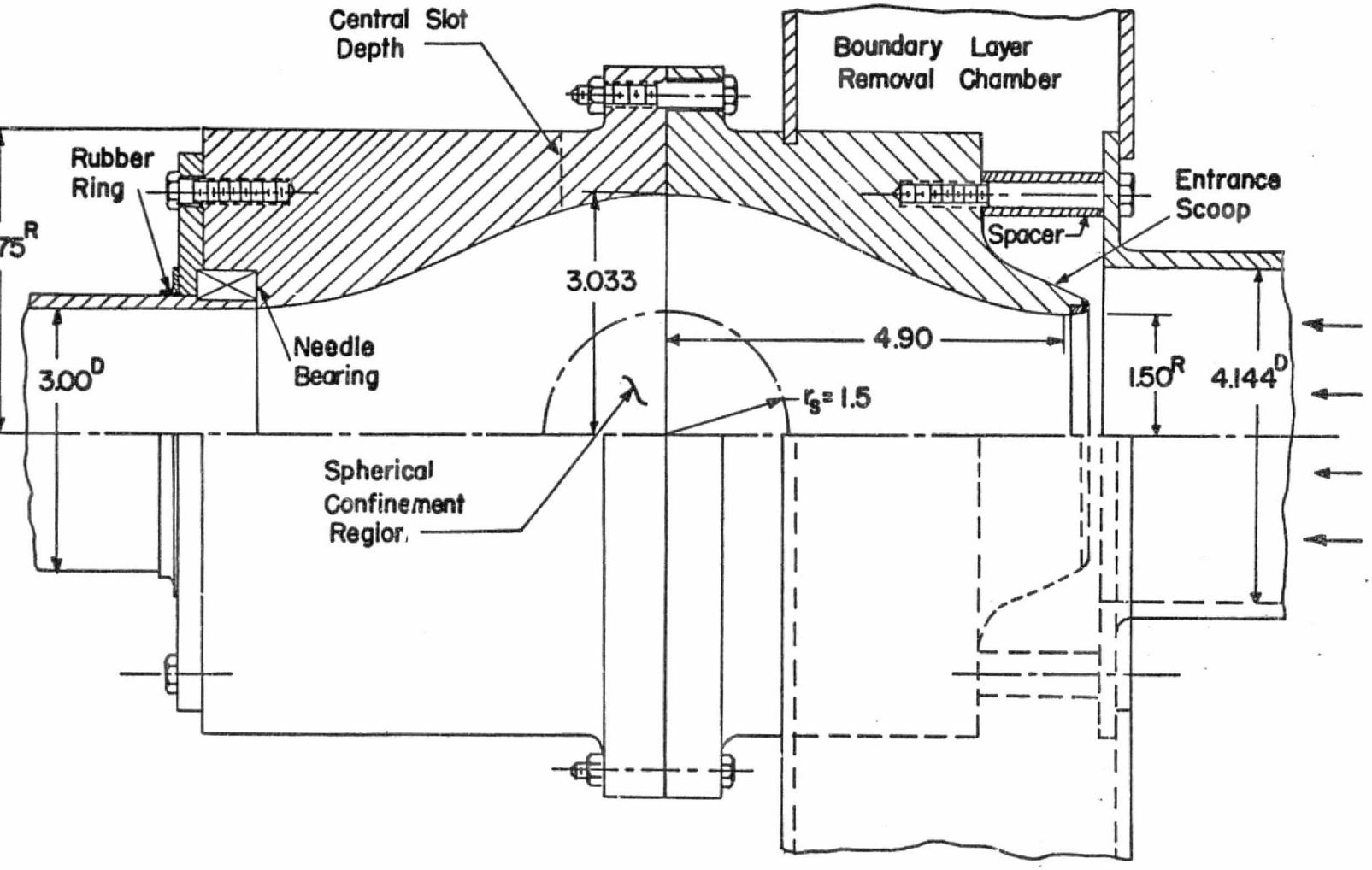


Figure 3-5. Layout for the test section

confined region was to appear. It consisted of two halfs, both machined out of solid Plexiglas material (Figures 3-5 & 3-8). The essential features of this section, besides the entrance scoop of the upstream half, was the special interior wall configuration of the whole section. It must be shaped as one of the stream surfaces as prescribed by equation (2-23) so that the condition of no flow across the stream surface was satisfied.

Before designing the test section for manufacturing, a series of streamline calculations were made. First, the stream function $\psi$ was non-dimensionalized with $a r_s^4$, and then the non-dimensionalized stream function $\psi'$ was assigned a series of constant values for streamline coordinate calculations. Namely:

$$\psi' = \frac{\psi}{a r_s^4} = (r')\left[\frac{1}{10}(R')^2 - \frac{1}{6} + \frac{1}{15}\frac{1}{(R')^3}\right] \qquad (3\text{-}2)$$

Different sets of streamline coordinate values calculated from equation (3-2) were then plotted on a graph for design purpose.

As stated in the last chapter, the constants M and N in the stream function solution of equation (2-16) were found by choosing a sphere of radius $r_s$ to be a stream surface $\psi = 0$ such that both velocity components, $u$ & $v$, vanished on the sphere. Now the size of this spherical confinement region was chosen to have a diameter of 3 inches, i.e. $r_s = 1.5$ inches. Then a value of $\psi' = 1$ was selected for the evaluation of wall configuration. This would give us a reasonable wall size of $r = 3.033$ inches at the center of the test section, and $r = 1.499$ inches at $x = 4.9$ inches at the entrance scoop. The final coor-

dinate values for the test section interior wall are shown in Table 1 in the Appendix.

At the very center of the test section wall, a slot was cut along the center line to provide access for various probes into the test chamber. This slot could be tightly sealed against air leaks with an insert, flush with the inside wall, without causing any disturbances in the flow. At the rear end of the downstream half, a precision traversing mechanism was mounted on a pipe through a needle bearing seated on the test section. On the outside, a rubber ring sealed the air passage so that the whole traversing mechanism and pipe assembly could rotate around with respect to the test section without any air leakage into the flow.

1.5. Exit section

The flow, coming out of the test chamber, went through a section of straight pipe (for mounting the traversing mechanism) into a conical diffuser, passed into the rear settling chamber, and then exited into the room at the blower outlet. The diffuser was made of sheet metal and had a small angle of divergence of $4.7^{\circ}$ in order to prevent separation. The diffuser had dimensions of 4 inches inside diameter at the inlet, 12 inches diameter at the outlet and a length of 49 inches. At the junction of the straight pipe and the diffuser inlet a thin layer of furnace filter material was placed across the entire area, supported by criss-crossed wires, in order to damp any downstream disturbances. For the same reason, a gauze wire screen was placed at the junction of the diffuser outlet and the rear settling chamber to insure that minimum chamber fluctuations could propagate upstream into the flow.

The rear settling chamber was constructed of heavy plywood panels. The diffuser exit and two boundary layer removal pipes were connected to this chamber as shown in Figure 3-1 & 3-2A. There were several baffle plates inside the settling chamber to further damp any fluctuation that might be caused by the downstream suction blower. A 5 HP centrifugal blower, made by Baffalo Forge Company, was connected to the rear end of the settling chamber. The maximum flow speed obtained in the incoming straight pipe, without the vorticity generator, was about 92 ft/sec. A gate valve with vernier scale was installed at the blower exit to control the flow rate through the apparatus.

2. Measuring equipment and traversing mechanism

The measuring equipment used in this experiment included pitot-static probes, manometers, micromanometers, tuft probes, thermocouples, the constant hot wire anemometer and its associated instrumentation, digital voltmeters, a microvoltmeter, an oscilloscope, a Dynograph chart recorder, etc. The arrangement of the equipment can be seen on Figures 3-1, 3-2, and 3-7. An instrumentation schematic is shown on Figure 3-6.

2.1. Pitot-static probes, manometers and thermocouples

The initial pipe flow velocity and its profiles were measured with standard pitot-static probes and a manometer. Later, a micromanometer was used with the standard pitot-static probes for more accurate measurements as well as for the hot wire calibrations. After the initial measurement stage, a pitot-static probe was permanently

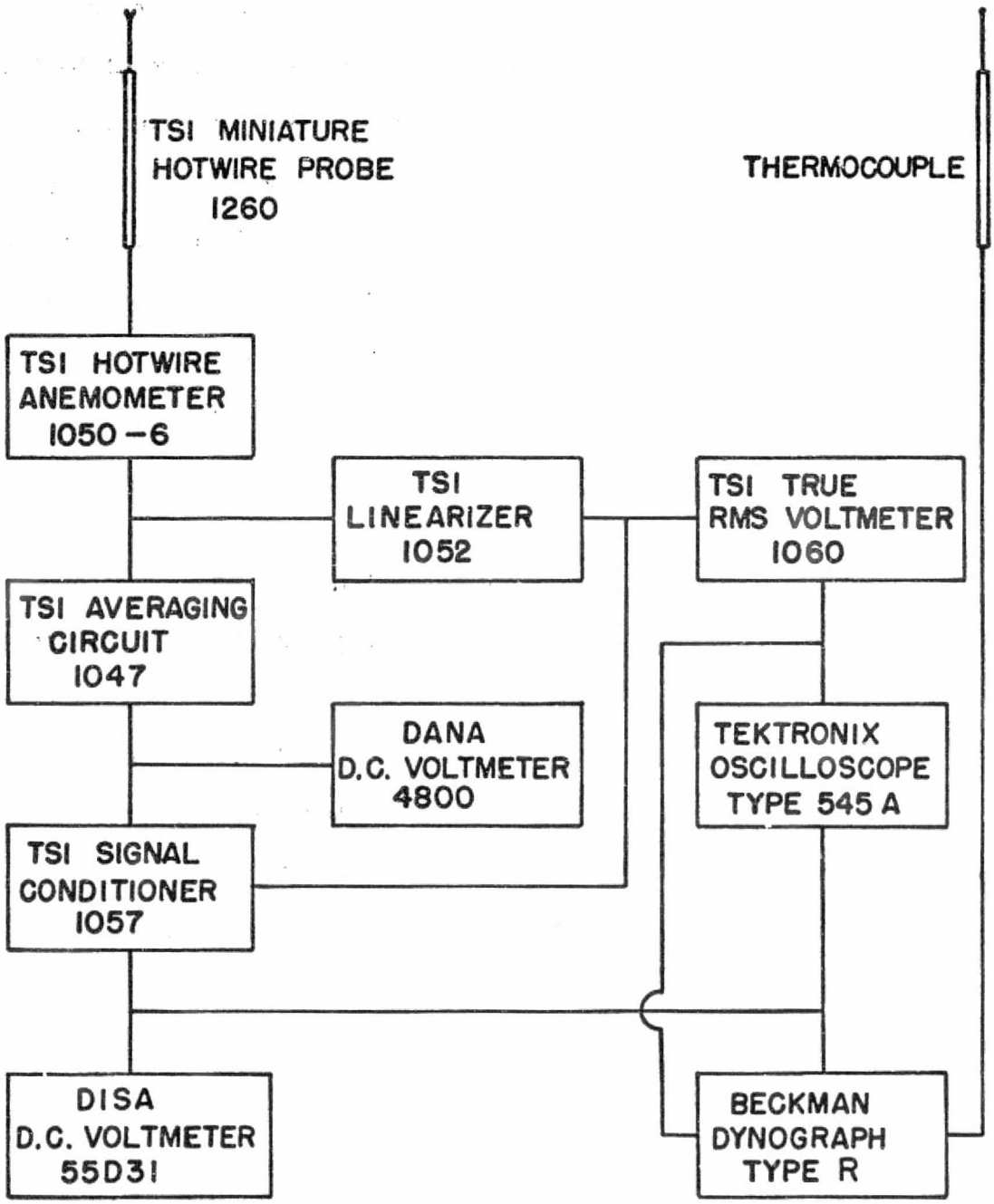


Figure 3-6. Instrumentation schematic

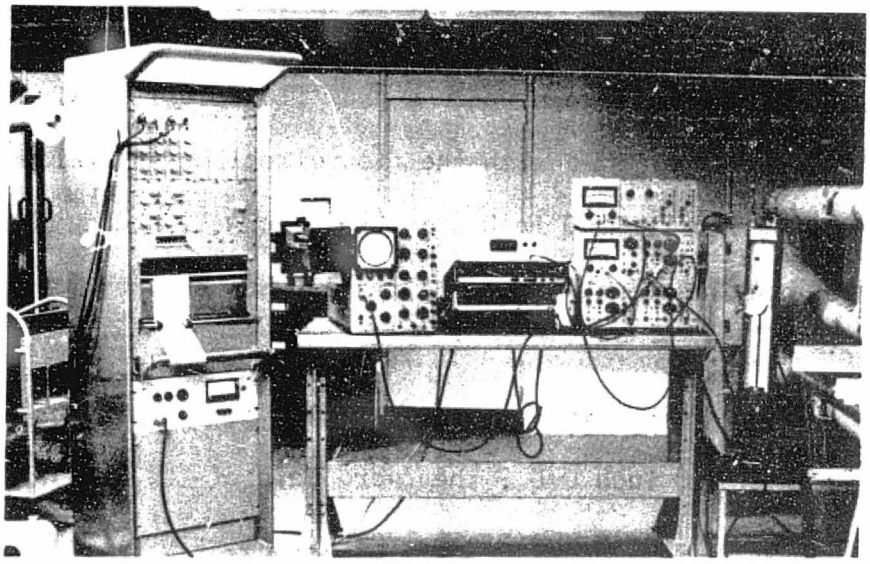

Figure 3-7. Instrumentation for flow measurement

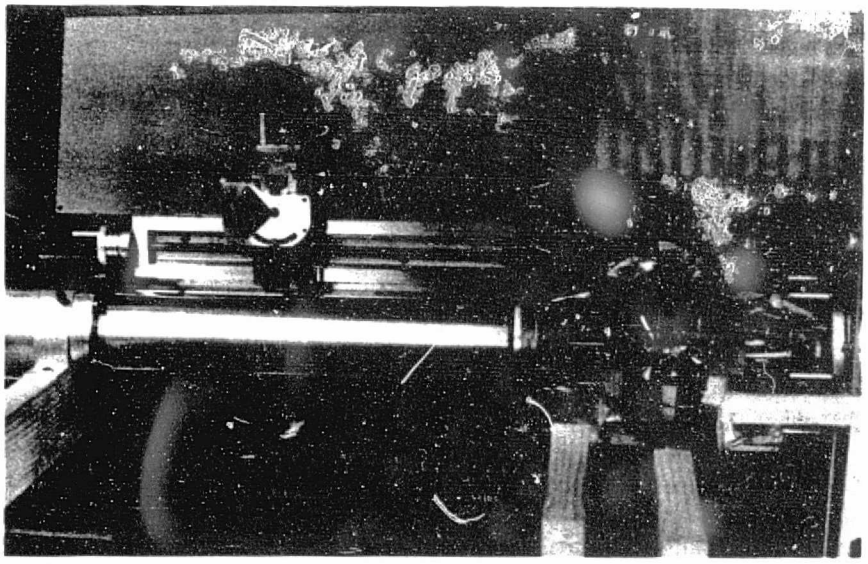

Figure 3-8. Test section and traversing mechanism

installed in the upstream section of the incoming pipe to continually monitor the flow velocity during the test. It was located 6.25 inches downstream of the flat screen where a plug flow profile existed. The probe was carefully aligned with the flow direction and raised above the pipe centerline to 0.50 inch away from the wall and outside the boundary layer so as to minimize the disturbance and obstruction caused by the probe stem.

Two sizes of the standard pitot-static probes were used, an 1/16 inch O.D. and an 1/8 inch O.D.; they were both of the Prandtl type and made by The United Sensor and Control Corp., Watertown, Mass. They were calibrated by the manufacturer and had an accuracy of 0.5% for a Mach number less than 0.5. The micromanometer was made by The Meriam Instrument Company, Cleveland, Ohio. It had a range of differential pressure readings of 0.001 inch to 10 inches of water. A special indicating fluid was used in the micromanometer for accurate readings; it was a mixture of 1 part of Meriam 1000 green fluid concentrate into 9 parts of distilled water such that the mixed green indicating fluid had a specific gravity of 1.000.

Another specially made miniature pitot-static probe was used to obtain qualitative velocity and pressure information of the flow in the test section. It was inserted from the top and away from the center of the test section so that the tip of the probe would measure the flow condition across the central diameter. Quantitative measurements were later carried out with the hot wire anemometer.

A copper-constantan thermocouple was also installed in the upstream section of the incoming pipe, in front of the permanent pitot-

static probe, to monitor the temperature of the flow. The thermocouple output signal was fed into a Keithley Model 149 milli-microvoltmeter and a Type R, Beckman Dynograph so that accurate temperature readings and a record could be obtained. These temperature measurements were important during the hot wire calibration and measurement.

2.2. Constant Temperature hot wire anemometer system

Because information on turbulence intensity was needed to provide some insight into the flow stability question, and also due to the divergent-convergent nature of the flow in the test section with curved streamlines, the hot wire was chosen over the standard pitot-static probes for the final quantitative measurements. The flow direction inside the straight pipe, except in the regions immediately behind the turbulence manipulator and the vorticity generator, was well defined. Also the flow in the test section was in the meridional plane (no swirling component). Therefore, as long as the sensing element of the hot wire probe was placed perpendicular to the meridional plane, both the turbulence intensity and flow speed could be measured without too much difficulty.

The instrument used for the final quantitative measurements was a constant temperature hot wire anemometer system made by the Thermo-systems Inc., St. Paul, Minn. The system was of a No. 1050 series consisting of the following components (Ref. 31):

Model 1051-6 monitor and power supply unit

Model 1050 constant temperature anemometer

Model 1052 signal linearizer

Model 1057 signal conditioner

Model 1047 averaging circuit

Model 1055 linearizer

Model 1060 true RMS voltmeter

Model 1015C correlator

Model 1260 straight miniature probe

The straight miniature probe had a main body size of 0.06 inch in diameter and 2 inches in length. Rooted on one end of the probe body were two small gold plated sensor supports. The distance between the tips of the sensor supports was enlarged from 0.06 inch to 0.082 inch. A plain platinum coated tungsten wire of 5 micron in diameter (instead of the TSI supplied sensor element) was stretched over this distance and spot welded at the tip of each support by a special welder equipped with a microscope. The reasons for this modification were to obtain a larger length to diameter ratio for the sensor and also that a damaged sensor could be more conveniently replaced by ourselves in the laboratory. In our case, a length to diameter ratio of 416 was achieved. According to Champagne, Sleicher and Wehrmann (Ref. 32), the correction factor due to sensor length ranged from 0.2 to 0.0 for length to diameter ratios of 200 and greater than 600 respectively. So in this experiment --- under most circumstances, the flow was perpendicular to the sensor --- the effect of the correction factor could be assumed to be very small.

The miniature probe was fitted into either a straight or a bent support tube. Both support tubes were made of 1/8 inch diameter, thick-walled stainless steel tubing. The straight tube, 6.785 inches in

length, was used for flow measurements in both the incoming straight pipe and in a 1.2 inches diameter cylindrical tunnel around the axis of the test section. For measurements in the incoming straight pipe, the support tube was inserted through the probing holes in the wall; for that in the test sectior, the support tube was inserted from the section exit for minimum disturbances. The bent tube, 7.643 inches in length, had a 45° bend 1.383 inches from the end. It was also inserted from section exit into the test section for flow measurements in the areas not reachable by the straight tube. Finally, there was a 12.97 inch long support tube extension. It was made of 3/16 inch diameter, thick-walled stainless steel tubing with a 90° bend 6 inches from the end. This extension was used to join the support tubes to the traversing mechanism for flow measurements in the test section.

Model 1051-6 monitor and power supply unit was a six channel unit. It was capable of supplying steady, regulated power to six hot wire channels. At the same time, it could monitor, on a taut-band panel meter with 1/2% of full scale accuracy, either the bridge output voltage or the linearized output voltage for any of the channel selected. Each model 1050 constant temperature anemometer unit was equipped to handle the input and output signals for a single hot wire channel. It had all the necessary electronic circuits for the bridge, feed back, amplifier, stability control, trim control, temperature and resistance measurement controls, square wave calibrations as well as filters and resistors. For more detailed information on both the model 1051-6 and 1050 units, readers are refered to the TSI Bulletins and Manuals (Refs. 31 and 33).

The Model 1052 signal linearizer was used to linearize the output of a constant temperature anemometer. Calibration curves of hot wire sensors generally would not follow any analytical expression and varies in shape for different sensors and fluids. These non-linear calibration curves were frequently linearized for convenient data analysis. Linearization was accomplished by approximating a curve with a fourth degree polynomial. The four coefficients of the polynomial were determined by using a computer program based on the standard least-square curve fitting technique. Then these four coefficients were set into the linearizer for a calibration run. If the result was good, the linearizer was ready for operation. Detailed information can be found in the TSI Bulletin and Instruction Manual (Refs. 31 and 34).

The Model 1057 signal conditioner was a precision device for making more accurate, controlled measurements with anemometer equipment. signals from either the anemometer, linearizer or other sources could be zero suppressed, filtered or amplified in various manners. The Model 1047 averaging circuit was a low pass filter used for mean flow measurements by averaging a voltage signal with selectable time constants. More information on these two units could be found in (Refs. 31, 33, and 35).

The primary function of the Model 1060 true RMS meter was to measure the true RMS value of a random signal or a turbulence quantity in the flow on a 1/2 % linearity taut-band panel meter. A mean square output was also provided. Now suppose that $f(t)$ is an arbitrary, time dependent function where t represents time. The mean square value of $f(t)$ is:

$$\overline{f^2(t)} = \lim_{t\to\infty} \frac{1}{t} \int_{-t/2}^{t/2} f^2(t)\, dt$$

and the root mean square value is:

$$\sqrt{\overline{f^2(t)}}$$

Normally a transducer is used to convert these to voltage signals for measurement purpose. In actual practice, the mean square meter or root mean square meter is generally coupled with a capacitor so D.C. voltages are not processed. Therefore, the measurement is really for a variance or standard deviation quantity. Variance is

$$\overline{f^2(t)} = \lim_{t\to\infty} \frac{1}{t} \int_{-t/2}^{t/2} \left[ f(t) - \overline{f(t)} \right]^2 dt \qquad (3\text{-}3)$$

and the standard deviation is:

$$\sqrt{\overline{f^2(t)}} = \left\{ \lim_{t\to\infty} \frac{1}{t} \int_{-t/2}^{t/2} \left[ f(t) - \overline{f(t)} \right]^2 dt \right\}^{1/2} \qquad (3\text{-}4)$$

Therefore, the mean square value with the Model 1060 meter is really a measurement of variance while the root mean square value is a standard deviation measurement. The term "true" root mean square meter is often utilized for a meter to distinguish it from the "untrue" meters. The later are essentially rectifier units that give an accurate root mean square reading only on a sine wave input. A "true" RMS meter gives an

accurate RMS reading independent of wave forms as long as the bandwidth and crest factor limitations of the meter are not exceeded. More detailed information can be found in (Refs. 31 and 36). The Model 1055 linearizer was modified to provide readings for the squared values of input signals. Both this unit and the Model 1015C correlator were not used for this experiment.

Three types of voltmeter were used. The first one, a DANA Model 4800 D.C. voltmeter was used to measure the D.C. component of an analog voltage. The anemometer bridge output signals were first routed to the Model 1047 averaging circuit then fed into this voltmeter to monitor the mean bridge output voltages for accurate mean velocity measurements through the use of the calibation curves. The second one was a DISA Model 55D31 D.C. voltmeter with a built-in averaging circuit. Linearized signals from Model 1052 linearizer went first to the Model 1057 signal conditioner for zero suppression, were then fed into this voltmeter to monitor the mean, linearized voltage for direct velocity measurements. The third one was a Keithley Model 149 milli-microvoltmeter. It was used in conjunction with a multi-channel, Beckman Type D Dynograph to simultaneously monitor the thermocouple signals so that a more accurate reading could be obtained when it was needed.

A Tektronix Type 545A oscilloscope with a Type CA plug in unit was used to monitor various fluctuating voltage signals. The stability and frequency response of the anemometer were set and adjusted with the aid of this oscilloscope. Both the mean flow and the turbulence quantities could be monitored and photographed by the scope.

2.3. Hot wire calibrations

The hot wire anemometer has been used for many years as a research tool in fluid mechanics and heat transfer fields. Recently, the application of anemometry has expanded greatly due to better equipments and more interest in details of fluid flow. A hot wire is a small, electrically heated element exposed to a fluid medium for purpose of measuring a property of that medium. Normally, the property being measured is the velocity. Since these elements are sensitive to heat transfer between the element and its environment, temperature and composition changes can also be sensed. Two types of anemometry are in general use, i.e., the constant current and the constant temperature anemometers. The constant current type of anemometer operates by taking the voltage signal caused by wire resistance changes and compensates for frequency lag with a non-linear amplifier while maintaining a constant current through the wire sensor. The constant temperature type of anemometer operates by utilizing a feedback controlled bridge circuit to maintain the sensor at a constant temperature. In this experiment a constant temperature anemometer was used. This type of anemometer has gained rapidly in acceptance recently because of its versatility over the constant current type. The performance characteristics of these anemometers can easily be found in numerous papers (see, for example, Refs. 31, 36 and 37).

The hot wire sensor is a small resistance element which is heated and controlled at an elevated temperature. The amount of electrical energy dissipated from the sensor is a measure of the cooling effect of the fluid flowing past the heated sensor. This cooling effect depends

on both the mass flow and temperature difference between the sensor and the fluid. The relationship, however, is a non-linear one. It could only be expressed in an empirical form. Calibration of a particular sensor in a certain fluid has to be done first before any quantitative measurement can be carried out. Generally, the basic bridge output signal of the anemometer is a voltage which is related to flow approximately as follows:

$$E^2 \sim \left[ A + B(\rho q)^{1/n} \right] (T_s - T_e) \qquad (3\text{-}5)$$

Where A and B are constants depending on fluid properties; $\rho$ is the fluid density; $q$ is the fluid velocity perpendicular to the sensor; $n$ is the exponent that varies with range and fluid (usually about 2); $T_s$ is the sensor operating temperature (hot); and $T_e$ is the fluid or environment temperature (cold). The original work on this relationship was done by King (Ref. 38). In practice, the cylindrical sensors do not follow the King's Law precisely. As shown by Colli and Williams (Ref. 39), the value of $n$ for a very long wire varies from 0.48 for low velocity ranges to 0.51 for higher velocity ranges. For sensors of finite length, the variation in $n$ is greater. Equation (3-5) illustrates the non-linearity of the anemometer output with the fluid density, velocity and temperature. Therefore a careful calibration of the hot wire is required for each particular test condition. It is clear that when fluid density and temperature are kept constant, velocity (both mean and fluctuating quantities) can be found.

Before taking the final quantitative measurements in this

experiment, many test runs as well as hot wire calibrations were carried out to make sure that the whole system was in good running condition. As mentioned previously in section III.1.1.1., the "Entrance section", there was a severe hot wire drift problem due to dust collection on the sensor in the beginning. This problem was later solved by using very high efficiency air filters at the flow inlet. From time to time, the hot wire sensor was cleaned by dipping into a solution of potassium dichromate in sulfuric acid, and then was rinsed in distilled water and acetone. This way a dry and clean sensor could be maintained.

Another common problem associated with the hot wire anemometer operation was due to the change in the environment (fluid) temperature or the change in the actual cold resistance of the sensor. Many methods can be used to correct this problem. However, if the amount of change is small, the problem can be corrected by slightly adjusting the overheat ratio so that the same zero flow bridge voltage is obtained as that in the original calibration. And then a few more calibration points are needed to verify the accuracy of hot wire outputs. This method has been used successfully in general practice with very little sacrifice in accuracy. Good results were reported in a study by Hollasch and Gebhart (Ref. 40) using variable overheat ratios for a hot wire calibration procedure at low velocities in water with variable fluid temperatures. Generally, as long as a large temperature difference is maintained between the fluid and the sensor, errors in the hot wire outputs are small even if the overheat ratio is not adjusted. For example, if the sensor is at 470° F, and the fluid at 70° F, a 4° F change would represent about a 1 % error without any correction.

All hot wire calibrations were performed in the far downstream side of the incoming straight pipe against a standard pitot-static tube and a micromanometer system. Sensors were carefully oriented so that they were normal to the flow. The flow there was well defined and had very low local turbulence intensity (about 1 %). Two hot wires, similar in their characteristics, were used for the final quantitative measurements. The calibration curve for the last hot wire used is shown in Figure 3-9, and the data are shown in Table 2 in the Appendix. In both cases, an overheat ratio of 1.6 were used. The overheat ratio is defined as the ratio of the hot sensor resistance, $R_H$, to that of the cold (unheated) resistance, $R_c$. The relationship between the overheat ratio and the operating temperature is as follows:

$$\frac{R_H}{R_c} = 1 + \alpha_c (T_s - T_e) \qquad (3\text{-}6)$$

Where $\alpha_c$ is the temperature coefficient of resistance for the sensor material referenced to temperature $T_e$. For a tungsten hot wire $\alpha_c$ = 0.00[illegible]/°F. Once an overheat ratio is selected, the hot wire operating temperature can be determined from equation (3-6). In our case, with an overheat ratio of 1.6 and 76°F room temperature, the sensor operating temperature was approximately at 336.9°F. When an accurate determination of sensor operating temperature is required, an actual temperature vs. resistance curve should be plotted for the specific sensor of interest. For most work with anemometers, the sensor is calibrated for flow measurement and knowledge of the exact sensor operating temperature is not important so long as conditions can be repeated. With this large

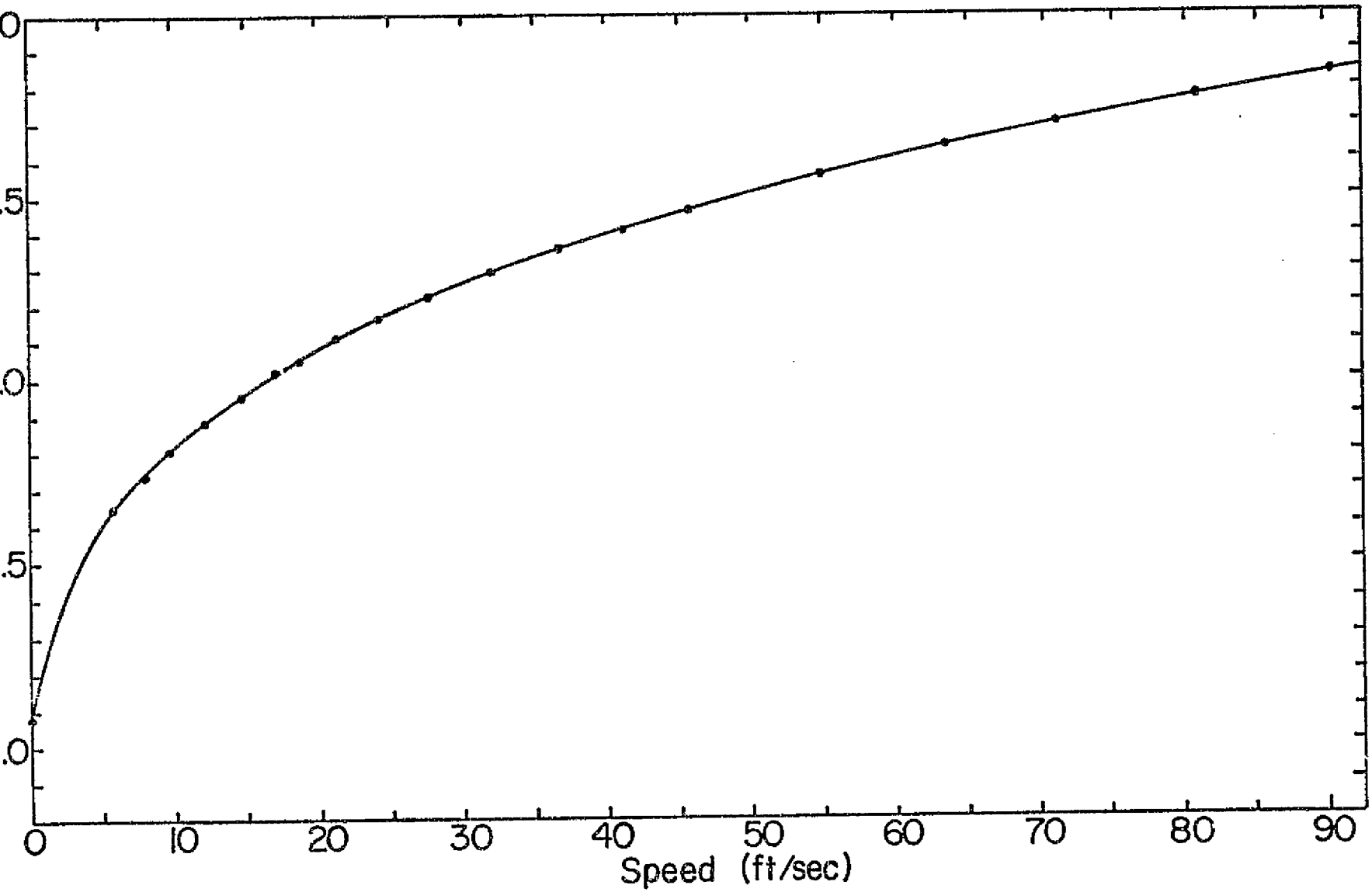


Figure 3-9. Hot wire calibration curve.

temperature difference between the hot sensor and fluid, very good sensitivity was achieved for velocity and turbulence measurements while maintaining a very low sensitivity to small temperature fluctuations.

Based on the final hot wire calibration data, a set of four linearizer coefficients was generated by fitting a fourth degree polynomial to the calibration curve. A computer program based on the standard, least square curve fitting technique was used for this procedure. Two sets of linearizer coefficients were found for the two hot wire sensors used in the final quantitative measurements. The first set, in ascending order, was 0.2071, 3.6907, 2.4803, and 3.6219. The second set was 0.8927, 2.2530, 2.0311, and 4.8222. Then the values of these coefficients were individually set into the potentiometers in the linearizer and a calibration run was carried out to determine the accuracy of the linearizer output. The linearizer calibration curve is shown in Figure 3-10, and the data are shown in Table 3 in the Appendix. During the experiments, output signals from the linearizer were fed both into a RMS meter for turbulence readings and into a signal conditioner then to a voltmeter for direct mean velocity readings. Detailed calibration procedures for the hot wire and linearizer can be found in (Refs. 31, 33 and 34).

## 2.4. Traversing mechanism

Three different traversing units were used in this experiment. To traverse the pitot-static probe which monitored the flow velocity, a traversing unit was mounted on the incoming straight pipe $6\frac{1}{4}$ inches downstream of the flat screen (Figure 3-2B). It had a micrometer to

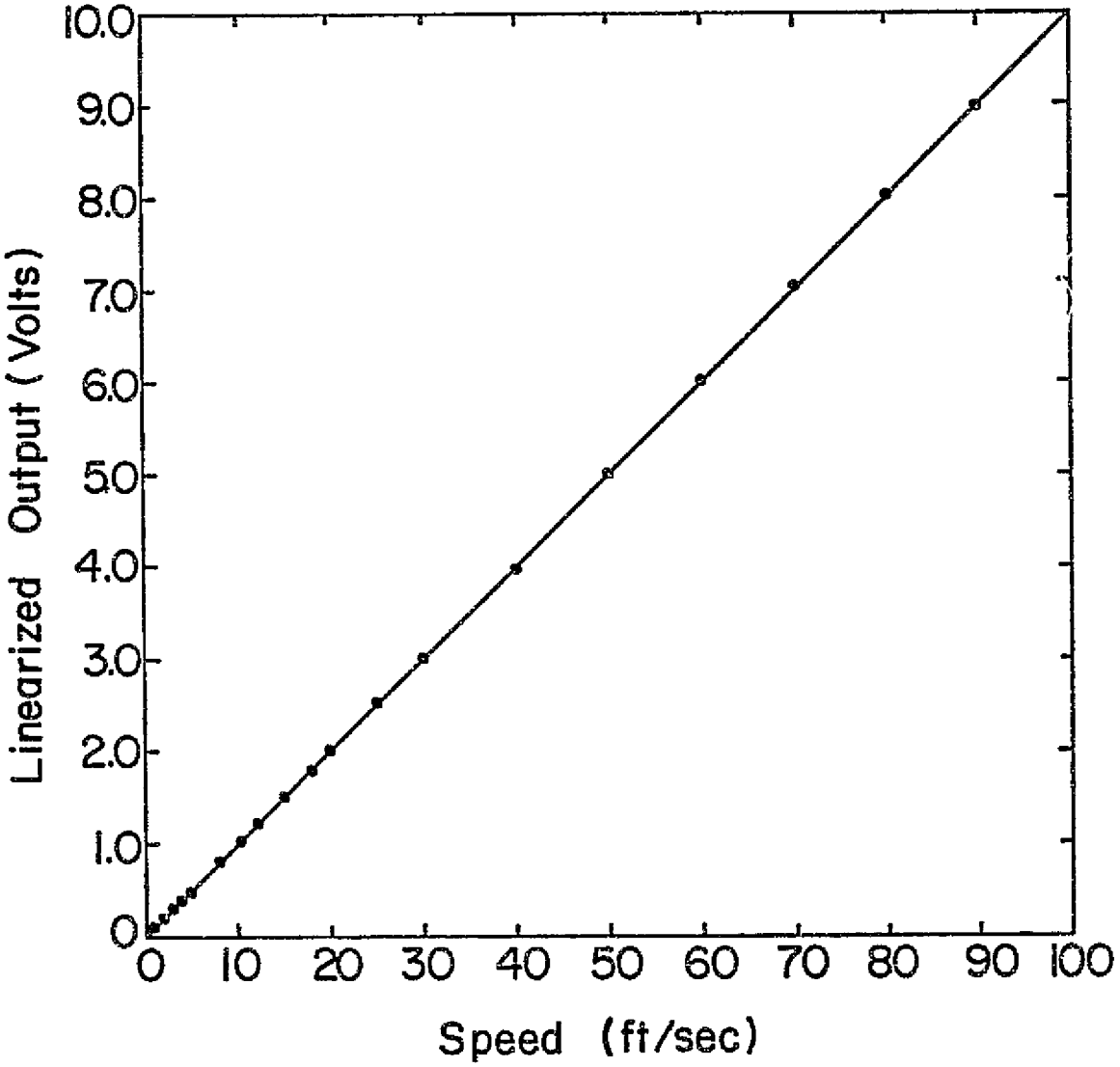


Figure 3-10. Linearizer calibration curve.

control the vertical position to within 0.001 inch and a protractor and a rotary vernier scale to control the yaw angle to within 6 minutes. The probe vertical position and the initial orientation were calibrated with a precision gage using the pipe wall as a reference. Another traversing unit of the similar type, except having a vertical slide and a linear vernier scale instead of the micrometer, was used to traverse the hot wire probe for pipe flow measurements. The unit could be moved from one axial location of the pipe to another without too much difficulty. Vertical position of the hot wire was also calibrated with the same precision gage against the pipe centerline. The yaw angle, however, was calibrated by the hot wire output signal. A maximum bridge output would indicate that the wire was perpendicular to the main flow.

Due to the particular test section configuration, a special traversing mechanism had to be developed to measure the flow inside the test chamber (see Figures 3-2B and 3-8). The chamber wall was machined according to a particular streamline shape which had a 3 inch diameter at the inlet and outlet, and 6.066 inch diameter at the center section. It also had a boundary layer removal section at the entrance. So it was impractical to drill probing holes through the chamber wall, and the hot wire probe had to come into the chamber through the exit. In order for the probe to reach all the places inside the test chamber, two probe support tubes were made (see section III.2.2.2., the section on "Constant temperature hot wire anemometer system"). The straight tube was for flow measurements in a 1.2 inch diameter cylindrical tunnel around the axis of symmetry in the test chamber, and the bent tube was for that of remaining areas. Either of these tubes was fitted into a support tube

extension and fixed onto the traversing slide.

This traversing mechanism consisted of a section of aluminum pipe, two precision Unislide assemblies, pitch control assembly, mounting blocks, bearings, housings, vernier scales, seals, adapters for the hot wire leads, etc. The straight pipe had an inside diameter of 3 inches and a length of 18.875 inches; and it was force fitted with a stainless steel sleeve as the hard bearing surface at each end. The ends of the pipe were then assembled into needle bearings housed in the test section on one side and a diffuser junction block on the other (see Figure 3-5). Both ends were sealed against air leak with rubber rings. A 0.75 inch wide by 13.25 inch long slot was machined out from the top of the pipe and a sealing lip, flush with inside wall surface, was molded into place with a silicone rubber compound. Through a slit in the rubber lip, the support tube extension could traverse back and forth in the pipe without any air leak. A Unislide assembly with a 15 inch travel was fixed to the pipe through a mounting block and plate to control the movement of the probe in the axial direction. Another Unislide assembly with $4\frac{1}{2}$ inch travel was then mounted on the slide of the first assembly to control the radial probe movement. Both Unislide assemblies, made by Velmex, Inc., E. Bloomfield, N. Y., were of the precision lead screw type capable of movements with 0.001 inch of accuracy. Lastly, a pitch control assembly was fastened to the slide of the second Unislide assembly. The support tube extension mounted on this control assembly could pitch with an accuracy of 6 minutes by readings on a set of protractor and a vernier gage.

Therefore, besides providing controlled movements for the probe

in axial, radial and pitching directions, the whole traversing mechanism could rotate in the azimuthal direction with an accuracy of 6 minutes by readings on a yet another set of protractor and vernier gage. Before the final flow measurements, position calibrations were performed for the probe with both the straight and bent support tubes. The test section center and the central cross-sectional plane were used as the bases for this calibration.

3. Some experimental procedures

In the early stage of the experiment, a long pipe with axial probing slot was installed downstream of the vorticity generator in order to find an appropriate length for the second part of the straight pipe. Measurements of the generated velocity profiles were taken at different locations along the axis to locate the position where it would have the desired profile shape without too much boundary layer build-up. This distance was found to be 12 inches downstream of the vorticity generator and then the second part of the straight pipe was fabricated to this length. The boundary layer thickness at this point was 0.3 inch and was subsequently removed before the flow entered the test section.

The opening of the valves in the boundary layer removal pipes were first approximately set with the aid of a tuft probe. A piece of short tuft at the end of a hypodermic tubing was used to indicate the flow pattern and to determine whether the boundary layer was properly removed into the removal section. Final adjustments of the valve opening ($56.25^{\circ}$ to the pipe axis) were done with reference to the quantitative velocity profile measurements at the test section entrance such

that the entering flow would have a negligible boundary layer and a good velocity profile.

During the initial test runs, the tuft probe was inserted into the test chamber from the downstream side by the traversing mechanism for flow visualization. The flow rate in the apparatus was varied from very small to full capacity; and for each flow rate, the tuft probe would traverse the entire test chamber to see whether there was a confinement region in the center, any separation along the wall, or just to find the approximate flow directions. This information was later combined with the initial hot wire test results to select a particular flow rate for detailed quantitative measurements.

The final phase of the experiment was the detailed hot wire measurements of the mean flow velocities and the turbulence intensities in both the pipe and the test section. Because the hot wire was a very delicate and difficult instrument to use, extreme care had to be taken in so far as to its physical conditions as well as to its calibration characteristics. First we must have accurate calibration curves and corresponding sets of good linearizer coefficients. Then at the beginning of each data taking session, these conditions were carefully checked to insure the repeatability of the instruments. Temperature was continuously monitored so that minor adjustment could be made on the hot wire overheat ratio if it was needed. A few points on the calibration curve were tested to make sure that the original calibration was still valid. Flow rate in the apparatus was also constantly watched with the pitot-static probe and micromanometer system, while the velocity profile at the test section was checked by hot wire measurements. After all

these steps were performed then the final measurements were carried out.

4. Stability of the generated velocity profile

As stated in section III.1.1.2. on "Vorticity generator", the velocity profile generated in the incoming pipe was of a parabolic form specified by equation (3-1). It consisted only of axial component yet had the same vorticity distribution as that in the theoretical model, i.e., $\omega_\theta = -ar$. The velocity had a larger magnitude further away from the axis. However, due to the no slip condition at the pipe wall, a thin boundary layer was built up. This would cause a inflection point to appear on the generated velocity profile (see Figure 3-4). Thus a question would be raised: due to the particular characteristics of this velocity profile, would inviscid instability occur in the flow?

The inviscid instability problem for the flow in a circular pipe had previously been studied. As shown by Shen (Ref. 41), in the case of an axially symmetric basic flow with rotationally symmetric disturbances, a stability criterion was established. Consider the case:

$$\overline{V} = \overline{W} = 0 \; ; \quad \overline{u} = \overline{u}(r)$$

Where $\overline{u}$, $\overline{V}$, and $\overline{W}$ are the velocity components of the basic, steady flow. Then inviscid instability would occur only if, within the fluid,

$$\frac{d^2\overline{u}}{dr^2} - \frac{1}{r}\frac{d\overline{u}}{dr} = 0 \tag{3-7}$$

Consequently, this term $\left[\overline{u}'' - (\overline{u}'/r)\right]$ played the part of $\overline{u}''$ in the

two-dimensional case. So a velocity profile with a point of inflection was no longer necessarily unstable, at least with respect to rotationally symmetric disturbances, in the inviscid limit.

In order to answer the inviscid instability question about the flow in our incoming straight pipe, equation (3-7) was used as a criterion for the test. However, before this test could be performed, the velocity profile, as a function of $r$ had to be found first. This function could be easily constructed such that the function would represent the velocity profile in the inviscid core as specified by equation (3-1) and represent the boundary layer profile adjacent to the pipe wall.

Assuming that the velocity inside the boundary layer slowed down exponentially from its maximum value of $u_m$ at the boundary layer edge to zero at the wall. As an approximation, a function of the following form was used.

$$\frac{u}{u_m} = \left[ 1 - e^{-Re^{0.25}\eta^3} \right] \tag{3-8}$$

$$\eta = \frac{R_p - r}{\delta} \quad , \qquad Re = \frac{uD}{\nu}$$

Where $R_p$ was the inside radius of the pipe, $\delta$ the boundary layer thickness, $Re$ the Reynolds number based on pipe diameter $D$, and $\nu$ the kinematic viscosity of the fluid. The boundary conditions for this function were (1) zero velocity at the wall, (2) maximum velocity at the boundary layer edge to match that of the inviscid core, (3) vanishing shear at the boundary layer edge.

It was a simple matter to check whether equation (3-8) met all

these three boundary conditions.

$$\frac{d}{d\eta}\left(\frac{u}{u_m}\right) = -e^{-Re^{0.25}\eta^3}\left(-3Re^{0.25}\eta^2\right)$$

at $\eta = 0$: $u/u_m = 0$

at $\eta = 1$: $u/u_m = 1 - \frac{1}{\sqrt[4]{Re}} \approx 1$ for large Re

$$\frac{d}{d\eta}\left(\frac{u}{u_m}\right) = 3\sqrt[4]{Re}\,/\,e^{\sqrt[4]{Re}} \approx 0 \text{ for large Re}$$

So equation (3-8) satisfied all the boundary conditions. It then could be combined with the velocity profile in the inviscid core to provide a composite velocity function valid for the whole cross-section. Equation (3-1) was simply multiplied by equation (3-8) to become:

$$\overline{u}(r) = \left[1 - e^{-Re^{0.25}\left(\frac{R_p - r}{\delta}\right)^3}\right]\left(\frac{a}{2}r^2 + u_0\right) \qquad (3\text{-}9)$$

Numerical evaluation of this profile for a Reynolds number of 150,000 in our experiment showed that the parabolic profile in the inviscid core was not disturbed by the modification in equation (3-9) and it had a very thin boundary layer adjacent to the pipe wall.

Now the criterion specified by equation (3-7) could be applied to the velocity profile of equation (3-9) to determine whether inviscid instability would occur in the pipe.

$$\bar{u}'(r) = \left[-e^{-Re^{0.25}\left(\frac{R_p - r}{\delta}\right)^3}\right]\left[\frac{3}{\delta}\left(\frac{R_p - r}{\delta}\right)^2 Re^{0.25}\right]\left(\frac{a}{2}r^2 + u_o\right) + \left[1 - e^{-Re^{0.25}\left(\frac{R_p - r}{\delta}\right)^3}\right]$$

$$\bar{u}''(r) = \left[-e^{-Re^{0.25}\left(\frac{R_p - r}{\delta}\right)^3}\right]\left\{\left[\frac{9}{\delta^2}\left(\frac{R_p - r}{\delta}\right)^4 Re^{0.5}\right]\left(\frac{a}{2}r^2 + u_o\right) - \left[\frac{6}{\delta^2}\left(\frac{R_p - r}{\delta}\right) Re^{0.25}\right]\left(\frac{a}{2}r^2 + u_o\right) + \left[\frac{3}{\delta}\left(\frac{R_p - r}{\delta}\right) Re^{0.25}\right](ar)\right\} - \left[1 - e^{-Re^{0.25}\left(\frac{R_p - r}{\delta}\right)^3}\right]a$$

If there was to be any inviscid instability, equation (3-7) must be satisfied, i.e.:

$$\bar{u}'' - \frac{\bar{u}'}{r} = 0 \quad , \quad or$$

$$(3a\,Re^{0.25})r^7 - (12a\,R_p\,Re^{0.25})r^6 + 6Re^{0.25}(3aR_p^2 + u_o)r^5 - (12\,Re^{0.25}a\,R_p^3 + 24Re^{0.25}R_p\,u_o - 5a\delta^3)r^4 + (3Re^{0.25}aR_p^4 + 36\,Re^{0.25}u_o R_p^2 - 8aR_p\delta^3)r^3 - (24Re^{0.25}u_o R_p^3 - 2u_o\delta^3 - 3aR_p^2\delta^3)r^2 + (6Re^{0.25}u_o R_p^4)r - u_o R^2\delta^3 = 0$$

To solve for this polynomial equation, a standard IBM 'POLRT' program was used. No real solution could be found, which meant that equation (3-7) could not be satisfied by any real values of $r$ inside the pipe. Therefore, inviscid instability would not occur anywhere inside the pipe

and the flow in the pipe was either stable or neutrally stable to any rotationally symmetric disturbances. Later quantitative measurements by the hot wire also confirmed that the flow inside the pipe was a very stable one.

# CHAPTER IV

# RESULTS

In order to see the unique phenomenon of this experiment, test runs were conducted for two different conditions. First, flow visualization with a tuft probe and hot wire measurements were performed without the vorticity generator in the incoming straight pipe to acquire some base information about the flow without the prescribed vorticity distribution. Then the vorticity generator was installed in the pipe and the same procedures were repeated. Finally detailed quantitative measurements were made. These results are presented in the following two sections. In the last section, mass flow rates at both the entrance and the central plane of the test section were calculated from the measured velocity profiles to verify the existence of a self-confined region as described in the second section of this chapter. A pitot-static probe inserted into the test chamber through the central slot and traversed along the vertical axis confirmed that the static pressure did increase from the center outwardly toward the wall as mentioned in Chapter II. However, no detailed pressure measurements inside the test chamber were made.

## 1. Visualization

A tuft probe, as described in the last chapter, was used to visualize the flow inside the test section. It was inserted into the test chamber through the central slot and traversed up and down the vertical axis. For the test condition without the vorticity generator,

flow rate was varied through the full range by changing the opening of the exit valve at the blower outlet. For all the flow rates, no self-confined region was indicated. At low flow rate, owing to the small amount of stiffness in the tuft and very low fluid speed, the tuft probe was not a good flow indicator. Therefore, a higher flow rate was used in the test.

Then by using the precision traversing mechanism, another tuft probe was inserted into the test chamber from the chamber exit to probe the entire region. Flow separation was seen to occur at the diverging wall almost immediately behind the entrance. A large, annular recirculating cell formed adjacent to the wall stretching from the separation point to a point about three quarters of the chamber length. The flow in the central portion of the chamber was similar to a straight jet issued from the entrance. There was no self-confined region at the central portion of the chamber. Figure 4-1 shows the general flow pattern inside the test chamber as indicated by the tuft when there is no vorticity generator in the straight pipe to produce the proper vorticity distribution.

The same procedures as those stated above were repeated for the test condition with vorticity generator installed in the straight pipe. For all the higher flow rates (in order to see the tuft movements), no flow separation could be seen anywhere along the chamber wall, and there was no recirculating cell adjacent to the wall. The flow was very orderly and the fluctuations were very small. In the central portion of the test chamber, a distinct region approximately the size as prescribed by the theory existed. Inside this region, very low flow speed

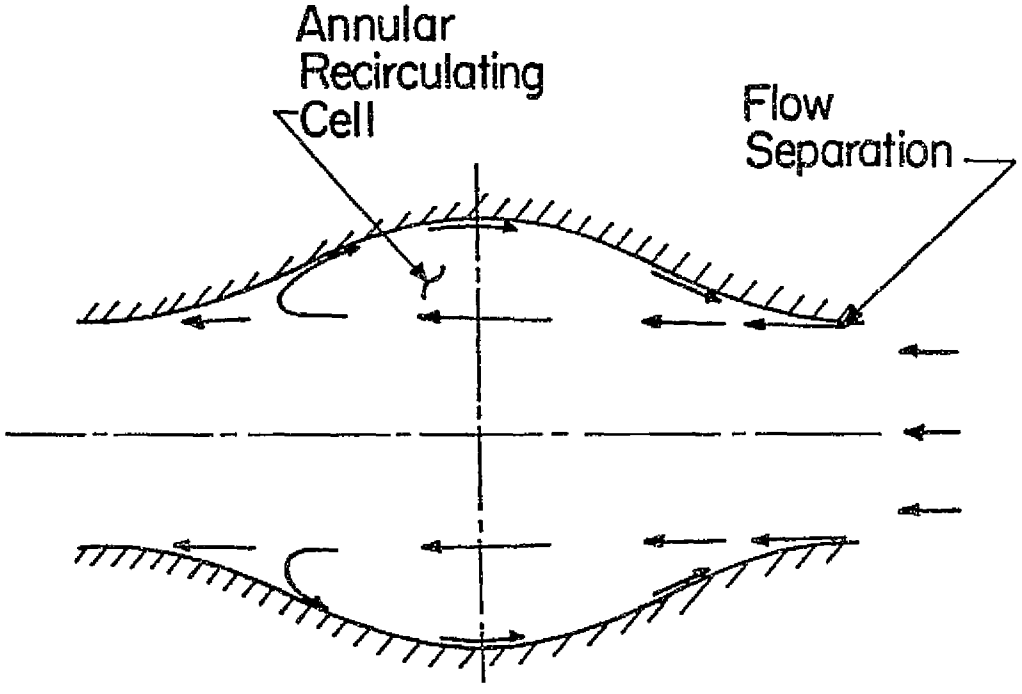


Figure 4-1. Flow pattern inside the test chamber as indicated by the tuft probe (without vorticity generator).

in the reversed flow direction (toward upstream) was indicated. Flow patterns in this case are shown in the figures of the next section as confirmed by the hot wire measurements.

Flow visualization by smoke was attempted, but no good result was obtained. A small cigar smoke generator was used to send smoke through a tube directly into the self-confined region from chamber exit. The amount of smoke was not large and dense enough to give any good flow visualization. Then a sky diver's smoke flare (Kilgore smoke signal) was used to send dense orange smoke into the flow apparatus from the inlet chamber. This did not work well either because the flare burning time was very short and the amount as well as the way to channel the smoke could not be controlled. For good flow visualization, a well designed, controllable smoke generator must be used along with a

proper ventilation system for the flow apparatus.

2. Quantitative results

The quantitative measurements were performed with a constant temperature anemometer system described in the last chapter. Preliminary measurements inside the test chamber were carried out for the two test conditions both with and without the vorticity generator in the straight pipe. When there was no vorticity generator, the hot wire measurements confirmed the general flow patterns as visualized by the tuft probe and shown in Figure 4-1. At the point of separation, large turbulence levels as well as base fluctuations were detected. There were also large fluctuations along the interface of the jet and the recirculating cell. Approximately one quarter of the chamber length downstream from the entrance, the flow became increasingly chaotic (about 15--20 % absolute turbulence intensity) then quieted down a little near the exit (about 14 % absolute turbulence intensity). After the vorticity generator was installed, the flow became very orderly at the former separation point with very small turbulence level. In the chamber center, a region of very low speed was found having about the same size and location as that indicated by the tuft probe. The situations were approximately the same for different flow rates. For the final detailed measurements, a higher flow rate was chosen so that more accurate hot wire readings could be obtained.

2.1. Incoming straight pipe

During the entire data taking period, flow rate was carefully

watched by the upstream pitot-static tube and micromanometer system to insure identical test conditions at all times. Fluid temperature was monitored by the thermocouple, chart recorder and a milli-micro voltmeter. Hot wire and linearizer calibrations were also checked every day for accuracy.

Results of the hot wire measurements in the straight pipe are presented in the graphs of Figures 4-2A & B, and 4-3A, B & C. In Figures 4-2A & B, local average fluid speeds (Q in ft/sec), and local turbulence intensities ($q'/Q$ in %) at different axial locations are plotted against pipe radius. For the test condition without vorticity generator (V.G.), local average fluid speeds are represented by thin solid lines and the local turbulence intensities by thin dashed lines. For the test condition with vorticity generator, the local average fluid speeds are represented by heavy solid lines, and the local turbulence intensities by heavy dashed lines.

From these results, one can see that the local turbulence intensity decreases quite rapidly to 1--2 % in a few pipe diameters downstream of either the flat screen or the vorticity generator. Without the vorticity generator, the speed profile at the location of $5\frac{1}{2}$ pipe diameters downstream of the flat screen is reasonably smooth over the central portion and has a boundary layer of 0.37 inch thick adjacent to the wall. After the vorticity generator is installed, it can be seen that the speed profile is inverted to have a higher speed at a larger radius and small speed at the center, and at the same time the boundary layer becomes thinner. Turbulence intensity is increased to 3--4 %. Further down the pipe, the inverted speed profile becomes smoother; the

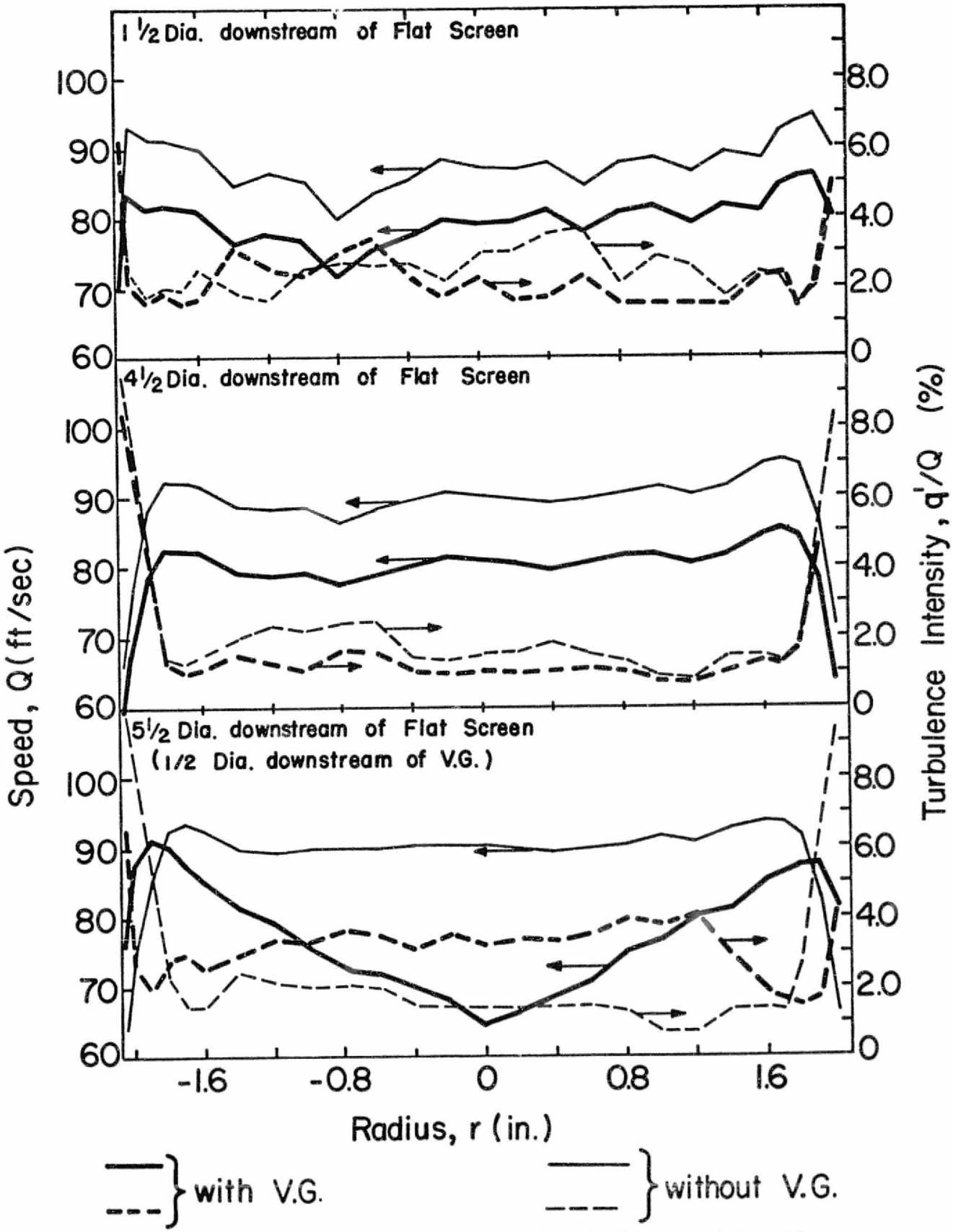


Figure 4-2A. Local average speed & turbulence intensity

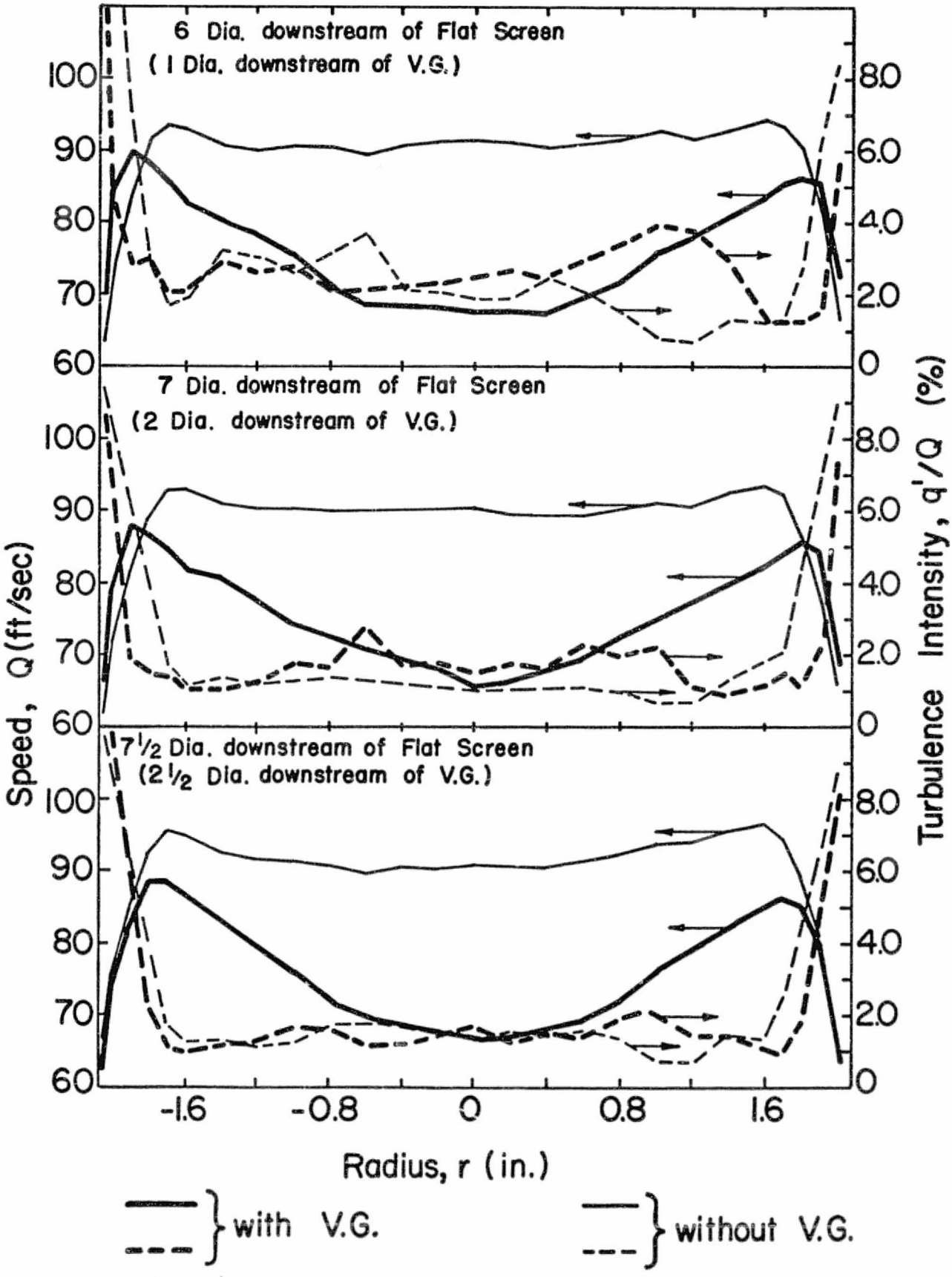


Figure 4-2B. Local average speed & turbulence intensity profiles in the straight pipe.

thickness of the boundary layer increases again; and the turbulence intensity dies down to 1--2 % at about half a pipe diameter upstream to the test section entrance. The boundary layer is subsequently removed and the flow entering the test section has a speed profile similar to the one shown in the last graph of Figure 4-2B (central portion of the heavy solid line on the last graph -- $2\frac{1}{2}$ diameter downstream of V.G.). The actual speed profile at the test section entrance are presented in the next section.

In order to find out the axisymmetric characteristics of the generated velocity profile, hot wire measurements of the local average velocities and turbulence intensities were made at an axial location one diameter downstream of the vorticity generator. The hot wire sensor was placed at a certain radial location and readings were taken while the vorticity generator was being rotated through twelve different azimuthal angles (30° apart). Then the sensor was moved to a new radial location, and the same procedure was repeated. In Figures 4-3A, B & C, for various radial locations, graphs are plotted with axial velocity deviation ($Q/Q_r$ in %), along the axis of ordinates and azimuthal angles of the vorticity generator ( $\theta$ in degree), along the axis of abscissa. Where Q is the local average speed and $Q_r$ is the average speed of twelve Q values at the same radius. It can be seen that the maximum axial velocity deviations from $Q_r$ are +3.9 % and - 4.8 %. In view of the fact that these data are taken only one pipe diameter downstream of the vorticity generator, the generated velocity profile can be considered to have a reasonably good axisymmetric property. Turbulence intensity along radial direction is generally lower at the center, increases, decreases

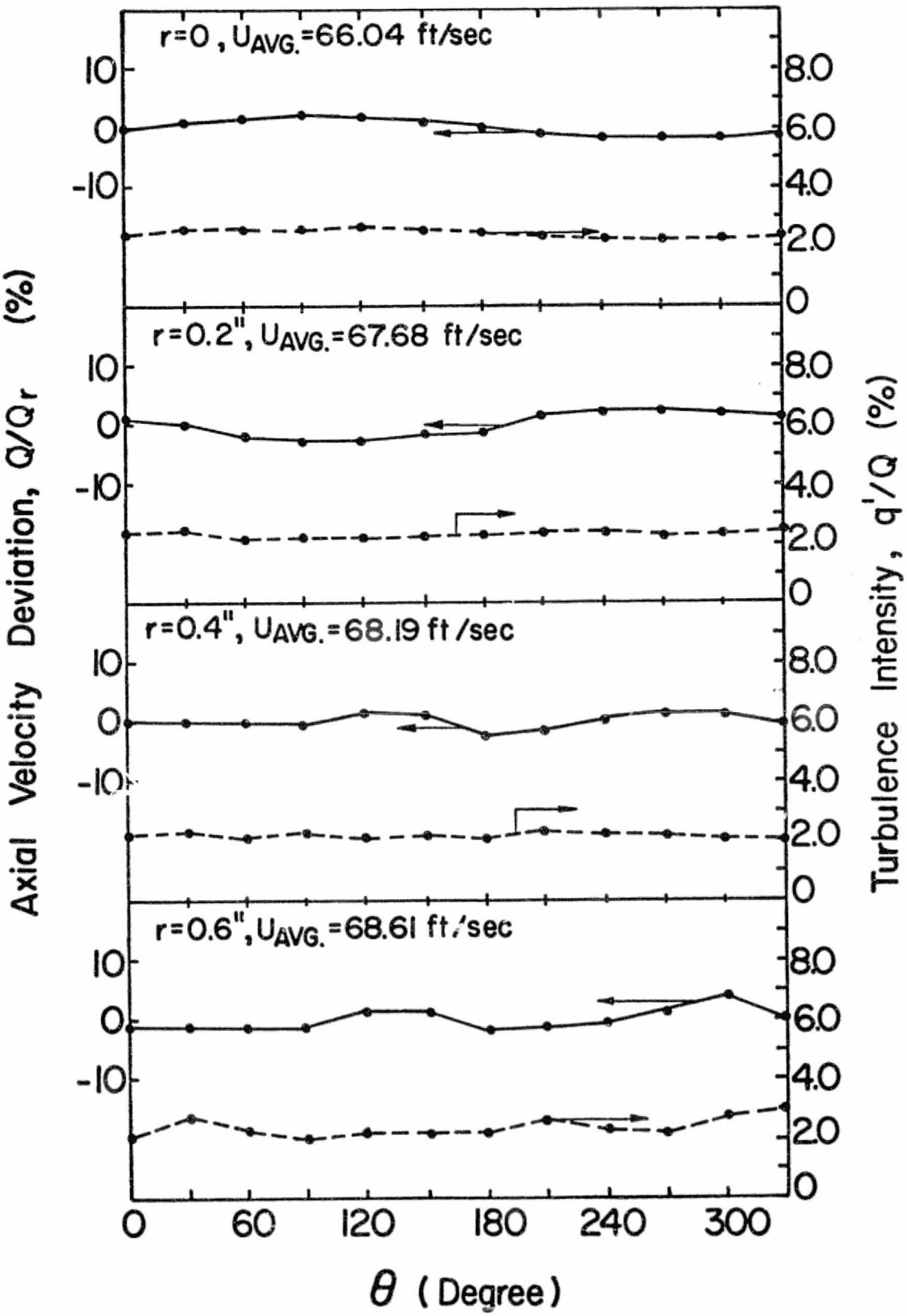


Figure 4-3A. Azimuthal distribution of velocity & turbulence intensity profiles in the straight pipe (6 dia. downstream of flat screen and 1 dia. downstream of the vorticity generator).

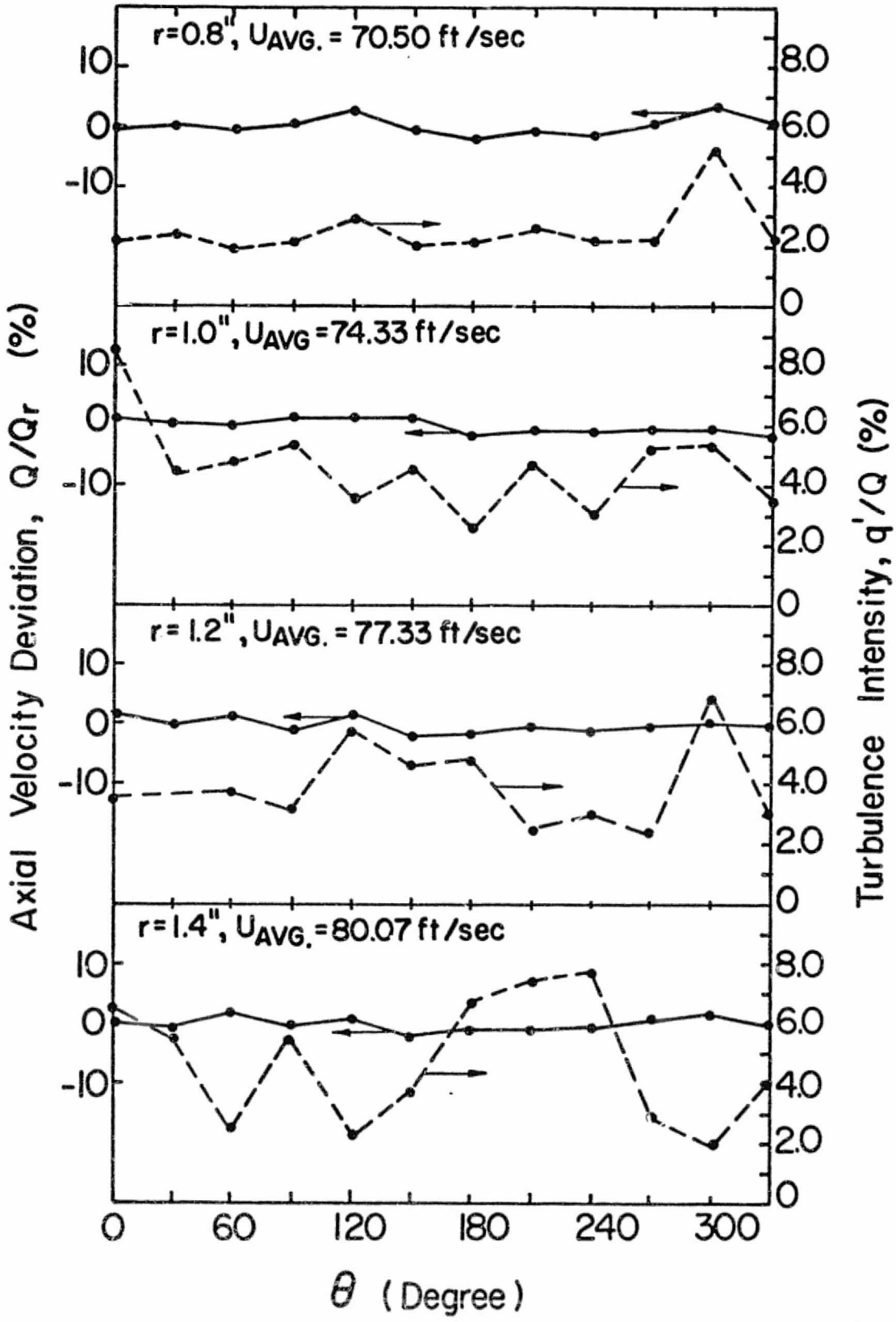


Figure 4-3B. Azimuthal distribution of velocity & turbulence intensity profiles in the straight pipe (6 dia. downstream of flat screen and 1 dia. downstream of the vorticity generator).

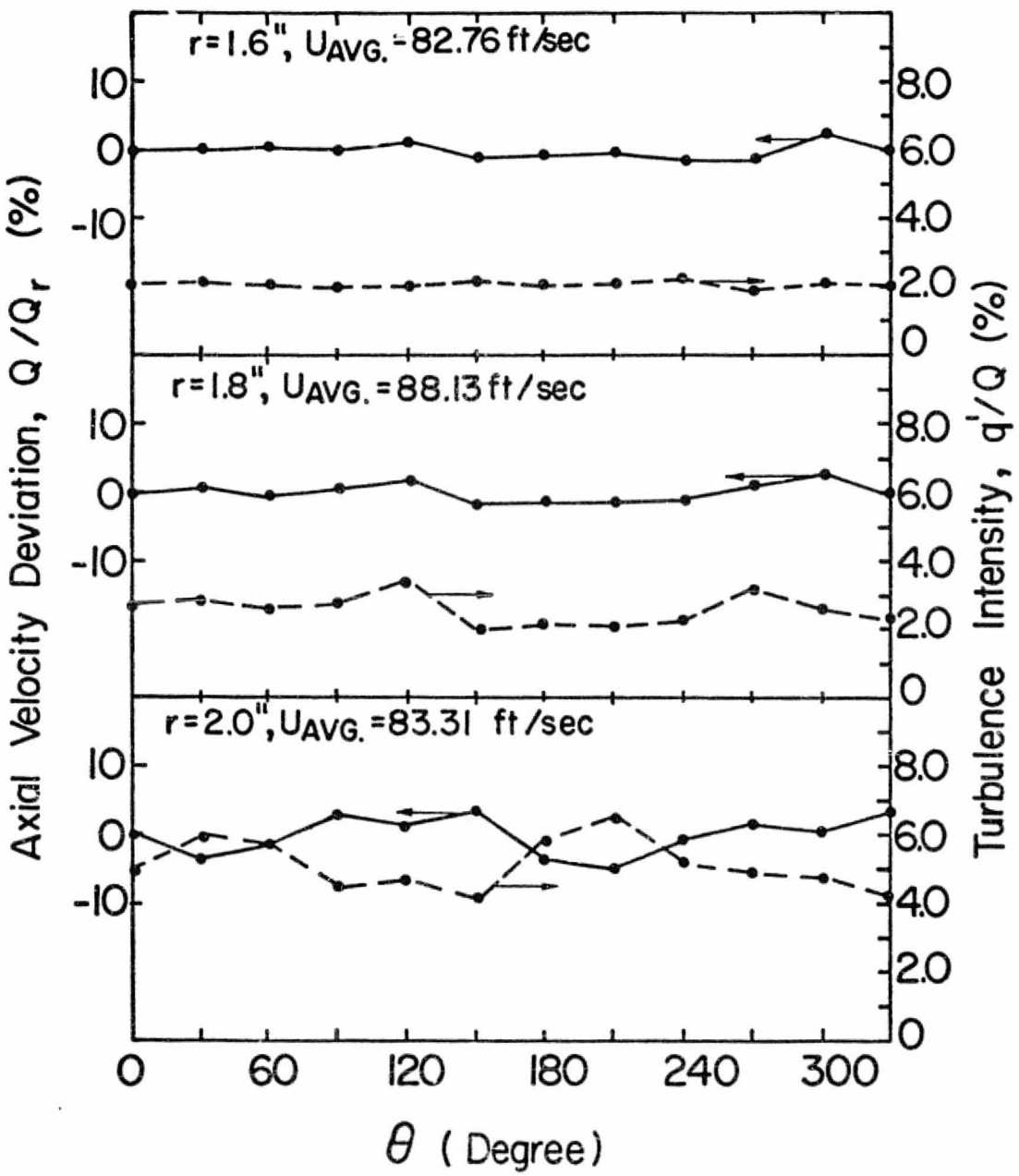


Figure 4-3C. Azimuthal distribution of velocity & turbulence intensity profiles in the straight pipe (6 dia. downstream of flat screen and 1 dia. downstream of the vorticity generator).

and finally increases somewhat close to the wall. This particular situation is directly related to the special properties of the vorticity generator. For different vorticity generators, turbulence characteristics are different. Immediately behind the shaped gauze screen, a large amount of flow is being diverted toward the outer region of the pipe and is subsequently forced to make an adjustment in its flow direction. This creates strong shearing effects at the middle range of the radius producing higher turbulence intensities at the same time. Further downstream, the turbulence levels are reduced as can be seen on Figure 4-2B.

Figures 4-4A and B are the oscilloscope pictures of some RMS signals of the linearized bridge output at three different axial locations on the axis of the straight pipe. These RMS signals represent the fluctuating velocity components perpendicular to the hot wire sensor. Two conditions are shown here, one with the vorticity generator installed in the pipe and the other without. It can be seen that the RMS values increase right behind the vorticity generator and decrease further down the pipe. Except for the magnitude differences, these signal traces appear to have the same general turbulence characteristics. Magnitudes of each trace are quite uniform, and the frequencies are all quite high (estimated at about 1200 -- 2000 Hz.).

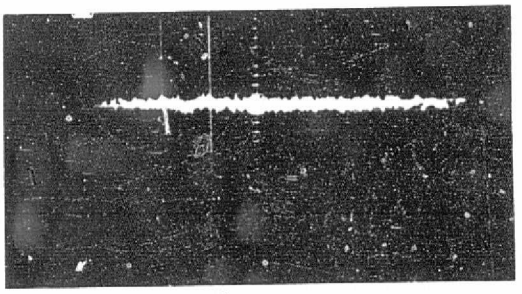

(a)

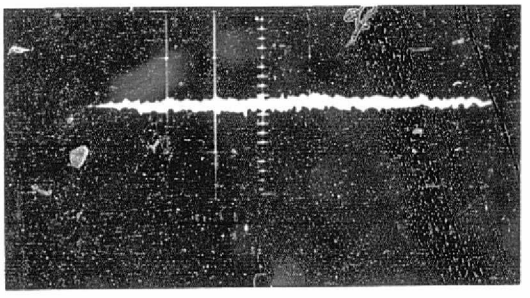

Q = 93.25 ft/sec
$RMS_L$ = 0.88 ft/sec

Q = 82.50 ft/sec
$RMS_L$ = 0.797 ft/sec
($\frac{1}{2}$ dia. upstream of V. G.)

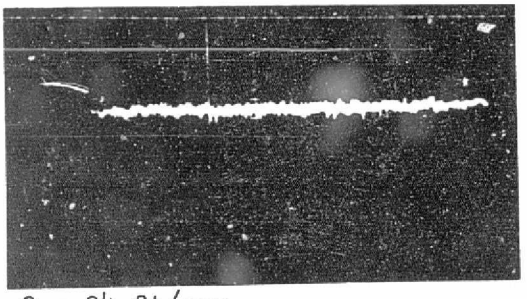

(b)

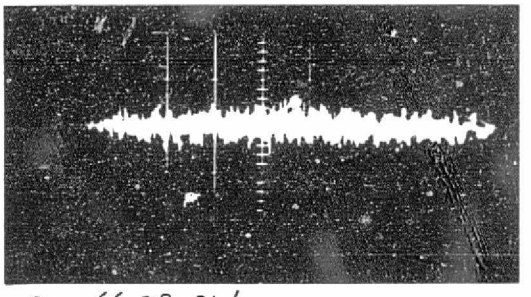

Q = 94 ft/sec
$RMS_L$ = 0.745 ft/sec

Q = 66.78 ft/sec
$RMS_L$ = 2.35 ft/sec
($\frac{1}{2}$ dia. downstream of V. G.)

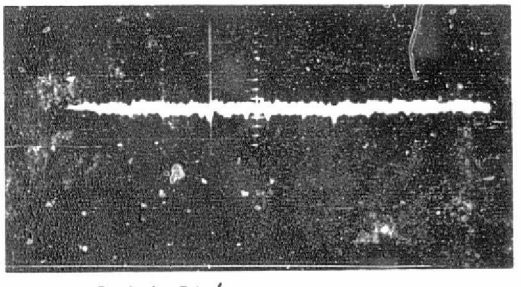

(c)

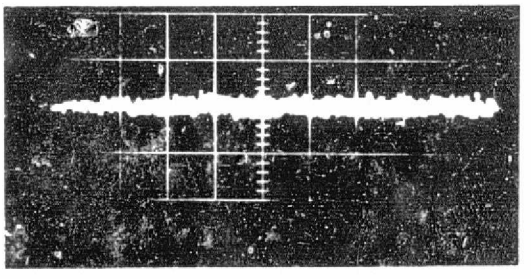

Q = 93.75 ft/sec
$RMS_L$ = 0.72 ft/sec

Q = 69 ft/sec
$RMS_L$ = 0.98 ft/sec
($2\frac{1}{2}$ dia. downstream of V. G.)

(4A) Without vorticity generator

(4B) With vorticity generator

Figure 4-4. RMS signals of the linearized bridge output at three different axial locations on the axis of the straight pipe.
(Scale: 1V/Cm--Vertical; 10 Milli Sec/Cm--Horizontal)
(a) 4 dia. downstream of flat screen
(b) 5 dia. downstream of flat screen
(c) 7 dia. downstream of flat screen

2.2. Test chamber

The detailed hot wire measurements inside the test chamber were conducted only for one flow rate and with the vorticity generator installed in the incoming straight pipe. Results for fluid speed and turbulence intensity measurements are summarized in the next ten figures (Figures 4-5, 4-6A, B, and C; 4-7A, B, and C; and 4-8A, B, and C). They are organized into three sets; each contains the information for one meridional plane. Therefore the three sets represent the three meridional planes of $0^\circ$ - $180^\circ$, $60^\circ$ - $240^\circ$, and $120^\circ$ - $300^\circ$ respectively. Each set represents the normalized speed profiles ($Q/Q_{ref}$), the local turbulence intensities ($q'/Q$) and the absolute turbulence intensities ($q'/Q_{ref}$). Where $Q_{ref}$ is the reference speed at the chamber entrance $x$ = +5.2 inches and on the axis $r$ = 0.0 inch.

Numerical data for these graphs are included in Table 4 of the Appendix. Actual measurements were carried out for stations along the axis in 0.5 inch increments and generally for 0.2 inch radial increments. For briefness and clarity, only the data on alternate axial cross-sections are presented here. The ones not presented show the same basic characteristics and trends. At locations $x$ = +1.75 inches and $x$ = -1.25 inches along the axis, hot wire measurements indicated two minimum average speeds of 1.58 ft/sec and 3.47 ft/sec respectively. Therefore, detailed measurements were taken for these two cross-sections also.

In Figure 4-5, each circular dot represents a single data point where hot wire measurement has been taken. Numerical values for these data points are shown in Table 4 of the Appendix. It can be seen that the velocity has very small magnitude in the central region of the test

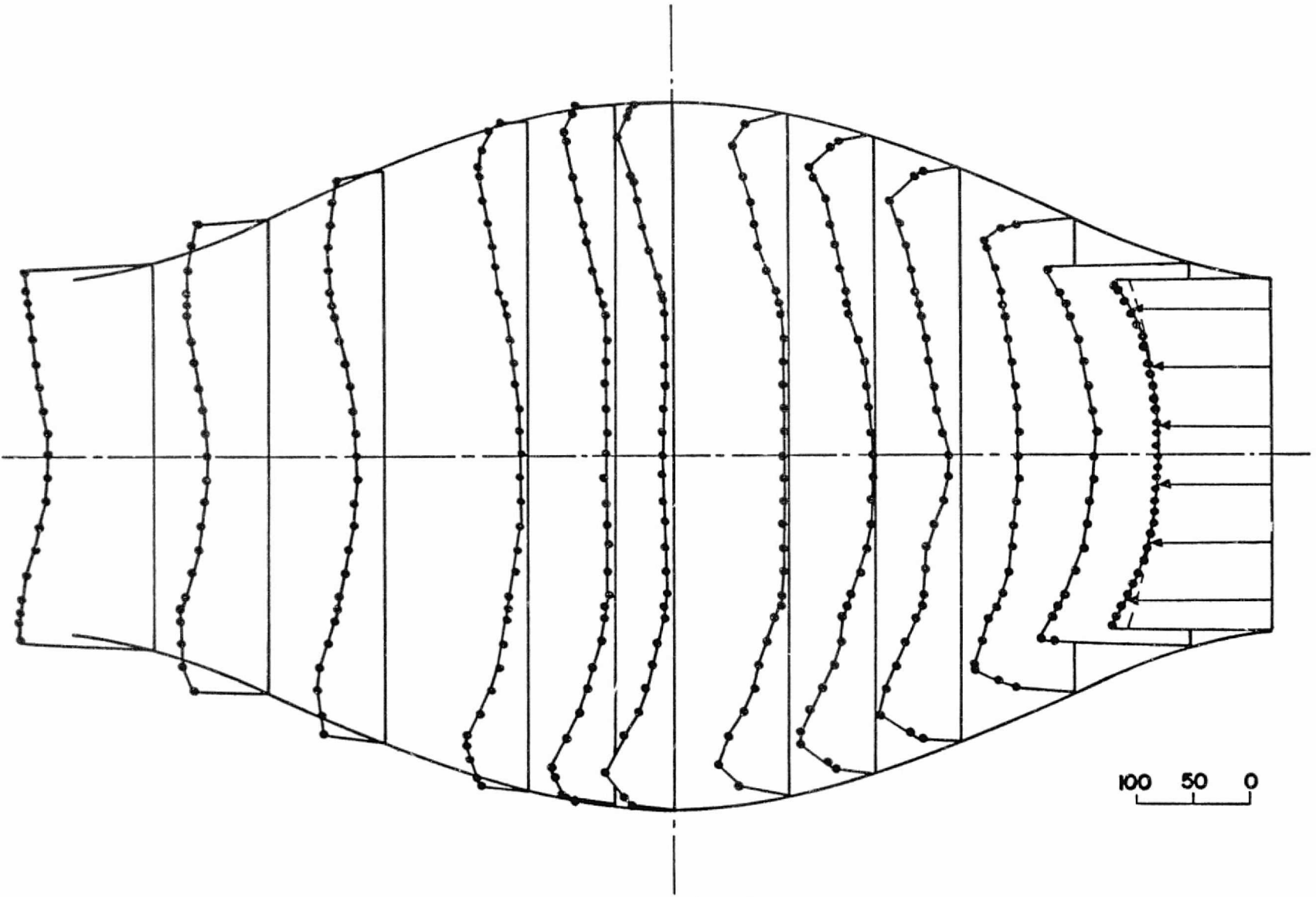


Figure 4-5. Normalized speed profiles ($Q/Q_{ref}$) in %, in the test chamber, 0°- 180° plane. Data points inside the confinement region are presented only as an indication for their possible maximum values.

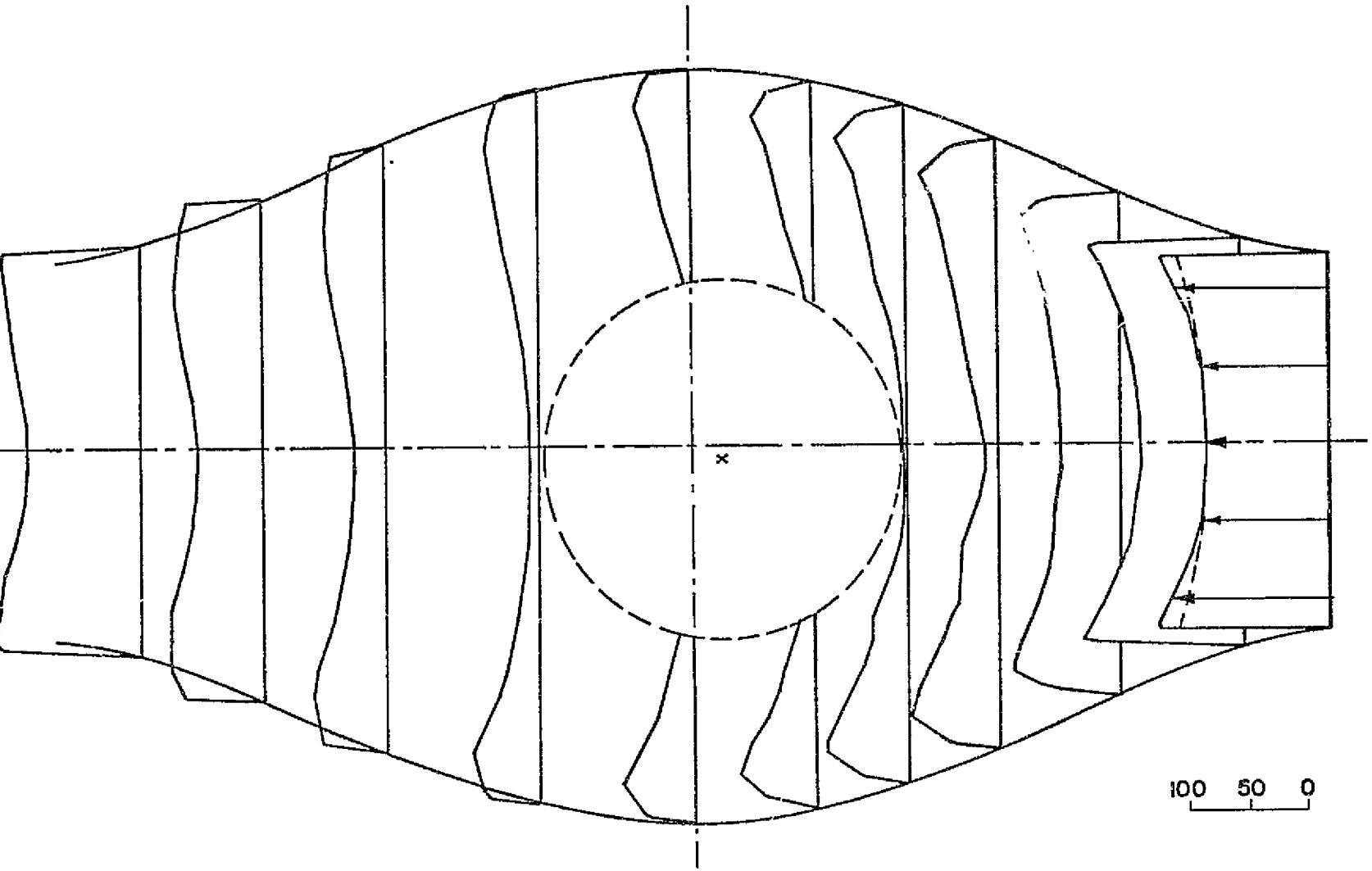


Figure 4-6A. Normalized speed profiles ($Q/Q_{ref}$) in %, in the test chamber, 0° - 180° plane.

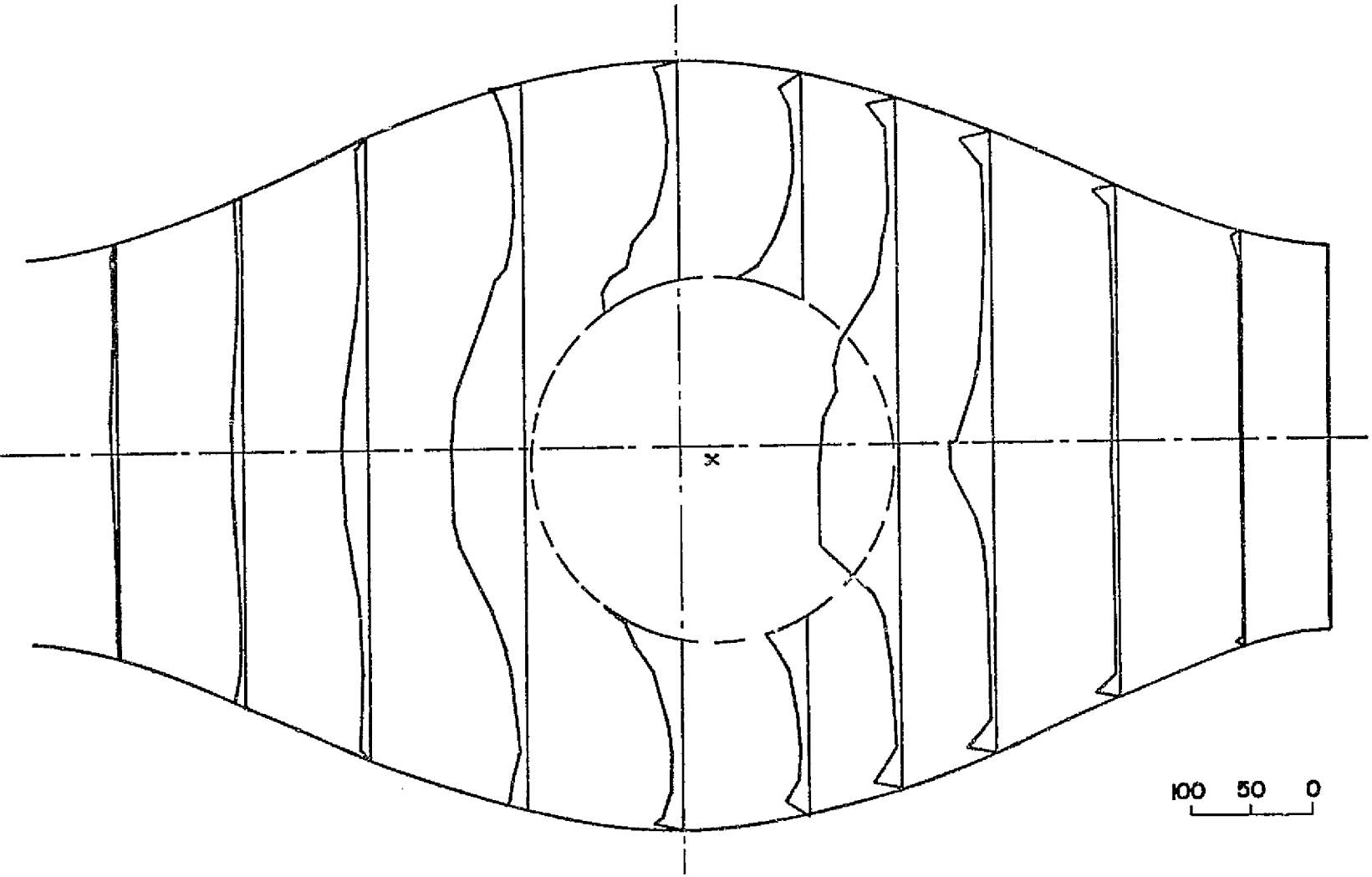


Figure 4-6B. Local turbulence intensity ($\sqrt{}/Q$) in %, in the test chamber, 0°- 180° plane.

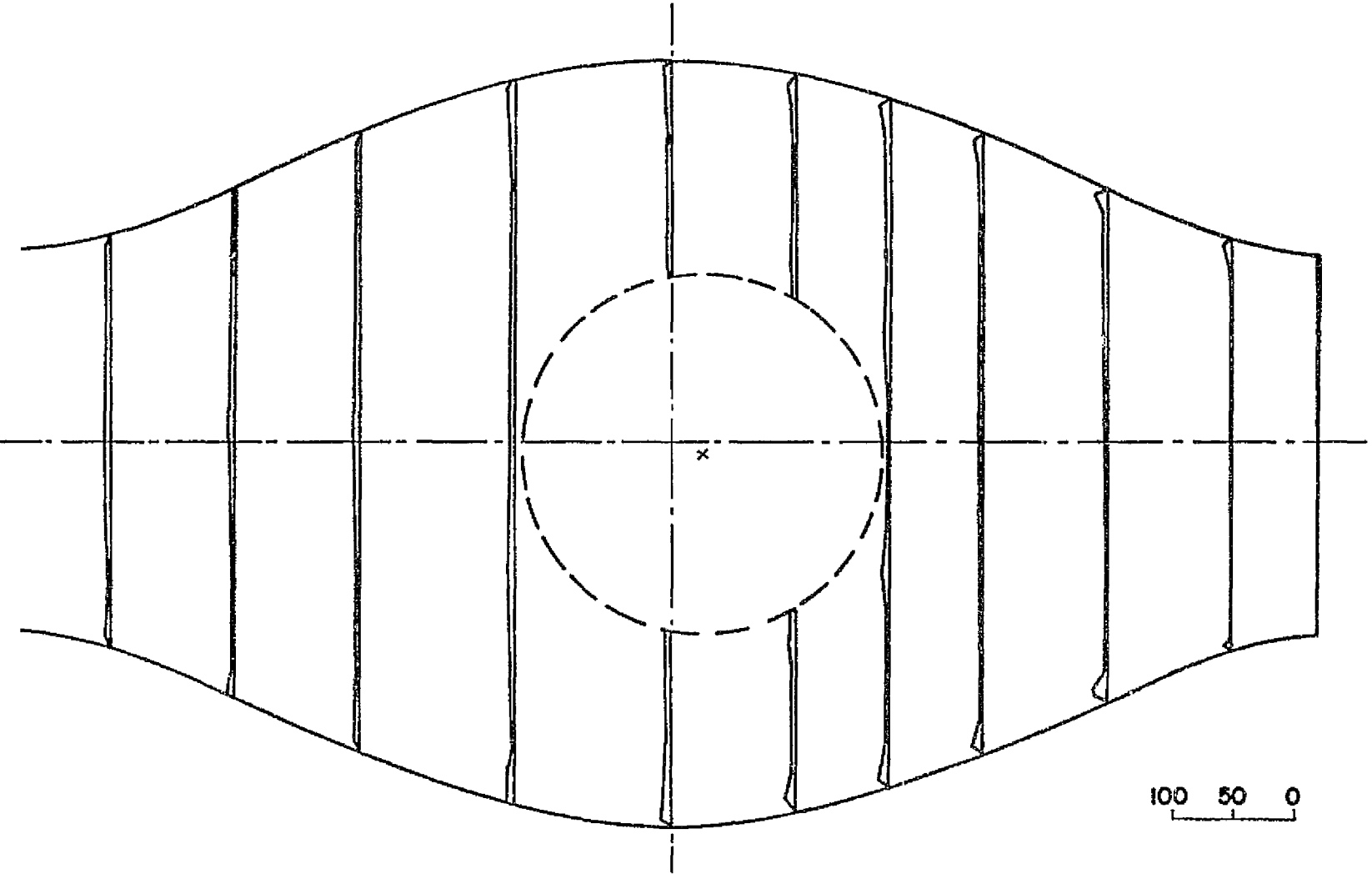


Figure 4-6C. Absolute turbulence intensity ($q'/Q_{ref}$) in %, in the test chamber, 0° - 180° plane.

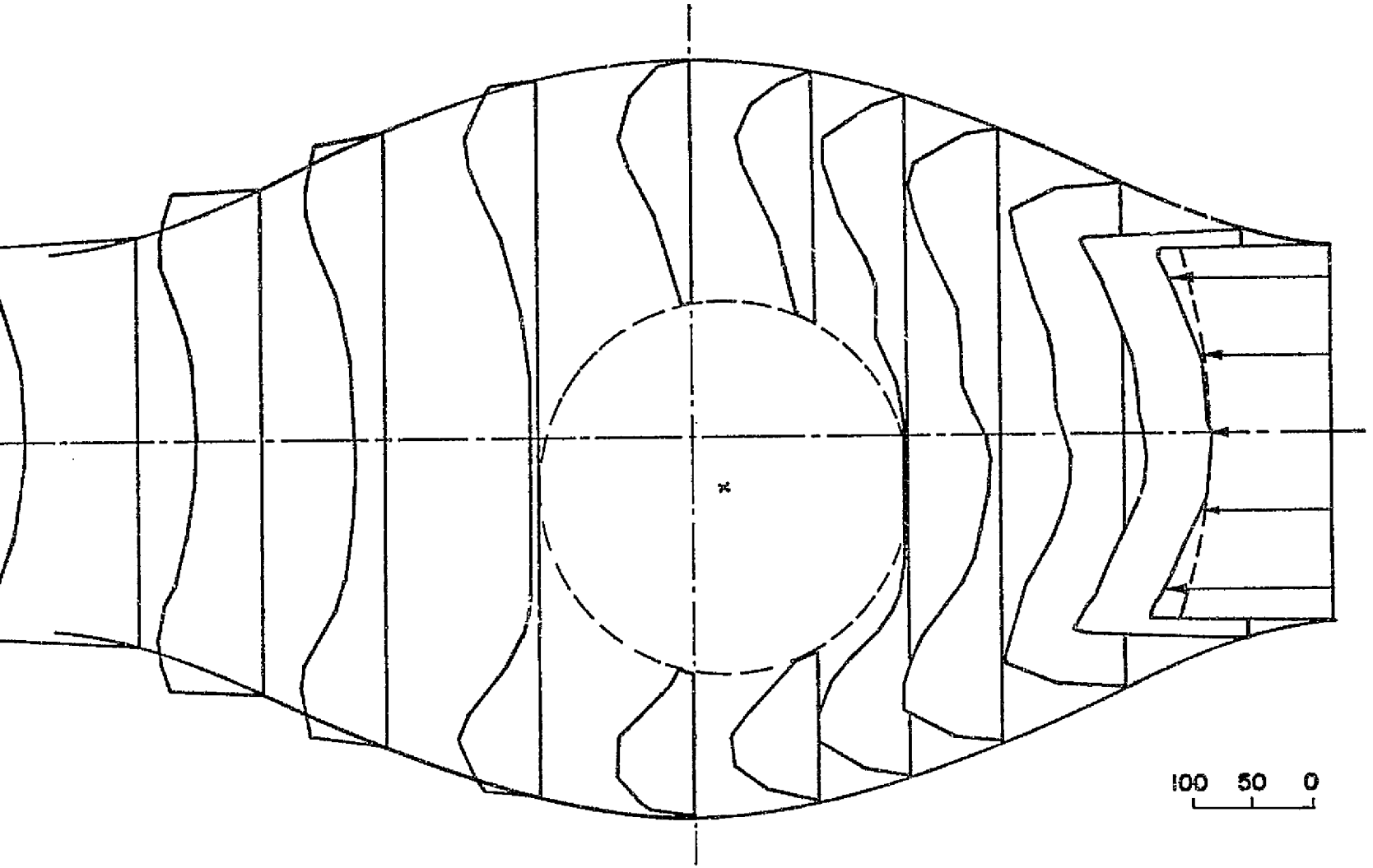


Figure 4-7A. Normalized speed profiles ($Q/Q_{ref}$) in %, in the test chamber, 60° - 240° plane.

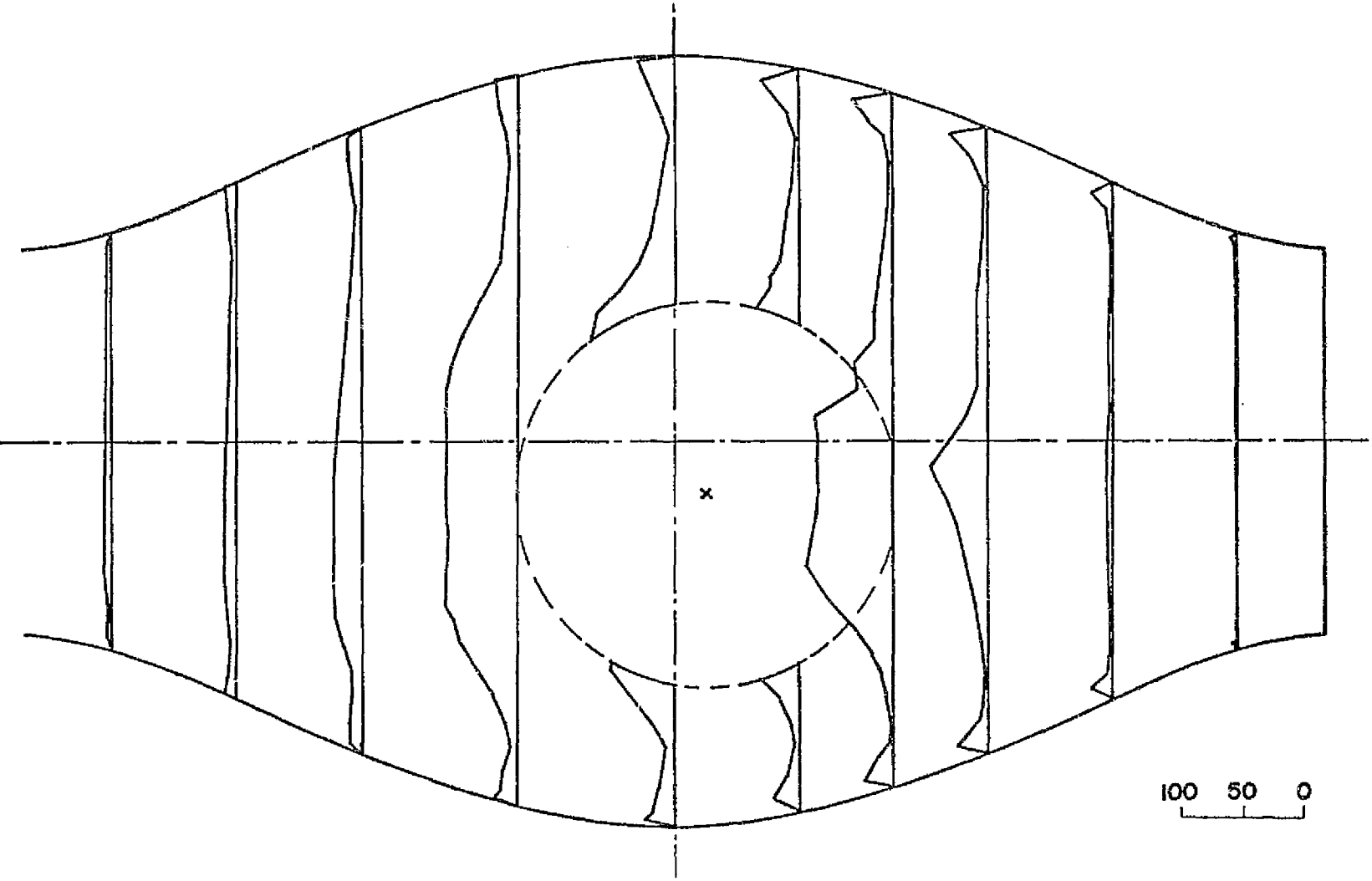


Figure 4-7B. Local turbulence intensity ($q'/Q$) in %, in the test chamber, 60° - 240° plane.

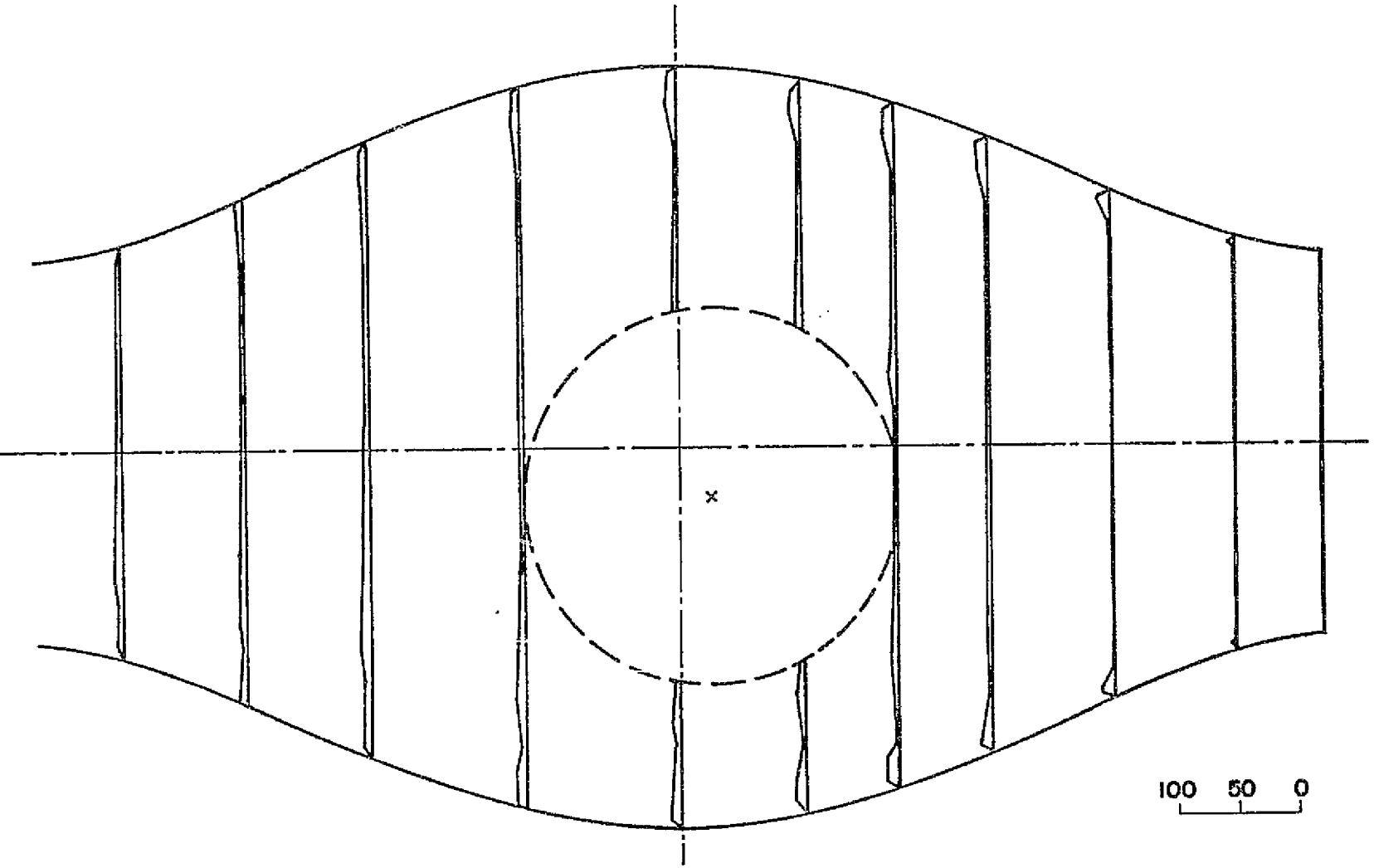


Figure 4-7C. Absolute turbulence intensity ($q'/Q_{ref}$) in %, in the test chamber, 60° - 240° plane.

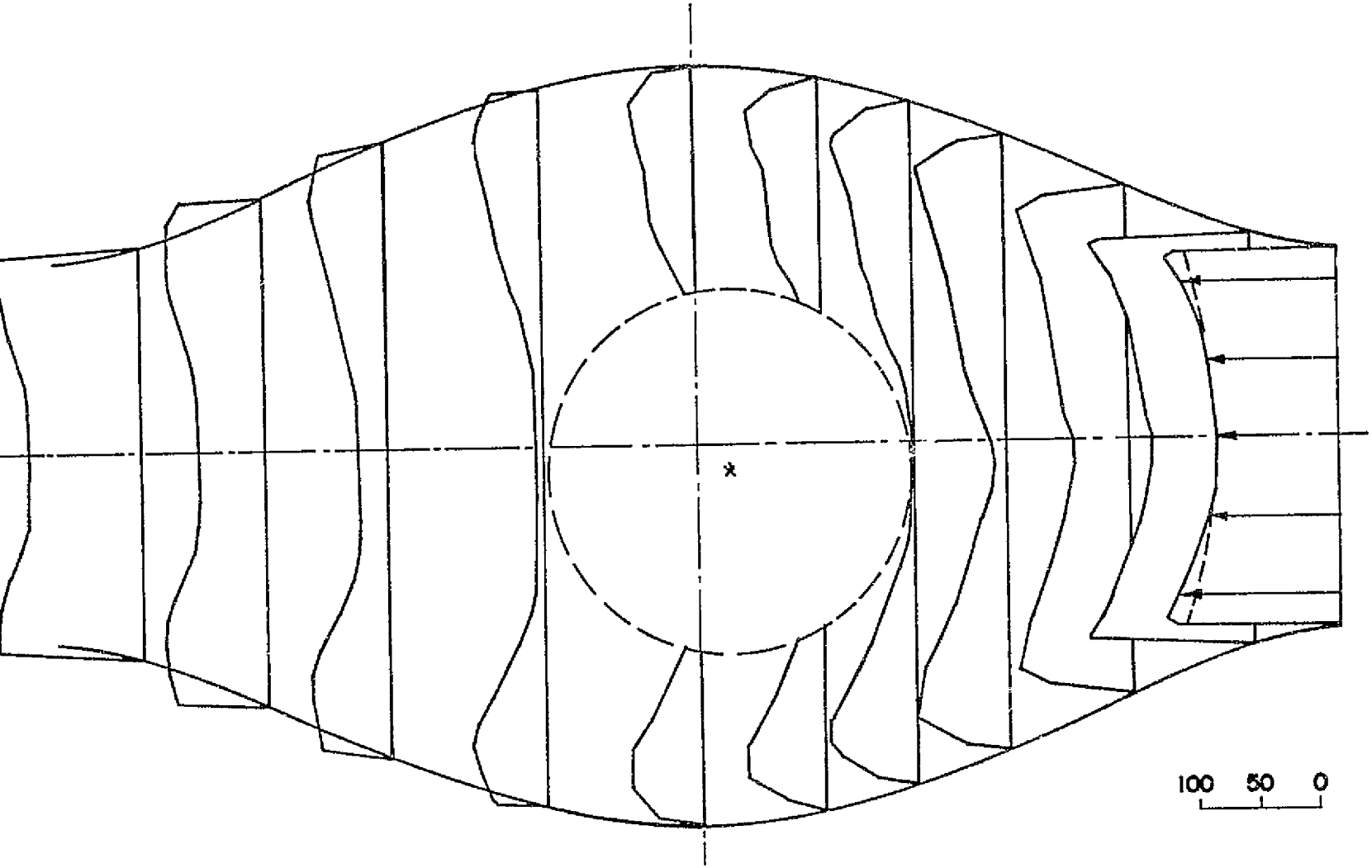


Figure 4-8A. Normalized speed profiles ($Q/Q_{ref}$) in %, in the test chamber, 120° - 300° plane.

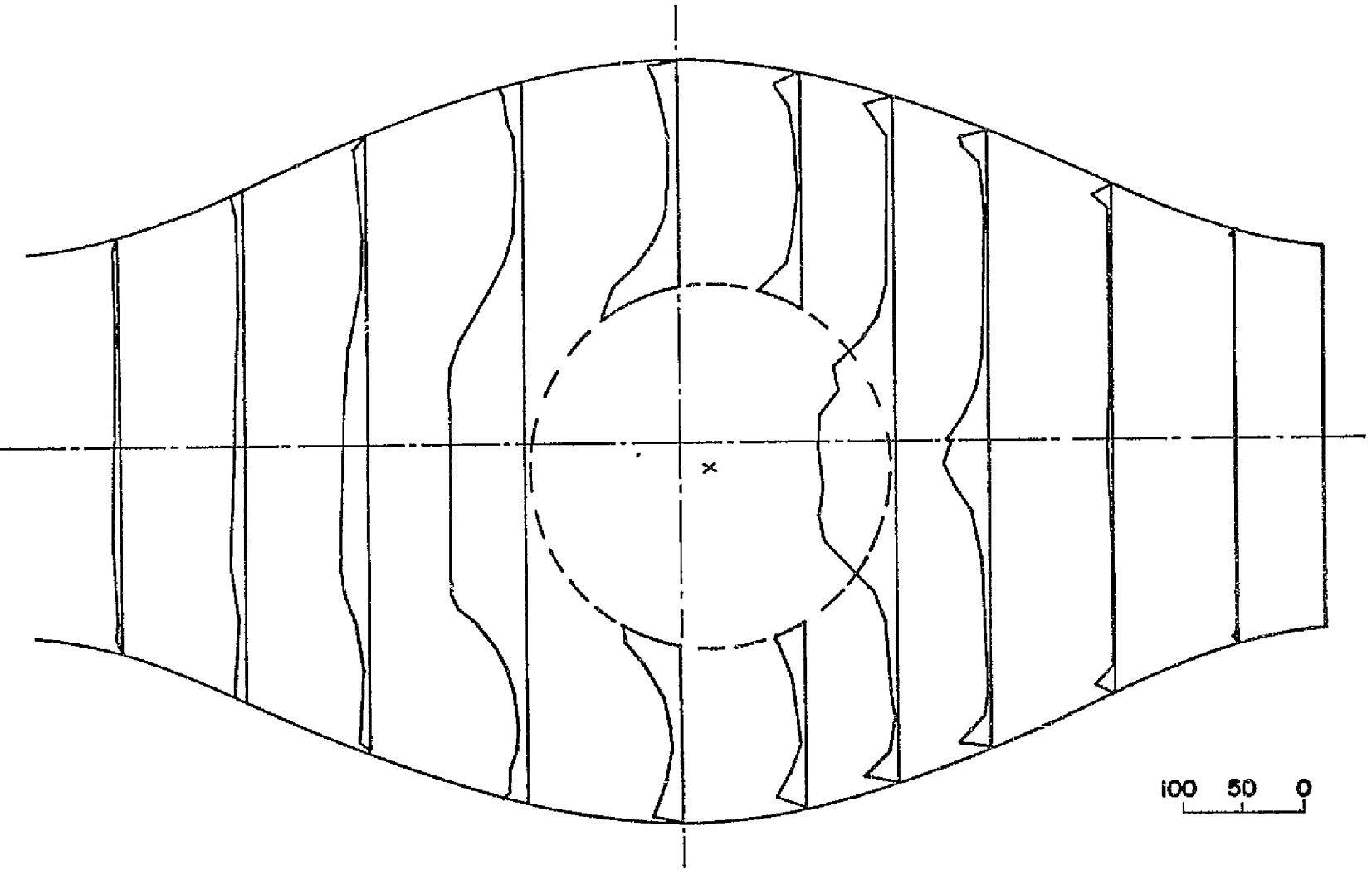


Figure 4-8B. Local turbulence intensity ($q'/Q$) in %, in the test chamber, 120° - 300° plane.

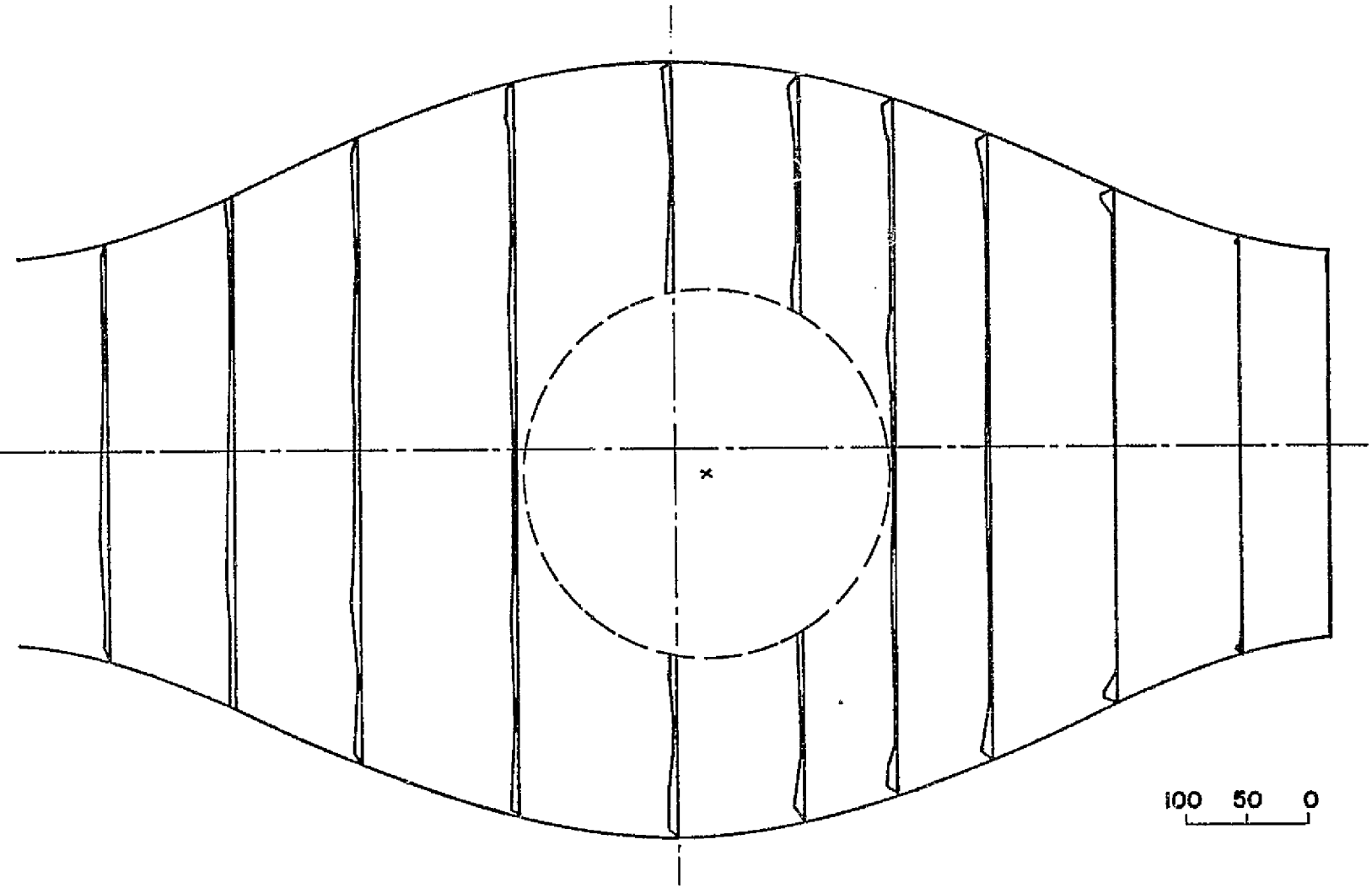


Figure 4-8C. Absolute turbulence intensity ($q'/Q_{ref}$) in %, in the test chamber, 120° - 300° plane.

chamber. Although the speed reading in this region is not very accurate (see later explanation), it still gives an indication for its possible maximum values. While all the profiles represent only the velocity magnitudes, not its directions, it should also be noted that there are flow reversals inside the central region as indicated by the tuft probe. Data for the other two meridional planes have the same general characteristics. A dashed circle of 1.5 inches in radius has been drawn in the central portion of the test chamber. It represents the spherical self-confined region as mentioned in the previous chapters. From tuft probe visualization results, we know that there is a self-confined region and its approximate location. With the aid of this rough picture and after the three normalized speed graphs (Figure 4-6A, 4-7A and 4-8A) are plotted, we then try to place a circle of 1.5 inches in radius in the central portion of the test chamber such that the speed on the boundary of this circle will be minimum (if not zero). The result is quite good; a self-confined spherical region fits into the graph very well. However, the center of this spherical region is shifted to 0.25 inch upstream of the chamber center and off the axis of symmetry by the amount shown in the Figure 4-9 below. In order to visualize such a confinement region in the test chamber more easily, the above mentioned circle is placed on to each of the remaining nine figures in the same manner, and inside the dashed circle speed profiles are not presented.

Because of the skewness of the confinement region, speed profiles on either sides of the region are not symmetrical as can be seen in the normalized speed profiles. Although the speed on the region boundary does not vanish, its magnitude is very small. The local turbulence

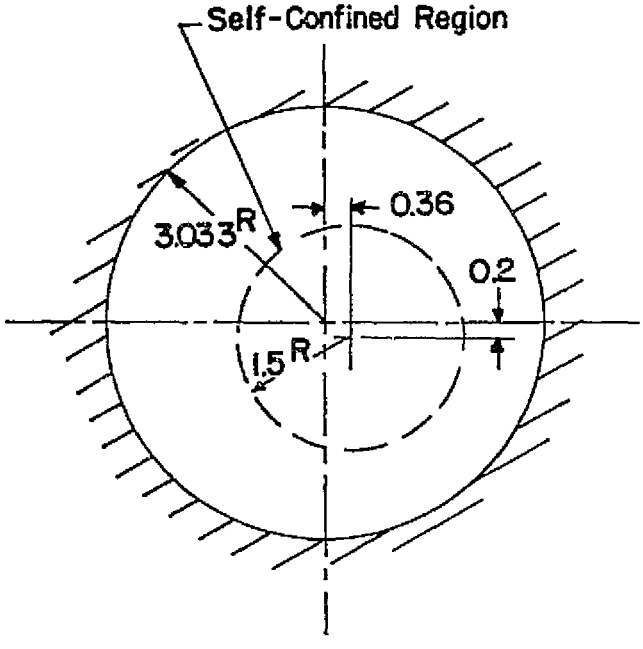


Figure 4-9. Location of the self-confined region at the cross-section of $\chi = + 0.25$ inch.

intensity there is high. This small speed is thought to be related to the local turbulence across the region interface. So the self-confined region does not have a very clear-cut, solid boundary. Rather, the boundary is a fuzzy zone with small turbulence velocities in different directions. Therefore the dashed circle only represents a time average position of the region. In spite of this situation, the confinement region still exists. The existence of the self-confined region as described above is further confirmed by the flow-rate calculation in the next section.

As indicated by the tuft probe, there are flow reversals inside this region and thus the flow would wash over the probe support first before it reaches the hot wire sensor. The disturbances created by the probe support would render the hot wire signals inaccurate. Besides, inside this region, the flow pattern may be very complicated. Further experimental work, especially good flow visualization, has to be done in order to completely understand the phenomenon. Nevertheless, hot wire measurements inside this region have indicated that the speeds are generally low with some regions having slightly higher speeds than others (Figure 4-5). Local turbulence intensities are high due to the low local mean speed, but the absolute turbulence remains low throughout the entire region (see numerical data in Table 4 of the Appendix).

A speed profile indicated by the dashed curve is also shown at the chamber entrance on each of the three normalized speed graphs. It represents the profile required by the theory in order to have the proper vorticity distribution. One can see clearly that the actual, generated speed profile at the chamber entrance pocesses a greater amount

C. 2

of vorticity than what is theoretically required. Therefore, it is conjectured that the shifting of the region position to an upstream location is caused by the excess in vorticity distribution of the generated speed profile. Furthermore, one can also notice that there is a certain amount of skewness in the actual, generated speed profile at the chamber entrance, and this corresponds very well with the dislocation of the confinement region to an off axis position. In other words, the location of the self-confined region can be directly related to the amount and the characteristics of the vorticity distribution in the generated speed profile. This phenomenon is certainly expected. As was noted in the second chapter, for a different vorticity distribution, we may very well obtain a different confinement region. It should be an easy matter to prove this conjecture in future experiments by using slightly different vorticity generators to generate slightly different input profiles, and then mapping out the confinement regions for comparison. More theoretical analysis on this situation will also be able to provide deeper insight into the confinement mechanism in this flow.

One of the remarkable characteristics of this flow shown on all the normalized speed profiles is that except for the smoothing effect of the viscosity, speed profiles have maintained and recovered their shapes quite well downstream of the self-confined region. No flow separation has occured anywhere inside the test chamber. Due to the small speeds in the central portion of the chamber, local turbulence intensities there are higher, but have returned to small magnitudes further downstream. Even the turbulence in the boundary layer are suppressed in the downstream part of the test chamber. Absolute turbulence

intensities have remained small throughout the entire test section. No flow instability has been detected.

Some oscilloscope pictures of the linearized RMS hot wire signals along the axis of the test section are given in Figures 4-10 and, 4-11A and B. In order to show the differences in the characteristics of the fluctuating velocities, these pictures were taken for two different conditions. Figure 4-10 is for the condition without the vorticity generator and Figure 4-11 is for the condition with the vorticity generator.

It can be seen that although the magnitudes of the fluctuating velocities at the chamber entrance ($\chi$ = +5.2 inches) in Figure 4-10 are slightly lower than that of the Figure 4-11A (larger fluctuating velocities caused by the vorticity generator), the fluctuating velocities generally have a much larger magnitude and higher frequencies for the former than that for the later. Especially at the chamber exit ($\chi$ = -5.2 inches), the difference in the magnitude of the fluctuating velocities is quite large. In addition to having smaller fluctuating velocities in the central portion of the test chamber, the frequencies of the RMS signal in Figure 4-11 are also much lower (about 150 - 500 Hz.). These results confirm the facts revealed by the tuft visulization that when the vorticity generator was installed in the pipe, the flow inside the test chamber became very orderly and a distinct flow region existed in the central part of the chamber.

3. Flow rate calculation

The mass flow rates both at the test chamber entrance ($\chi$ = +5.2 inches) and at the chamber central cross-section ($\chi$ = 0.0 inch) are

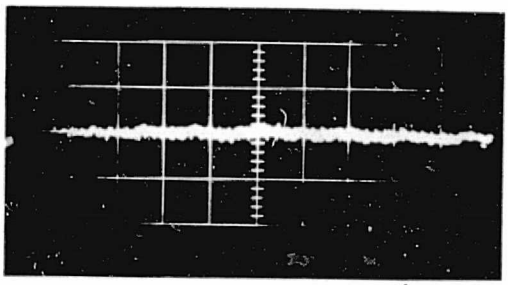

$\chi$ = +5.2", Q = 58.12 ft/sec
$RMS_L$ = 0.64 ft/sec

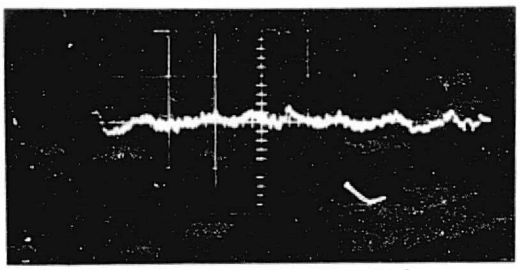

$\chi$ = +2.5", Q = 50.62 ft/sec
$RMS_L$ = 1.61 ft/sec

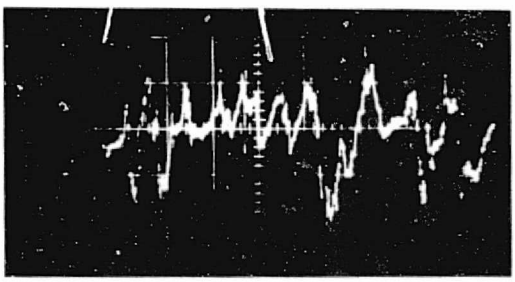

$\chi$ = 0.0", Q = 45.50 ft/sec
$RMS_L$ = 7.6 ft/sec

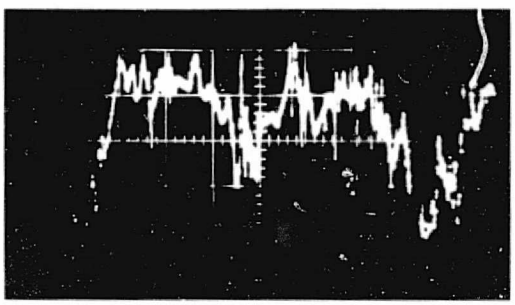

$\chi$ = -2.5", Q = 33.73 ft/sec
$RMS_L$ = 11.70 ft/sec

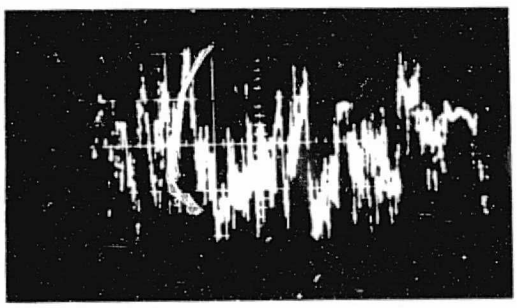

$\chi$ = -5.2", Q = 52.75 ft/sec
$RMS_L$ = 9.78 ft/sec

Figure 4-10. Linearized RMS hot wire signals along the axis of the test section (without V.G.). Scale: 1V/Cm-Vertical, 10 Milli Sec/Cm-Horizontal

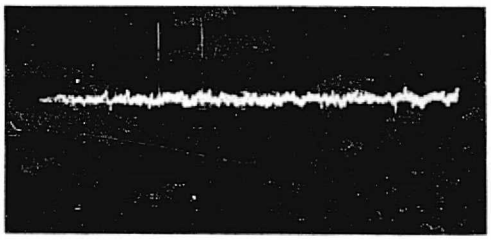

$\chi$ = +5.2", Q = 46.8 ft/sec
$RMS_L$ = 0.92 ft/sec

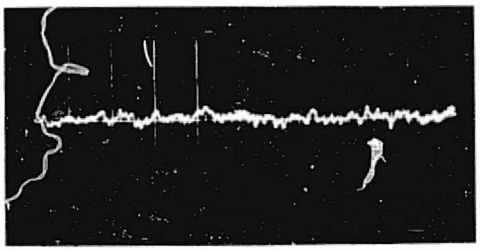

$\chi$ = +3.0", Q = 14.1 ft/sec
$RMS_L$ = 1.50 ft/sec

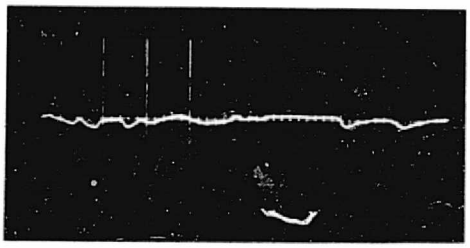

$\chi$ = +2.0", Q = 1.62 ft/sec
$RMS_L$ = 1.03 ft/sec

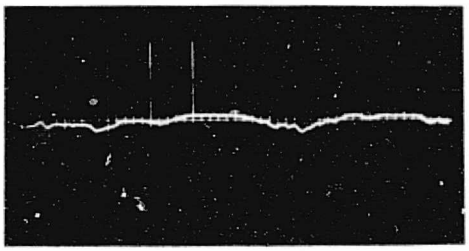

$\chi$ = +1.75", Q = 1.55 ft/sec
$RMS_L$ = 0.98 ft/sec

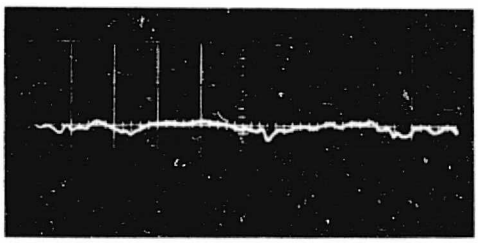

$\chi$ = +1.25", Q = 2.00 ft/sec
$RMS_L$ = 1.22 ft/sec

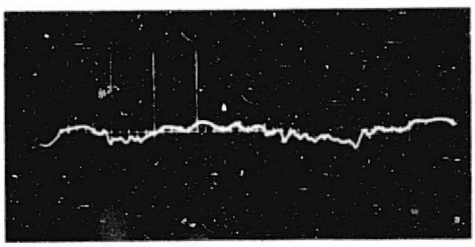

$\chi$ = +1.00", Q = 2.12 ft/sec
$RMS_L$ = 1.31 ft/sec

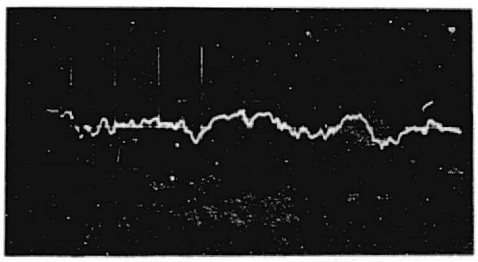

$\chi$ = 0.0", Q = 4.25 ft/sec
$RMS_L$ = 1.73 ft/sec

Figure 4-11A. Linearized RMS hot wire signals along the axis ofthe test section (with V.G.)
Scale: 1V/Cm-Vertical, 10 Milli Sec/Cm-Horizontal

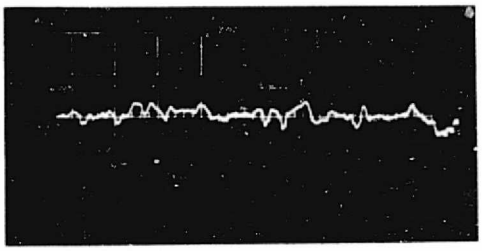

$\chi$= -1.0", Q = 3.77 ft/sec
$RMS_L$ = 1.98 ft/sec

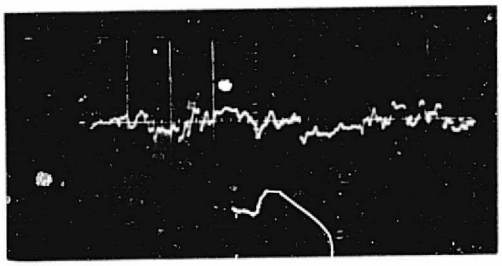

$\chi$ = -1.25", Q = 3.71 ft/sec
$RMS_L$ = 2.14 ft/sec

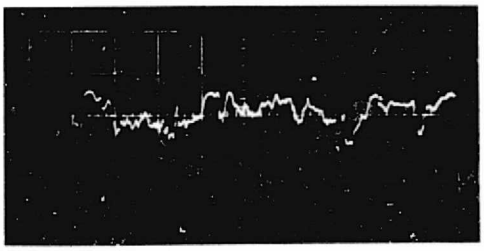

$\chi$= -1.75", Q = 5.40 ft/sec
$RMS_L$ = 2.56 ft/sec

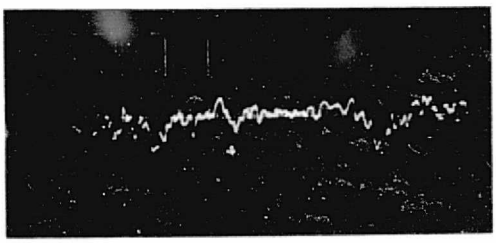

$\chi$= -2.0", Q = 6.82 ft/sec
$RMS_L$ = 2.55 ft/sec

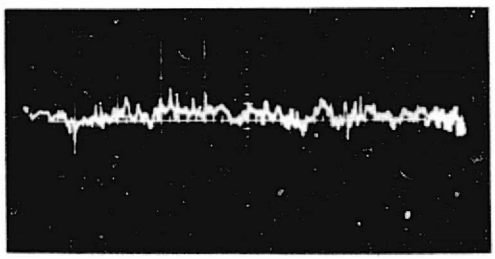

$\chi$= -3.0", Q = 18.12 ft/sec
$RMS_L$ = 2.49 ft/sec

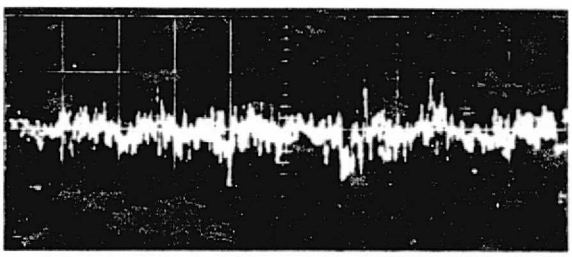

$\chi$= -5.2", Q = 51.3 ft/sec
$RMS_L$ = 2.58 ft/sec

Figure 4-11B. Linearized RMS hot wire signals along the axis of the test section (with V.G.)
Scale: 1V/Cm-Vertical, 10 Milli Sec/Cm-Horizontal

calculated. For this purpose, it is assumed that the self-confined region in the chamber center is stationary with respect to the main flow, just as if the spherical region was a solid sphere. Then the mass flow rate at the entrance must be the same as that through the skewed annulus (similar to the one shown in Figure 4-9) at the central cross-section in order to meet the continuity requirement.

References are made to the normalized speed profiles in Figures 4-6A, 4-7A, and 4-8A, and the numerical data in Table 4 of the Appendix. At each radial position, six speed measurements have been taken (i.e. every 60° in the azimuthal direction) for a certain radius $r$. Mass flow rate calculations are carried out by numerical integrations over both sections. The speed is assumed to be constant over a sector of annulus with radius $r$, width $\pm\frac{\Delta r}{2}$, and an included angle of 60° centered around the measuring station. Where $\Delta r$ is the radial increment for the measuring stations. For entrance section $\Delta r$ = 0.1 inch and for central section $\Delta r$ = 0.2 inch.

The two mass flow rates thus found are surprisingly close to each other. Except for the third decimal figure, they are identical.

Mass flow rate at entrance section ($\chi$ = +5.2 inches)

= Mass flow rate at the central annular section ($\chi$ = 0.0 inch)

= 2.85$\rho$ lb/sec

This mass flow rate calculation is based on the measured speed data and the flow geometry as shown in Figures 4-6A, 4-7A, and 4-8A. There is a small degree of uncertainty involved in the mass flow rate calculation for the central annular section. As discussed in section IV.2.2.2, there is no clear-cut, solid boundary at the confinement region inter-

face. The dashed circles only represent the time average position of a certain fuzzy zone with low average speed (about 1.5 - 5.5 ft/sec) and locally high relative intensity of turbulence (about 40-60 % ). Therefore there is considerable amount of turbulent diffusion between the fluids of the main flow and that of the confinement region across the fuzzy zone. This would affect the accuracy of the hot wire measurements. Nevertheless, this uncertainty would have little effect on the flow rate calculation. If the velocity at the region interface has an error of 50%, by a very rough estimate, the local position of the time average boundary will have a possible maximum error of less than 4% of the region diameter (3 inches) so as to meet the continuity requirement. In addition, the accuracy of the hot wire anemometer in the day to day measurements is estimated to be less than 4%. In any event, the above uncertainty or the possible errors involved will not affect the mass flow rate calculation a great deal. The closeness of the mass flow rates at the two sections helps us determine, with a reasonable accuracy the size and location of the self-confined region.

# CHAPTER V

# CONCLUSIONS

To a great extent, the original goals set for this experimental study have been successfully achieved, and most of the questions raised in the beginning have also been answered. However, in order to have a more complete understanding of this problem, further theoretical as well as experimental studies are required. Some suggestions on the direction for future studies are presented in the later section. Based on the results obtained in this experiment, some possible applications for this self-confined flow are also outlined here. The major findings of this study are now summarized below.

## 1. Summary

The theoretical model based on an inviscid, incompressible, steady-state analysis showed that an isolated, stagnant, self-confined region of constant pressure might be produced by suitable choices of flow parameters. The main concern, however, was that in a real situation, would this flow exist? Either the turbulence, instability, or separation of the flow, or any combination of these factors could undermine the confinement mechanism and made the theoretical model unrealistic. There were also questions about how to properly produce the required vorticity distributions. Now with the results presented in Chapter IV, these questions have been settled and the existence of such a self-confined region in a flow with a specified ring-vorticity distribution is confirmed. Furthermore, the flow appears to be unique and

stable. Even in the actual situation of this experiment, where the generated velocity profile deviated from the theoretical value (too much vorticity and some skewness in its distribution), the spherical self-confined region of the right size still existed at the same location every time the experiment was carried out. The only deviation from the theoretical model indicated was that the position of the confinement region was shifted to 0.25 inch upstream of the theoretical center and off the axis of symmetry by 0.41 inch. It is this author's opinion that such a deviation in the location of the confinement region is directly related to the shape of the generated velocity profile. Both the vorticity distribution and the symmetry of this velocity profile are important in determining the location of the confinement region. However, the detailed relationship between the generated velocity profile and the location of the confinement region are yet to be determined.

This experiment has shown that there has been no undue influence of the low turbulence level in the incoming stream on the confinement mechanism, except for the possible effects on the turbulence characteristics at the interface between the self-confined region and the main flow. Again, this is the area which requires more detailed study in the future so that the relationship between the turbulence in the incoming stream and that of the region interface can be better understood. In the initial stage of the experiment, flow separation was found at the sharp leading edge of the test section entrance scoop. This problem was subsequently corrected by blunting out the sharp leading edge to a semi-circle shape. With this problem eliminated and the introduction of the generated velocity profile into the test section, a self-confined

region was formed in the central part of the test chamber. The flow was very orderly and no flow separation was found anywhere along the chamber wall. This contrasted dramatically to the situation when the vorticity generator was not used in the incoming straight pipe (see Chapter IV for detailed descriptions). The velocity profile produced by the vorticity generator definitely contributed to the formation of the self-confined region and the orderliness of the flow in the test chamber.

2. Application

The author feels that the self-confined flow studied here could offer a new range of important possibilities for fluid mechanical confinement. If the other known confining mechanisms, such as the vortex breakdown phenomenon or the electromagnetic pinch effect, could be combined with this ring-vorticity case, a very powerful confinement method could be devised. Although the concept of a nuclear core reactor can not be realized yet, it could be brought closer to reality if a good confinement scheme could be found. The confinement mechanism illustrated in this experimental study could certainly make some contribution toward that end.

Most importantly, this method of flow confinement could be developed so as to have immediate benefit for some practical applications. For example, the concept of self-confined flow could be incorporated into a turbine combustor design such that the fuel could be confined in the combustor and with the help of the turbulent diffusion across the region interface, the combustion process might be better controlled. Of course, the concept of the vortex breakdown could also be

incorporated into the design to further enhance the confinement process. There also could be useful applications for this type of self-confined flow in the fields of chemical processes where a region of fluid must be contained within a flowing medium without touching the chamber walls.

One interesting result revealed by this experimental study was that the flow inside the test chamber was very orderly and no flow separation was found anywhere in the chamber. In view of the large area ratio (3 to 1) between the central section annulus to the entrance of the test chamber in such a short distance (5.2 inches which is shorter than the diameter of the central cross-section), an oddly shaped but very effective flow diffuser can be made. Such a diffuser has a peculiar shape because the central self-confined region is relatively stagnant to the main flow, just as if the whole spherical volume was a solid block standing there with respect to the main flow. Also the test chamber has a certain specific contour as required by Equation (3-2). A more practical diffuser could be made if the rear half section of the test chamber could be eliminated, or even if the contour of the chamber could be modified to have a simpler shape. These modifications are considered to be possible but more studies are certainly needed before any definite relationship or rule could be established.

## 3. Suggestions

The experimental study performed here is only the first effort made to establish such a self-confined flow in the real situation. For a new flow phenomenon like this, there will certainly be a lot of questions and also difficult problems associated with its practical

applications. This study has only broken the ground and a great deal of research work still remains to be done before all the questions could be answered and the whole phenomenon fully understood. Some areas for the future study on this problem are suggested below.

Flow visualization for this experiment was carried out with a tuft probe which was good only for general flow indications. Smoke visualization was tried but it was not very successful. It is strongly recommended that a good smoke visualization method be used as the next step in this experiment. A controllable smoke generator with sufficient amount of dense smoke is needed. Smoke could be introduced into the confinement region from downstream side to occupy the self-confined region, or a sheet of smoke could be introduced into the incoming stream so that the smoke would follow the main flow and passes around the confinement region. Then good photographs could be taken for better understanding of the flow patterns inside the test chamber.

One of the special features of this self-confined flow was in the generated velocity profile of the incoming flow such that it had a prescribed vorticity distribution. The vorticity generators tested in this experiment were all passive devices, i.e. they provided different resistances across the pipe diameter to create different velocities. Pressure drops (or losses) were incurred through this process. There were also problems with the axisymmetry with the generated velocity profiles. Unless a series of different devices are made, it is difficult to study the effect of the vorticity distribution and symmetry on the formation or the characteristics of the confinement region by varying the generated velocity profiles. One plausible remedy for this problem is to use an

array of tiny jets compactly arranged in a series of concentric rings. Flow rate from each tiny jet can be individually adjusted to give a desirable downstream velocity profile. If more sophistication is allowed, the flow rate of each jet can be controlled independently by a small computer so that quick and accurate changes can be made with very simple commands to the computer.

As stated in the third chapter, in order to simplify the construction, a straight pipe was used upstream of the test section for the velocity profile generation. Even though a reasonably good vorticity distribution could be produced in the straight pipe, there was no radial velocity component as required by the theory. The experimental results have shown that the confinement mechanism was not significantly affected. The theoretical model could be more realistically approached in any future study if a properly contoured incoming pipe is used to develop the correct amount of radial velocity before the test section.

In this experiment, the boundary layer was removed immediately before the flow entered the test chamber. Effects of the boundary layer build-up could be studied by eliminating the boundary layer removal section. Also, for a more sophisticated set-up, boundary layer suction arrangements could be applied to the test section walls to study the effect of the boundary layer on the confinement region.

The effect of density difference and of energy evolution and transfer require much further theoretical as well as experimental studies before practical containment applications can be claimed. Heavier fluid could be introduced into the confinement region to see whether it could be contained. However, stability theory suggests that it would indeed

be desirable for a rotationally confined heavy fluid to be at rest (Ref. 17). The diffusion rate across the region boundary as well as the total leakage rate of the fluid from the region should be investigated. Both the diffusion and the leakage would actually help the combustion process if fuel is confined in the central region.

Theoretical, experimental, and numerical work could also be performed to study the relationship among the incoming velocity profiles, the chamber contour and the shape and location of the self-confined region. Further work could also be done for the cases where $F(\psi)$ in Equation (2-14) takes on different values other than constant. Maybe more detailed turbulence work (e.g. scales, spectra, Reynolds stress, etc.) could be done in order to understand the connections between the turbulence of the incoming stream and that of the region interface. This understanding is essential for the practical combustion processes. Also Laser Doppler Anemometer could be used to measure the flow speed, direction as well as turbulence characteristics. However, in order to accommodate the LDA system, the entire test section may have to be redesigned.

Finally, a simpler variation of this experiment could be performed for some useful applications. As mentioned in the last section that suppose the rear half of test chamber is eliminated, what would happen to the confinement region? The flow could simply exit into the open air, or into a straight pipe of 6.066 inches in diameter. The simpliest case would be just to let the generated velocity profile (maybe from a straight tappered pipe in order to have proper radial velocity component) exit into the open air like a jet, or into a straight pipe similar to the arrangement

in a combustor canister. More understanding for these phenomena would certainly be very important for the practical application of such a self-confined flow in combustion, turbine combustor design and other general fluid mechanical confinement processes.

BIBLIOGRAPHY

1. Werlé, H.: "Sur l'éclatemant des tourbillons dápex dúne aile delta aux faibles vibles vitesses". La Recherche Aeronautique, pp. 23-30, No. 74, 1960

2. Elle, B. J.: "On the Breakdown at High Incidences of the Leading Edge Vortices on Delta Wings". Journal of the Royal Aeronautical Society, p. 491, Vol. 64, 1960

3. Peckham, D. H.: "Low Speed Wind Tunnel Tests on a Series of Uncambered Slender Pointed Wings with Sharp Edges". ARC RM 3186, 1961

4. Lambourne, N. C. and Bryer, D. W.: "The Bursting of Leading Edge Vortices. Some Observations and Discussion of the Phenomenon". ARC RM 3282, 1962

5. Lowson, M. V.:"Some Experiments with Vortex Breakdown". Journal of the Royal Aeronautical Society, pp. 343-346, Vol. 68, 1964

6. Hummel, D.: "Unterschuchungen uber das Aufplatzen der Wirbel en schlanken Deltaflugeln". Zeitschr. Flugwiss, S 158-168, Vol. 13, 1965

7. Hummel, D. and Srinivasan, P. S.: "Vortex Breakdown Effects on the Slow-Speed Aerodynamic Characteristics of Slender Delta Wings in Symmetric Flow". Journal of the Royal Aeronautical Society, pp. 319-322, Vol. 71, 1967

8. Harvey, J. K.: "Some Observations of the Vortex Breakdown Phenomenon". Journal of Fluid Mechanics, Vol. 14, pp. 585-592, 1962

9. Benjamin, T. B.: "Some Developments in the Theory of Vortex Breakdown". Journal of Fluid Mechanics, Vol. 28, p. 65, 1967

10. Sarpkaya, Turgut: "An Experimental Investigation of the Vortex-Breakdown Phenomenon". Report NPS-59SL0071A, U.S.Naval Postgraduate School, July 1970

11. Hall, M. G.: "Vortex Breakdown". Annual Review of Fluid Mechanics, Vol. 4, 1972, pp. 195-218

12. Mager, A.: "Dissipation and Breakdown of a Wing-Tip Vortex". Journal of Fluid Mechanics, Vol. 55, p. 609, 1972

13. Randall, J. D. and Leibovich, S.: "The Critical State: A Trapped Wave Model of Vortex Breakdown". Journal of Fluid Mechanics, Vol. 58, pp. 495-515, 1973

14. Kubo, I.: "A Numerical Study of Confined, Coaxial, Turbulent Swirling Flows". Ph.D. Thesis, 1974, Cornell University, N. Y.

15. Faler, J.: "Some Experiments in Swirling Flows: Detailed Velocity Measurements of a Vortex Breakdown Using a Laser Doppler Anemometer". Ph.D. Thesis, 1976, Cornell University, Ithaca,N.Y.

16. Hall, M. G.: "The Structure of Concentrated Vortex Cores". Article in Progress in Aeronautical Sciences, 7, Edited by Küchemann et al, Pergamon Press, 1966

17. Moore, F. K., and Leibovich, S: "Self-Confined Rotating Flows for Containment". NASA, SP-236, 1973

18. Lamb, H.: "Hydrodynamics". Dover Pub. (New York, N. Y.),1932, pp. 245-246

19. Batchelor, G. K.: "An Introduction to Fluid Dynamics". Cambridge University Press, 1967, p.526

20. Ragsdale, R. G., and Lanzo, C. D.: "Summary of Recent Gaseous Reactors Fluid Mechanics Experiments". NASA, TM X-1847, 1969

21. Shapiro, A. H., Jaffrin, M. Y. and Weinberg, S. L.: "Peristaltic Pumping with Long Wavelengths at low Reynolds Number". Journal of Fluid Mechanics (1969), Vol. 37, pp. 799-825

22. Jaffrin, M.Y., and Shapiro, A. H.: "Peristaltic Pumping". Annual Review of Fluid Mechanics, Vol. 3, 1971, pp. 13-35

23. Hung, Tin-Kan, and Brown, Thomas D.: "Solid-Particle Motion in Two-Dimensional Peristaltic Flows". Journal of Fluid Mechanics (1976), Vol. 73, pp. 77-96

24. Lighthill, M. J.: "Dynamics of a Dissociating Gas, Part I. Equilibrium Flow". Journal of Fluid Mechanics (1957), Vol. 2, pp. 1-32

25. Manual for Air Filtration Systems, Flanders Filters Inc. Washington, North Carolina, 1972

26. Loehrke, R. I., and Najib, H. M.: "Experiments on Management of Free-Stream Turbulence". AGARD Report No. 598, 1972

27. Vidal, R. J., and Curtis, J. T.: "The Effects of Axisymmetric Shear on Airfoil Characteristics". TCREC Technical Report T61-138, Cornell Aeronautical Laboratory, Inc. 1961

28. Livesey, J. L., and Laws, E. M.: "Simulation of Velocity Profiles by Shaped Gauze Screens". AIAA Journal, Vol. 11, No. 2, pp. 184-188, 1973

29. Livesey, J. L., and Laws, E. M.: "Flow Through Non-Uniform Gauze Screens". Journal of Fluid Mechanics (1973), Vol. 59, pp. 737-743

30. Sajben, M., Kroutil, J. C., Hoffman, G. H., and Sedrick, A. V.: "Generation of Velocity Profiles Using Screens of Nonuniform Solidity". AIAA Paper No. 73-1229, 1973

31. TSI Manual for Anemometry, Thermo-Systems Inc., St. Paul, Minn. 1973

32. Champagne, F. H., Sleicher, C. A., and Wehrmann, O. H.: "Turbulence Measurements with Inclined Hot-Wires". Part 1 & 2, Journal of Fluid Mechanics, Vol. 28, pp. 153 & 177, 1967

33. Operating and Service Manual, 1050 Series Constant Temperature Anemometers and Related Accessories., Thermo-Systems Inc., St. Paul, Minn., 1970

34. Instruction Manual for Model 1052 Linearizer, Thermo-Systems Inc., St. Paul, Minn., 1971

35. Model 1047 Instruction Manual, Thermo-Systems Inc., St. Paul, Minn., 1974

36. Bradshaw, P.: "An Introduction to Turbulence and Its Measurement". Pergamon Press, 1971

37. Hinze, J. O.: "Turbulence, An Introduction to Its Mechanism and Theory". McGraw-Hill Book Co. Inc. 1959

38. King, L. V.: "On the Convection of Heat from Small Cylinders in a Stream of Fluid: Determination of the Convective Constants of Small Platinum Wires with Applications to Hot-Wire Anemometry". Proc. of Roy. Society, Vol. 214A, No. 14, p.373, 1914

39. Collis, D. C., and Williams, M. J.: "Two-Dimensional Convection from Heated Wires at Low Reynolds Numbers". Journal of Fluid Mechanics (1959), Vol. 6, p. 357

40. Hollasch, K., and Gebhart B.: "Calibration of Constant-Temperature Hot-Wire Anemometer at Low Velocities in Water with Variable Fluid Temperature". ASME Paper No. 71-HT-9, 1971

41. Shen, S. F.: The section on "Stability of Laminar Flows". p.788, in the book: "Theory of Laminar Flows". Edited by Moore, F. K., Prinston University Press, 1964

APPENDIX

Table 1

Coordinates for the test section interior wall

| $x$ (inch) | $r$ (inch) |
|---|---|
| 0.000 | 3.033 |
| 0.146 | 3.018 |
| 0.212 | 3.015 |
| 0.339 | 3.008 |
| 0.456 | 2.999 |
| 0.548 | 2.989 |
| 0.608 | 2.982 |
| 0.728 | 2.966 |
| 0.920 | 2.934 |
| 1.218 | 2.871 |
| 1.441 | 2.813 |
| 1.505 | 2.795 |
| 1.810 | 2.698 |
| 2.060 | 2.609 |
| 2.274 | 2.526 |
| 2.464 | 2.450 |
| 2.635 | 2.377 |
| 2.939 | 2.246 |
| 3.206 | 2.131 |
| 3.447 | 2.027 |
| 3.671 | 1.934 |
| 3.881 | 1.850 |
| 4.080 | 1.773 |
| 4.272 | 1.703 |
| 4.365 | 1.670 |
| 4.548 | 1.609 |
| 4.726 | 1.552 |
| 4.900 | 1.499 |

Table 2

Hot wire calibration data

| P-S Reading (in.-water) | Speed (ft/sec) | Bridge Voltage (volt) |
|---|---|---|
| 0.0000 | 0.00 | 2.082 |
| 0.0070 | 5.64 | 2.656 |
| 0.0135 | 7.83 | 2.736 |
| 0.0200 | 9.53 | 2.803 |
| 0.0320 | 12.06 | 2.888 |
| 0.0465 | 14.53 | 2.956 |
| 0.0630 | 16.92 | 3.014 |
| 0.0760 | 18.58 | 3.048 |
| 0.0985 | 21.15 | 3.105 |
| 0.1280 | 24.11 | 3.161 |
| 0.1675 | 27.59 | 3.218 |
| 0.2250 | 31.97 | 3.288 |
| 0.2955 | 36.64 | 3.355 |
| 0.3710 | 41.05 | 3.409 |
| 0.4600 | 45.71 | 3.461 |
| 0.6615 | 54.82 | 3.558 |
| 0.8890 | 63.55 | 3.639 |
| 1.1180 | 71.27 | 3.703 |
| 1.4380 | 80.83 | 3.774 |
| 1.7950 | 90.30 | 3.834 |

Room temperature: 76°F

Sensor cold resistance: 5.022 Ohms

Overheat ratio: 1.6

Operating resistance: 8.04

Table 3

Linearizer calibration data

| Speed* (ft/sec) | Bridge* Voltage (volt) | Linearizer Output (volt) |
|---|---|---|
| 0 | 2.082 | 0.000 |
| 1 | 2.243 | 0.100 |
| 2 | 2.358 | 0.200 |
| 3 | 2.450 | 0.302 |
| 4 | 2.526 | 0.405 |
| 5 | 2.587 | 0.501 |
| 8 | 2.739 | 0.808 |
| 10 | 2.818 | 1.014 |
| 12 | 2.884 | 1.214 |
| 15 | 2.970 | 1.517 |
| 18 | 3.043 | 1.816 |
| 20 | 3.086 | 2.017 |
| 25 | 3.182 | 2.518 |
| 30 | 3.263 | 3.015 |
| 40 | 3.397 | 3.999 |
| 50 | 3.509 | 5.000 |
| 60 | 3.605 | 6.002 |
| 70 | 3.691 | 7.031 |
| 80 | 3.765 | 8.031 |
| 90 | 3.831 | 9.000 |

* Values of the speed and bridge voltage used in this table are taken from the hot wire calibration curve plotted on a large graph paper for accuracy (the curve is similar to the one shown on Figure 3-9).

Table 4

Detailed hot wire measurement data for the test section
(partial list)

Nomenclature

ANGLE: Azimuthal angle in degrees, starting from the twelve o'clock position and in the counterclockwise direction

SPEED: Fluid speed in the meridional plane in ft/sec

SPEED RATIO: Ratio of the local average speed to the reference speed at $x = +5.2$ inches and $r = 0.0$ inch, i.e., $Q/Q_{ref}$

RMS SPEED: The fluctuating speed $q'$ in ft/sec

LOCAL INT: Local turbulence intensity in %, $q'/Q$

TURB INT: Absolute turbulence intensity in %, $q'/Q_{ref}$

| ANGLE | SPEED | SPEED RATIO | RMS SPEED | LOCAL INT | TURB INT |
|---|---|---|---|---|---|
| | | X= 5.20 | | R=0.000 | |
| 0 | 47.62 | 1.012 | 0.940 | 1.974 | 1.997 |
| 30 | 47.62 | 1.012 | 0.960 | 2.016 | 2.040 |
| 60 | 47.05 | 1.000 | 0.940 | 1.998 | 1.997 |
| 90 | 46.95 | 0.998 | 0.960 | 2.045 | 2.040 |
| 120 | 46.87 | 0.996 | 0.930 | 1.984 | 1.976 |
| 150 | 46.80 | 0.994 | 0.910 | 1.944 | 1.934 |
| 180 | 46.80 | 0.994 | 0.920 | 1.966 | 1.955 |
| 210 | 46.80 | 0.994 | 0.930 | 1.987 | 1.976 |
| 240 | 46.80 | 0.994 | 0.950 | 2.030 | 2.019 |
| 270 | 46.95 | 0.998 | 0.920 | 1.960 | 1.955 |
| 300 | 47.13 | 1.001 | 0.950 | 2.016 | 2.019 |
| 330 | 47.35 | 1.006 | 0.930 | 1.964 | 1.976 |
| | | X= 5.20 | | R=0.100 | |
| 0 | 47.64 | 1.012 | 0.890 | 1.868 | 1.891 |
| 30 | 47.90 | 1.018 | 0.910 | 1.900 | 1.934 |
| 60 | 48.25 | 1.025 | 0.900 | 1.865 | 1.912 |
| 90 | 48.10 | 1.022 | 0.910 | 1.892 | 1.934 |
| 120 | 47.85 | 1.017 | 0.950 | 1.985 | 2.019 |
| 150 | 47.35 | 1.006 | 0.920 | 1.943 | 1.955 |
| 180 | 46.60 | 0.990 | 0.910 | 1.953 | 1.934 |
| 210 | 46.17 | 0.981 | 0.830 | 1.798 | 1.764 |
| 240 | 46.04 | 0.978 | 0.800 | 1.738 | 1.700 |
| 270 | 46.40 | 0.986 | 0.820 | 1.767 | 1.742 |
| 300 | 46.55 | 0.989 | 0.830 | 1.783 | 1.764 |
| 330 | 46.85 | 0.996 | 0.860 | 1.836 | 1.827 |
| | | X= 5.20 | | R=0.200 | |
| 0 | 47.62 | 1.012 | 0.820 | 1.722 | 1.742 |
| 30 | 47.85 | 1.017 | 0.850 | 1.776 | 1.806 |
| 60 | 48.62 | 1.033 | 0.820 | 1.687 | 1.742 |
| 90 | 48.80 | 1.037 | 0.770 | 1.578 | 1.636 |
| 120 | 48.62 | 1.033 | 0.800 | 1.645 | 1.700 |
| 150 | 47.90 | 1.018 | 0.840 | 1.754 | 1.785 |
| 180 | 47.07 | 1.000 | 0.840 | 1.785 | 1.785 |
| 210 | 46.40 | 0.986 | 0.830 | 1.789 | 1.764 |
| 240 | 46.10 | 0.980 | 0.750 | 1.627 | 1.594 |
| 270 | 46.56 | 0.989 | 0.770 | 1.654 | 1.636 |
| 300 | 46.75 | 0.993 | 0.800 | 1.711 | 1.700 |
| 330 | 46.85 | 0.996 | 0.820 | 1.750 | 1.742 |

| ANGLE | SPEED | SPEED RATIO | RMS SPEED | LOCAL INT | TURB INT |
|---|---|---|---|---|---|
| | | X= 5.20 | | R=0.300 | |
| 0 | 47.64 | 1.012 | 0.810 | 1.700 | 1.721 |
| 30 | 47.66 | 1.013 | 0.820 | 1.721 | 1.742 |
| 60 | 48.72 | 1.035 | 0.870 | 1.786 | 1.849 |
| 90 | 49.55 | 1.053 | 0.710 | 1.433 | 1.509 |
| 120 | 49.00 | 1.041 | 0.690 | 1.408 | 1.466 |
| 150 | 48.60 | 1.033 | 0.710 | 1.461 | 1.509 |
| 180 | 48.00 | 1.020 | 0.750 | 1.563 | 1.594 |
| 210 | 46.90 | 0.997 | 0.890 | 1.898 | 1.891 |
| 240 | 46.60 | 0.990 | 0.790 | 1.695 | 1.679 |
| 270 | 47.64 | 1.012 | 0.790 | 1.658 | 1.679 |
| 300 | 47.70 | 1.014 | 0.760 | 1.593 | 1.615 |
| 330 | 47.85 | 1.017 | 0.830 | 1.735 | 1.764 |
| | | X= 5.20 | | R=0.400 | |
| 0 | 48.00 | 1.020 | 0.860 | 1.792 | 1.827 |
| 30 | 47.80 | 1.016 | 0.810 | 1.695 | 1.721 |
| 60 | 48.78 | 1.037 | 0.910 | 1.866 | 1.934 |
| 90 | 49.75 | 1.057 | 0.720 | 1.447 | 1.530 |
| 120 | 49.77 | 1.058 | 0.690 | 1.386 | 1.466 |
| 150 | 49.72 | 1.057 | 0.700 | 1.408 | 1.487 |
| 180 | 48.65 | 1.034 | 0.710 | 1.459 | 1.509 |
| 210 | 47.87 | 1.017 | 0.900 | 1.880 | 1.912 |
| 240 | 47.62 | 1.012 | 0.820 | 1.722 | 1.742 |
| 270 | 48.65 | 1.034 | 0.780 | 1.603 | 1.657 |
| 300 | 48.47 | 1.030 | 0.700 | 1.444 | 1.487 |
| 330 | 48.75 | 1.036 | 0.790 | 1.621 | 1.679 |
| | | X= 5.20 | | R=0.500 | |
| 0 | 48.70 | 1.035 | 0.850 | 1.745 | 1.806 |
| 30 | 48.60 | 1.033 | 0.930 | 1.914 | 1.976 |
| 60 | 49.55 | 1.053 | 0.890 | 1.796 | 1.891 |
| 90 | 50.25 | 1.068 | 0.730 | 1.453 | 1.551 |
| 120 | 50.50 | 1.073 | 0.710 | 1.406 | 1.509 |
| 150 | 50.72 | 1.078 | 0.750 | 1.479 | 1.594 |
| 180 | 48.75 | 1.036 | 0.700 | 1.436 | 1.487 |
| 210 | 48.62 | 1.033 | 0.890 | 1.831 | 1.891 |
| 240 | 48.48 | 1.030 | 0.880 | 1.815 | 1.870 |
| 270 | 49.77 | 1.058 | 0.790 | 1.587 | 1.679 |
| 300 | 48.92 | 1.040 | 0.710 | 1.451 | 1.509 |
| 330 | 49.65 | 1.055 | 0.740 | 1.490 | 1.572 |

| ANGLE | SPEED | SPEED RATIO | RMS SPEED | LOCAL INT | TURB INT |
|---|---|---|---|---|---|
| | | X= 5.20 | | R=0.600 | |
| 0 | 48.82 | 1.037 | 0.820 | 1.680 | 1.742 |
| 10 | 48.70 | 1.035 | 0.840 | 1.725 | 1.785 |
| 30 | 49.60 | 1.054 | 1.050 | 2.117 | 2.231 |
| 60 | 49.72 | 1.057 | 0.980 | 1.971 | 2.082 |
| 90 | 50.13 | 1.065 | 0.720 | 1.436 | 1.530 |
| 120 | 50.80 | 1.079 | 0.690 | 1.358 | 1.466 |
| 150 | 51.53 | 1.095 | 0.740 | 1.436 | 1.572 |
| 180 | 48.77 | 1.036 | 0.730 | 1.497 | 1.551 |
| 210 | 49.55 | 1.053 | 0.840 | 1.695 | 1.785 |
| 240 | 49.77 | 1.058 | 0.990 | 1.989 | 2.104 |
| 270 | 51.20 | 1.088 | 0.780 | 1.523 | 1.657 |
| 300 | 50.45 | 1.072 | 0.750 | 1.487 | 1.594 |
| 330 | 50.58 | 1.075 | 0.700 | 1.384 | 1.487 |
| | | X= 5.20 | | R=0.700 | |
| 0 | 50.60 | 1.075 | 0.780 | 1.542 | 1.657 |
| 10 | 50.45 | 1.072 | 0.790 | 1.566 | 1.679 |
| 30 | 51.75 | 1.100 | 1.190 | 2.300 | 2.529 |
| 60 | 52.25 | 1.110 | 1.050 | 2.010 | 2.231 |
| 90 | 51.20 | 1.088 | 0.730 | 1.426 | 1.551 |
| 120 | 51.85 | 1.102 | 0.680 | 1.311 | 1.445 |
| 150 | 52.83 | 1.123 | 0.770 | 1.458 | 1.636 |
| 180 | 50.60 | 1.075 | 0.710 | 1.403 | 1.509 |
| 210 | 51.00 | 1.084 | 0.810 | 1.588 | 1.721 |
| 240 | 52.70 | 1.120 | 1.030 | 1.954 | 2.189 |
| 270 | 53.52 | 1.137 | 0.830 | 1.551 | 1.764 |
| 300 | 52.50 | 1.116 | 0.820 | 1.562 | 1.742 |
| 330 | 52.25 | 1.110 | 0.780 | 1.493 | 1.657 |
| | | X= 5.20 | | R=0.800 | |
| 0 | 51.53 | 1.095 | 0.800 | 1.552 | 1.700 |
| 30 | 53.90 | 1.145 | 1.230 | 2.282 | 2.614 |
| 60 | 53.60 | 1.139 | 1.030 | 1.922 | 2.189 |
| 90 | 52.25 | 1.110 | 0.850 | 1.627 | 1.806 |
| 120 | 52.72 | 1.120 | 0.720 | 1.366 | 1.530 |
| 150 | 53.50 | 1.137 | 0.790 | 1.477 | 1.679 |
| 180 | 51.63 | 1.097 | 0.710 | 1.375 | 1.509 |
| 210 | 52.68 | 1.119 | 0.920 | 1.746 | 1.955 |
| 240 | 55.48 | 1.179 | 0.940 | 1.694 | 1.997 |
| 270 | 54.88 | 1.166 | 0.810 | 1.476 | 1.721 |
| 300 | 53.75 | 1.142 | 0.880 | 1.637 | 1.870 |
| 330 | 53.55 | 1.138 | 0.870 | 1.625 | 1.849 |

| ANGLE | SPEED | SPEED RATIO | RMS SPEED | LOCAL INT | TURB INT |
|---|---|---|---|---|---|
| | | X= 5.20 | | R=0.900 | |
| 0 | 52.53 | 1.116 | 0.830 | 1.580 | 1.764 |
| 30 | 56.00 | 1.190 | 1.070 | 1.911 | 2.274 |
| 60 | 55.66 | 1.183 | 0.840 | 1.509 | 1.785 |
| 90 | 54.15 | 1.151 | 0.990 | 1.828 | 2.104 |
| 120 | 53.68 | 1.141 | 0.690 | 1.285 | 1.466 |
| 150 | 54.52 | 1.159 | 0.730 | 1.339 | 1.551 |
| 180 | 53.10 | 1.128 | 0.750 | 1.412 | 1.594 |
| 210 | 54.75 | 1.163 | 0.950 | 1.735 | 2.019 |
| 240 | 57.70 | 1.226 | 0.810 | 1.404 | 1.721 |
| 270 | 56.75 | 1.206 | 0.760 | 1.339 | 1.615 |
| 300 | 55.75 | 1.185 | 0.890 | 1.596 | 1.891 |
| 330 | 55.20 | 1.173 | 0.920 | 1.667 | 1.955 |
| | | X= 5.20 | | R=1.000 | |
| 0 | 53.65 | 1.140 | 0.920 | 1.715 | 1.955 |
| 30 | 57.87 | 1.230 | 0.920 | 1.590 | 1.955 |
| 60 | 57.65 | 1.225 | 0.700 | 1.214 | 1.487 |
| 90 | 56.50 | 1.201 | 0.880 | 1.558 | 1.870 |
| 120 | 54.87 | 1.166 | 0.720 | 1.312 | 1.530 |
| 150 | 55.75 | 1.185 | 0.730 | 1.309 | 1.551 |
| 180 | 55.35 | 1.176 | 0.770 | 1.391 | 1.636 |
| 210 | 57.50 | 1.222 | 0.790 | 1.374 | 1.679 |
| 240 | 59.80 | 1.271 | 0.690 | 1.154 | 1.466 |
| 270 | 59.00 | 1.254 | 0.680 | 1.153 | 1.445 |
| 300 | 57.87 | 1.230 | 0.720 | 1.244 | 1.530 |
| 330 | 56.72 | 1.205 | 0.920 | 1.622 | 1.955 |
| | | X= 5.20 | | R=1.100 | |
| 0 | 55.63 | 1.182 | 1.100 | 1.977 | 2.337 |
| 30 | 60.05 | 1.276 | 0.870 | 1.449 | 1.849 |
| 60 | 59.25 | 1.259 | 0.640 | 1.080 | 1.360 |
| 90 | 58.63 | 1.246 | 0.650 | 1.109 | 1.381 |
| 120 | 56.70 | 1.205 | 0.770 | 1.356 | 1.636 |
| 150 | 57.75 | 1.227 | 0.790 | 1.368 | 1.679 |
| 162 | 56.70 | 1.205 | 0.820 | 1.446 | 1.742 |
| 180 | 57.70 | 1.226 | 0.750 | 1.300 | 1.594 |
| 210 | 60.00 | 1.275 | 0.720 | 1.200 | 1.530 |
| 240 | 61.60 | 1.309 | 0.660 | 1.071 | 1.402 |
| 270 | 61.30 | 1.303 | 0.650 | 1.060 | 1.381 |
| 300 | 59.86 | 1.272 | 0.590 | 0.986 | 1.254 |
| 330 | 58.63 | 1.246 | 0.970 | 1.654 | 2.061 |

| ANGLE | SPEED | SPEED RATIO | RMS SPEED | LOCAL INT | TURB INT |
|---|---|---|---|---|---|
| | | X= 5.20 | | R=1.200 | |
| 0 | 57.85 | 1.229 | 1.100 | 1.901 | 2.337 |
| 30 | 62.40 | 1.326 | 0.900 | 1.442 | 1.912 |
| 60 | 61.10 | 1.298 | 0.620 | 1.015 | 1.317 |
| 90 | 60.03 | 1.276 | 0.580 | 0.966 | 1.232 |
| 120 | 58.80 | 1.249 | 0.700 | 1.190 | 1.487 |
| 150 | 60.00 | 1.275 | 0.840 | 1.400 | 1.785 |
| 168 | 58.75 | 1.248 | 0.780 | 1.328 | 1.657 |
| 180 | 60.00 | 1.275 | 0.720 | 1.200 | 1.530 |
| 210 | 62.25 | 1.323 | 0.580 | 0.932 | 1.232 |
| 240 | 63.70 | 1.354 | 0.590 | 0.926 | 1.254 |
| 270 | 63.80 | 1.356 | 0.700 | 1.097 | 1.487 |
| 300 | 61.25 | 1.302 | 0.610 | 0.996 | 1.296 |
| 330 | 60.03 | 1.276 | 1.060 | 1.766 | 2.252 |
| | | X= 5.20 | | R=1.300 | |
| 0 | 60.87 | 1.293 | 1.000 | 1.643 | 2.125 |
| 30 | 65.20 | 1.385 | 0.920 | 1.411 | 1.955 |
| 60 | 63.68 | 1.353 | 0.590 | 0.927 | 1.254 |
| 90 | 62.55 | 1.329 | 0.630 | 1.007 | 1.339 |
| 120 | 61.80 | 1.313 | 0.710 | 1.149 | 1.509 |
| 150 | 63.35 | 1.346 | 0.800 | 1.263 | 1.700 |
| 180 | 62.43 | 1.327 | 0.680 | 1.089 | 1.445 |
| 210 | 64.28 | 1.366 | 0.560 | 0.871 | 1.190 |
| 240 | 66.24 | 1.408 | 0.610 | 0.921 | 1.296 |
| 270 | 66.76 | 1.419 | 0.660 | 0.989 | 1.402 |
| 300 | 63.72 | 1.354 | 0.660 | 1.036 | 1.402 |
| 330 | 63.50 | 1.349 | 1.080 | 1.701 | 2.295 |
| | | X= 5.20 | | R=1.400 | |
| 0 | 63.25 | 1.344 | 1.200 | 1.897 | 2.550 |
| 30 | 68.50 | 1.456 | 0.850 | 1.241 | 1.806 |
| 60 | 66.20 | 1.407 | 0.620 | 0.937 | 1.317 |
| 90 | 66.20 | 1.407 | 0.700 | 1.057 | 1.487 |
| 120 | 65.30 | 1.388 | 0.780 | 1.194 | 1.657 |
| 150 | 66.30 | 1.409 | 0.760 | 1.146 | 1.615 |
| 180 | 64.86 | 1.378 | 0.710 | 1.095 | 1.509 |
| 210 | 67.30 | 1.430 | 0.630 | 0.936 | 1.339 |
| 240 | 70.00 | 1.487 | 0.690 | 0.986 | 1.466 |
| 270 | 70.10 | 1.490 | 0.650 | 0.927 | 1.381 |
| 300 | 66.37 | 1.410 | 0.670 | 1.009 | 1.424 |
| 330 | 66.13 | 1.405 | 1.030 | 1.558 | 2.189 |

| ANGLE | SPEED | SPEED RATIO | RMS SPEED | LOCAL INT | TURB INT |
|---|---|---|---|---|---|
| | | X= 5.20 | | R=1.450 | |
| 0 | 64.32 | 1.367 | 1.450 | 2.254 | 3.081 |
| 30 | 68.75 | 1.461 | 0.800 | 1.164 | 1.700 |
| 60 | 66.80 | 1.419 | 0.660 | 0.988 | 1.402 |
| 90 | 67.20 | 1.428 | 0.670 | 0.997 | 1.424 |
| 120 | 66.80 | 1.419 | 0.790 | 1.183 | 1.679 |
| 150 | 67.70 | 1.439 | 0.730 | 1.078 | 1.551 |
| 180 | 66.05 | 1.404 | 0.770 | 1.166 | 1.636 |
| 210 | 68.20 | 1.449 | 0.650 | 0.953 | 1.381 |
| 240 | 71.25 | 1.514 | 0.680 | 0.954 | 1.445 |
| 270 | 70.45 | 1.497 | 0.650 | 0.923 | 1.381 |
| 300 | 67.45 | 1.433 | 0.690 | 1.023 | 1.466 |
| 330 | 61.05 | 1.297 | 0.960 | 1.572 | 2.040 |
| | | X= 4.50 | | R=0.000 | |
| 0 | 39.87 | 0.847 | 1.000 | 2.508 | 2.125 |
| 60 | 39.62 | 0.842 | 1.030 | 2.600 | 2.189 |
| 120 | 39.05 | 0.830 | 1.020 | 2.612 | 2.167 |
| 180 | 39.05 | 0.830 | 1.020 | 2.612 | 2.167 |
| 240 | 39.40 | 0.837 | 1.000 | 2.538 | 2.125 |
| 300 | 39.80 | 0.846 | 1.020 | 2.563 | 2.167 |
| | | X= 4.50 | | R=0.200 | |
| 0 | 39.87 | 0.847 | 0.900 | 2.257 | 1.912 |
| 60 | 41.75 | 0.887 | 0.840 | 2.012 | 1.785 |
| 90 | 42.13 | 0.895 | 0.800 | 1.899 | 1.700 |
| 120 | 41.50 | 0.882 | 0.840 | 2.024 | 1.785 |
| 180 | 39.72 | 0.844 | 0.950 | 2.392 | 2.019 |
| 240 | 38.20 | 0.812 | 0.840 | 2.199 | 1.785 |
| 300 | 38.90 | 0.827 | 0.870 | 2.237 | 1.849 |
| | | X= 4.50 | | R=0.400 | |
| 0 | 40.50 | 0.861 | 0.930 | 2.296 | 1.976 |
| 60 | 42.20 | 0.897 | 0.940 | 2.227 | 1.997 |
| 90 | 43.00 | 0.914 | 0.740 | 1.721 | 1.572 |
| 120 | 42.90 | 0.912 | 0.700 | 1.632 | 1.487 |
| 180 | 41.50 | 0.882 | 0.750 | 1.807 | 1.594 |
| 235 | 39.23 | 0.834 | 0.910 | 2.320 | 1.934 |
| 240 | 39.25 | 0.834 | 0.920 | 2.344 | 1.955 |
| 300 | 40.80 | 0.867 | 0.790 | 1.936 | 1.679 |

| ANGLE | SPEED | SPEED RATIO | RMS SPEED | LOCAL INT | TURB INT |
|---|---|---|---|---|---|
| | | X= 4.50 | | R=0.600 | |
| 0 | 42.37 | 0.900 | 0.840 | 1.983 | 1.785 |
| 60 | 43.20 | 0.918 | 1.000 | 2.315 | 2.125 |
| 120 | 44.75 | 0.951 | 0.710 | 1.587 | 1.509 |
| 140 | 45.50 | 0.967 | 0.770 | 1.692 | 1.636 |
| 180 | 42.50 | 0.903 | 0.690 | 1.624 | 1.466 |
| 225 | 41.50 | 0.882 | 1.000 | 2.410 | 2.125 |
| 240 | 42.50 | 0.903 | 1.050 | 2.471 | 2.231 |
| 300 | 43.27 | 0.919 | 0.760 | 1.756 | 1.615 |
| | | X= 4.50 | | R=0.800 | |
| 0 | 44.22 | 0.940 | 0.800 | 1.809 | 1.700 |
| 60 | 46.77 | 0.994 | 1.160 | 2.480 | 2.465 |
| 120 | 46.25 | 0.983 | 0.710 | 1.535 | 1.509 |
| 135 | 48.00 | 1.020 | 0.740 | 1.542 | 1.572 |
| 180 | 44.25 | 0.940 | 0.710 | 1.605 | 1.509 |
| 240 | 47.90 | 1.018 | 1.100 | 2.296 | 2.337 |
| 263 | 48.50 | 1.031 | 0.960 | 1.979 | 2.040 |
| 270 | 48.45 | 1.030 | 0.880 | 1.816 | 1.870 |
| 300 | 46.87 | 0.996 | 0.920 | 1.963 | 1.955 |
| | | X= 4.50 | | R=1.000 | |
| 0 | 46.55 | 0.989 | 0.870 | 1.869 | 1.849 |
| 60 | 50.72 | 1.078 | 0.810 | 1.597 | 1.721 |
| 120 | 48.55 | 1.032 | 0.710 | 1.462 | 1.509 |
| 180 | 47.87 | 1.017 | 0.810 | 1.692 | 1.721 |
| 240 | 53.00 | 1.126 | 0.790 | 1.491 | 1.679 |
| 300 | 51.00 | 1.084 | 0.890 | 1.745 | 1.891 |
| | | X= 4.50 | | R=1.200 | |
| 0 | 49.63 | 1.055 | 1.150 | 2.317 | 2.444 |
| 40 | 55.50 | 1.179 | 0.670 | 1.207 | 1.424 |
| 60 | 54.25 | 1.153 | 0.630 | 1.161 | 1.339 |
| 120 | 51.72 | 1.099 | 0.760 | 1.469 | 1.615 |
| 180 | 52.68 | 1.119 | 0.780 | 1.481 | 1.657 |
| 240 | 56.75 | 1.206 | 0.640 | 1.128 | 1.360 |
| 300 | 54.62 | 1.161 | 0.590 | 1.080 | 1.254 |
| | | X= 4.50 | | R=1.300 | |
| 0 | 52.00 | 1.105 | 1.150 | 2.212 | 2.444 |
| 35 | 57.48 | 1.221 | 0.790 | 1.374 | 1.679 |

| ANGLE | SPEED | SPEED RATIO | RMS SPEED | LOCAL INT | TURB INT |
|---|---|---|---|---|---|
| 60 | 56.20 | 1.194 | 0.610 | 1.085 | 1.296 |
| 120 | 53.82 | 1.144 | 0.700 | 1.301 | 1.487 |
| 180 | 55.00 | 1.169 | 0.730 | 1.327 | 1.551 |
| 240 | 58.75 | 1.248 | 0.590 | 1.004 | 1.254 |
| 300 | 56.20 | 1.194 | 0.620 | 1.103 | 1.317 |
| | | X= 4.50 | | R=1.400 | |
| 0 | 53.87 | 1.145 | 1.080 | 2.005 | 2.295 |
| 60 | 58.90 | 1.252 | 0.610 | 1.036 | 1.296 |
| 120 | 57.62 | 1.224 | 0.740 | 1.284 | 1.572 |
| 180 | 57.78 | 1.228 | 0.700 | 1.211 | 1.467 |
| 240 | 62.30 | 1.324 | 0.640 | 1.027 | 1.360 |
| 300 | 58.12 | 1.235 | 0.680 | 1.170 | 1.445 |
| | | X= 4.50 | | R=1.575 | |
| 0 | 58.72 | 1.248 | 3.140 | 5.347 | 6.672 |
| 60 | 63.70 | 1.354 | 2.120 | 3.328 | 4.505 |
| 120 | 63.25 | 1.344 | 0.990 | 1.565 | 2.104 |
| 180 | 62.40 | 1.326 | 1.080 | 1.731 | 2.295 |
| 240 | 67.50 | 1.434 | 1.080 | 1.600 | 2.295 |
| 300 | 64.25 | 1.365 | 2.120 | 3.300 | 4.505 |
| | | X= 4.50 | | R=1.600 | |
| 0 | 58.00 | 1.232 | 3.520 | 6.069 | 7.480 |
| 60 | 61.15 | 1.299 | 3.020 | 4.939 | 6.417 |
| 120 | 58.90 | 1.252 | 1.770 | 3.005 | 3.761 |
| 155 | 51.63 | 1.097 | 4.210 | 8.154 | 8.946 |
| 180 | 56.82 | 1.207 | 3.410 | 6.001 | 7.246 |
| 240 | 63.27 | 1.344 | 3.220 | 5.089 | 6.842 |
| 260 | 64.50 | 1.371 | 2.750 | 4.264 | 5.844 |
| 300 | 62.28 | 1.323 | 3.060 | 4.913 | 6.502 |
| | | X= 3.50 | | R=0.000 | |
| 0 | 23.00 | 0.489 | 1.180 | 5.130 | 2.507 |
| 60 | 22.87 | 0.486 | 1.180 | 5.160 | 2.507 |
| 120 | 22.35 | 0.475 | 1.180 | 5.280 | 2.507 |
| 180 | 22.50 | 0.478 | 1.180 | 5.244 | 2.507 |
| 240 | 22.95 | 0.488 | 1.200 | 5.229 | 2.550 |
| 300 | 23.00 | 0.489 | 1.180 | 5.130 | 2.507 |

| ANGLE | SPEED | SPEED RATIO | RMS SPEED | LOCAL INT | TURB INT |
|---|---|---|---|---|---|
| | | X= 3.50 | | R=0.200 | |
| 0 | 23.75 | 0.505 | 1.060 | 4.463 | 2.252 |
| 60 | 25.84 | 0.549 | 1.000 | 3.870 | 2.125 |
| 90 | 25.95 | 0.551 | 1.000 | 3.854 | 2.125 |
| 120 | 25.30 | 0.538 | 1.060 | 4.190 | 2.252 |
| 180 | 22.90 | 0.487 | 1.160 | 5.066 | 2.465 |
| 240 | 20.30 | 0.431 | 1.080 | 5.320 | 2.295 |
| 300 | 21.50 | 0.457 | 1.080 | 5.023 | 2.295 |
| | | X= 3.50 | | R=0.400 | |
| 0 | 24.10 | 0.512 | 0.960 | 3.983 | 2.040 |
| 60 | 26.50 | 0.563 | 1.020 | 3.849 | 2.167 |
| 90 | 27.50 | 0.584 | 0.800 | 2.909 | 1.700 |
| 120 | 27.18 | 0.578 | 0.790 | 2.907 | 1.679 |
| 180 | 24.90 | 0.529 | 0.910 | 3.655 | 1.934 |
| 240 | 21.20 | 0.450 | 1.060 | 5.000 | 2.252 |
| 300 | 23.70 | 0.504 | 0.970 | 4.093 | 2.061 |
| | | X= 3.50 | | R=0.600 | |
| 0 | 25.30 | 0.538 | 1.050 | 4.150 | 2.231 |
| 60 | 26.60 | 0.565 | 1.080 | 4.060 | 2.295 |
| 90 | 28.50 | 0.606 | 0.840 | 2.947 | 1.785 |
| 120 | 28.55 | 0.607 | 0.800 | 2.802 | 1.700 |
| 140 | 29.00 | 0.616 | 0.910 | 3.138 | 1.934 |
| 180 | 25.95 | 0.551 | 0.800 | 3.083 | 1.700 |
| 240 | 23.50 | 0.499 | 1.070 | 4.553 | 2.274 |
| 300 | 25.80 | 0.548 | 0.830 | 3.217 | 1.764 |
| 340 | 26.00 | 0.552 | 0.940 | 3.615 | 1.997 |
| | | X= 3.50 | | R=0.800 | |
| 0 | 26.55 | 0.564 | 0.960 | 3.616 | 2.040 |
| 60 | 28.30 | 0.601 | 1.320 | 4.664 | 2.805 |
| 120 | 30.00 | 0.637 | 0.790 | 2.633 | 1.679 |
| 140 | 31.75 | 0.675 | 0.880 | 2.772 | 1.870 |
| 180 | 26.50 | 0.563 | 0.800 | 3.019 | 1.700 |
| 225 | 25.70 | 0.546 | 1.120 | 4.358 | 2.380 |
| 240 | 26.70 | 0.567 | 1.280 | 4.794 | 2.720 |
| 275 | 29.60 | 0.629 | 0.970 | 3.277 | 2.061 |
| 300 | 28.82 | 0.612 | 0.950 | 3.296 | 2.019 |

| ANGLE | SPEED | SPEED RATIO | RMS SPEED | LOCAL INT | TURB INT |
|---|---|---|---|---|---|
| | | X= 3.50 | | R=1.000 | |
| 0 | 27.90 | 0.593 | 0.920 | 3.297 | 1.955 |
| 50 | 33.75 | 0.717 | 1.350 | 4.000 | 2.869 |
| 60 | 32.10 | 0.682 | 1.400 | 4.361 | 2.975 |
| 90 | 29.75 | 0.632 | 0.920 | 3.092 | 1.955 |
| 120 | 31.25 | 0.664 | 0.810 | 2.592 | 1.721 |
| 140 | 33.95 | 0.721 | 0.810 | 2.386 | 1.721 |
| 180 | 27.82 | 0.591 | 0.840 | 3.019 | 1.785 |
| 195 | 27.25 | 0.579 | 0.840 | 3.083 | 1.785 |
| 240 | 32.40 | 0.688 | 1.450 | 4.475 | 3.081 |
| 260 | 33.40 | 0.710 | 1.240 | 3.713 | 2.635 |
| 300 | 31.25 | 0.664 | 1.080 | 3.456 | 2.295 |
| | | X= 3.50 | | R=1.200 | |
| 0 | 29.25 | 0.622 | 0.970 | 3.316 | 2.061 |
| 60 | 35.77 | 0.760 | 1.040 | 2.907 | 2.210 |
| 120 | 32.60 | 0.693 | 0.820 | 2.515 | 1.742 |
| 180 | 31.00 | 0.659 | 0.950 | 3.065 | 2.019 |
| 240 | 38.10 | 0.810 | 1.060 | 2.782 | 2.252 |
| 300 | 35.20 | 0.748 | 1.140 | 3.239 | 2.422 |
| | | X= 3.50 | | R=1.300 | |
| 0 | 29.97 | 0.637 | 1.030 | 3.437 | 2.189 |
| 60 | 37.32 | 0.793 | 0.870 | 2.331 | 1.849 |
| 120 | 33.65 | 0.715 | 0.870 | 2.585 | 1.849 |
| 140 | 36.53 | 0.776 | 0.700 | 1.916 | 1.487 |
| 180 | 32.75 | 0.696 | 1.040 | 3.176 | 2.210 |
| 240 | 39.80 | 0.846 | 0.870 | 2.186 | 1.849 |
| 300 | 37.30 | 0.793 | 1.010 | 2.708 | 2.146 |
| | | X= 3.50 | | R=1.400 | |
| 0 | 30.70 | 0.652 | 1.100 | 3.583 | 2.337 |
| 60 | 38.50 | 0.818 | 0.800 | 2.078 | 1.700 |
| 120 | 35.90 | 0.763 | 0.900 | 2.507 | 1.912 |
| 180 | 35.30 | 0.750 | 0.980 | 2.776 | 2.082 |
| 240 | 41.60 | 0.884 | 0.920 | 2.212 | 1.955 |
| 300 | 39.10 | 0.831 | 0.970 | 2.481 | 2.061 |
| | | X= 3.50 | | R=1.600 | |
| 0 | 33.80 | 0.718 | 1.450 | 4.290 | 3.081 |
| 60 | 41.00 | 0.871 | 0.670 | 1.634 | 1.424 |

| ANGLE | SPEED | SPEED RATIO | RMS SPEED | LOCAL INT | TURB INT |
|---|---|---|---|---|---|
| 120 | 38.80 | 0.824 | 0.870 | 2.242 | 1.849 |
| 180 | 39.25 | 0.834 | 0.870 | 2.217 | 1.849 |
| 240 | 44.15 | 0.938 | 0.660 | 1.495 | 1.402 |
| 300 | 40.95 | 0.870 | 0.700 | 1.709 | 1.487 |
| | | X= 3.50 | | R=1.800 | |
| 0 | 37.62 | 0.799 | 1.600 | 4.253 | 3.400 |
| 60 | 43.05 | 0.915 | 1.510 | 3.508 | 3.209 |
| 120 | 42.20 | 0.897 | 1.340 | 3.175 | 2.847 |
| 180 | 42.40 | 0.901 | 1.140 | 2.689 | 2.422 |
| 240 | 46.72 | 0.993 | 1.350 | 2.890 | 2.869 |
| 270 | 47.50 | 1.009 | 1.450 | 3.053 | 3.081 |
| 300 | 43.45 | 0.923 | 1.260 | 2.900 | 2.677 |
| | | X= 3.50 | | R=1.840 | |
| 0 | 38.00 | 0.807 | 1.920 | 5.053 | 4.080 |
| 60 | 42.37 | 0.900 | 2.560 | 6.042 | 5.440 |
| 120 | 42.45 | 0.902 | 1.880 | 4.429 | 3.995 |
| 180 | 42.55 | 0.904 | 1.660 | 3.901 | 3.527 |
| 240 | 46.22 | 0.982 | 2.190 | 4.738 | 4.654 |
| 265 | 46.82 | 0.995 | 2.250 | 4.806 | 4.781 |
| 300 | 43.32 | 0.921 | 2.010 | 4.640 | 4.271 |
| | | X= 3.50 | | R=1.950 | |
| 0 | 31.50 | 0.669 | 4.890 | 15.524 | 10.391 |
| 45 | 28.37 | 0.603 | 5.700 | 20.092 | 12.112 |
| 60 | 31.00 | 0.659 | 5.510 | 17.774 | 11.708 |
| 120 | 32.80 | 0.697 | 5.210 | 15.884 | 11.071 |
| 180 | 32.28 | 0.686 | 5.200 | 16.109 | 11.050 |
| 240 | 33.10 | 0.703 | 5.700 | 17.221 | 12.112 |
| 270 | 33.18 | 0.705 | 5.820 | 17.541 | 12.367 |
| 300 | 32.12 | 0.683 | 5.510 | 17.154 | 11.708 |
| | | X= 3.50 | | R=1.990 | |
| 0 | 26.62 | 0.566 | 5.030 | 18.896 | 10.688 |
| 45 | 22.72 | 0.483 | 5.110 | 22.491 | 10.858 |
| 60 | 25.25 | 0.537 | 5.100 | 20.198 | 10.837 |
| 120 | 26.68 | 0.567 | 4.910 | 18.403 | 10.433 |
| 180 | 25.30 | 0.538 | 4.810 | 19.012 | 10.221 |
| 240 | 26.82 | 0.570 | 5.180 | 19.314 | 11.007 |
| 265 | 27.75 | 0.590 | 5.290 | 19.063 | 11.241 |
| 300 | 25.97 | 0.552 | 5.100 | 19.638 | 10.837 |

| ANGLE | SPEED | SPEED RATIO | RMS SPEED | LOCAL INT | TURB INT |
|---|---|---|---|---|---|
| | | X= 2.50 | | R=0.000 | |
| 0 | 6.10 | 0.130 | 1.900 | 31.148 | 4.037 |
| 60 | 6.02 | 0.128 | 1.840 | 30.565 | 3.910 |
| 120 | 5.30 | 0.113 | 1.900 | 35.849 | 4.037 |
| 180 | 5.30 | 0.113 | 1.880 | 35.472 | 3.995 |
| 240 | 5.70 | 0.121 | 1.860 | 32.632 | 3.952 |
| 300 | 6.15 | 0.131 | 1.920 | 31.220 | 4.080 |
| | | X= 2.50 | | R=0.200 | |
| 0 | 7.75 | 0.165 | 1.790 | 23.097 | 3.804 |
| 60 | 11.00 | 0.234 | 1.810 | 16.455 | 3.846 |
| 120 | 9.50 | 0.202 | 1.940 | 20.421 | 4.122 |
| 180 | 5.13 | 0.109 | 1.750 | 34.113 | 3.719 |
| 240 | 3.51 | 0.075 | 1.620 | 46.154 | 3.442 |
| 300 | 4.65 | 0.099 | 1.700 | 36.559 | 3.612 |
| | | X= 2.50 | | R=0.400 | |
| 0 | 9.45 | 0.201 | 1.480 | 15.661 | 3.145 |
| 60 | 14.75 | 0.313 | 1.270 | 8.610 | 2.699 |
| 90 | 15.55 | 0.330 | 1.270 | 8.167 | 2.699 |
| 120 | 13.50 | 0.287 | 1.480 | 10.963 | 3.145 |
| 180 | 7.20 | 0.153 | 1.780 | 24.722 | 3.782 |
| 240 | 4.37 | 0.093 | 1.600 | 36.613 | 3.400 |
| 300 | 6.25 | 0.133 | 1.670 | 26.720 | 3.549 |
| | | X= 2.50 | | R=0.600 | |
| 0 | 11.45 | 0.243 | 1.340 | 11.703 | 2.847 |
| 60 | 15.25 | 0.324 | 1.250 | 8.197 | 2.656 |
| 90 | 17.30 | 0.368 | 0.940 | 5.434 | 1.997 |
| 120 | 16.25 | 0.345 | 1.000 | 6.154 | 2.125 |
| 180 | 11.25 | 0.239 | 1.550 | 13.778 | 3.294 |
| 225 | 5.80 | 0.123 | 1.620 | 27.931 | 3.442 |
| 240 | 6.15 | 0.131 | 1.620 | 26.341 | 3.442 |
| 300 | 10.00 | 0.212 | 1.480 | 14.800 | 3.145 |
| | | X= 2.50 | | R=0.800 | |
| 0 | 13.10 | 0.278 | 1.320 | 10.076 | 2.805 |
| 60 | 15.00 | 0.319 | 1.300 | 8.667 | 2.762 |
| 90 | 18.20 | 0.387 | 0.930 | 5.110 | 1.976 |
| 120 | 18.00 | 0.382 | 0.910 | 5.056 | 1.934 |
| 180 | 14.30 | 0.304 | 1.100 | 7.692 | 2.337 |

| ANGLE | SPEED | SPEED RATIO | RMS SPEED | LOCAL INT | TURB INT |
|---|---|---|---|---|---|
| 240 | 8.30 | 0.176 | 1.720 | 20.723 | 3.655 |
| 300 | 13.30 | 0.283 | 1.180 | 8.872 | 2.507 |
| | | X= 2.50 | | R=1.000 | |
| 0 | 14.70 | 0.312 | 1.320 | 8.980 | 2.805 |
| 60 | 16.40 | 0.348 | 1.490 | 9.085 | 3.166 |
| 90 | 19.20 | 0.408 | 0.940 | 4.896 | 1.997 |
| 120 | 19.90 | 0.423 | 0.930 | 4.673 | 1.976 |
| 140 | 21.30 | 0.453 | 1.050 | 4.930 | 2.231 |
| 180 | 15.30 | 0.325 | 0.990 | 6.471 | 2.104 |
| 240 | 11.25 | 0.239 | 1.730 | 15.378 | 3.676 |
| 300 | 16.00 | 0.340 | 1.030 | 6.437 | 2.189 |
| | | X= 2.50 | | R=1.200 | |
| 0 | 16.30 | 0.346 | 1.230 | 7.546 | 2.614 |
| 60 | 20.70 | 0.440 | 1.860 | 8.986 | 3.952 |
| 120 | 21.25 | 0.452 | 0.890 | 4.188 | 1.891 |
| 140 | 24.25 | 0.515 | 0.980 | 4.041 | 2.082 |
| 180 | 15.70 | 0.334 | 0.970 | 6.178 | 2.061 |
| 225 | 14.60 | 0.310 | 1.690 | 11.575 | 3.591 |
| 240 | 16.10 | 0.342 | 1.880 | 11.677 | 3.995 |
| 270 | 21.50 | 0.457 | 1.420 | 6.605 | 3.017 |
| 300 | 18.70 | 0.397 | 1.200 | 6.417 | 2.550 |
| | | X= 2.50 | | R=1.300 | |
| 0 | 17.10 | 0.363 | 1.130 | 6.608 | 2.401 |
| 60 | 23.30 | 0.495 | 1.780 | 7.639 | 3.782 |
| 120 | 21.80 | 0.463 | 0.900 | 4.128 | 1.912 |
| 138 | 25.75 | 0.547 | 0.930 | 3.612 | 1.976 |
| 180 | 16.30 | 0.346 | 1.020 | 6.258 | 2.167 |
| 189 | 15.80 | 0.336 | 1.000 | 6.329 | 2.125 |
| 240 | 19.75 | 0.420 | 2.010 | 10.177 | 4.271 |
| 270 | 23.60 | 0.501 | 1.390 | 5.890 | 2.954 |
| 300 | 20.60 | 0.438 | 1.280 | 6.214 | 2.720 |
| | | X= 2.50 | | R=1.400 | |
| 0 | 18.80 | 0.399 | 1.020 | 5.426 | 2.167 |
| 38 | 28.05 | 0.596 | 1.560 | 5.561 | 3.315 |
| 60 | 24.80 | 0.527 | 1.500 | 6.048 | 3.187 |
| 120 | 24.20 | 0.514 | 0.960 | 3.967 | 2.040 |
| 135 | 27.70 | 0.589 | 0.760 | 2.744 | 1.615 |
| 180 | 19.04 | 0.405 | 1.040 | 5.462 | 2.210 |

| ANGLE | SPEED | SPEED RATIO | RMS SPEED | LOCAL INT | TURB INT |
|---|---|---|---|---|---|
| 189 | 17.92 | 0.381 | 1.050 | 5.859 | 2.231 |
| 240 | 23.80 | 0.506 | 1.860 | 7.815 | 3.952 |
| 300 | 22.68 | 0.482 | 1.310 | 5.776 | 2.784 |
| | | X= 2.50 | | R=1.600 | |
| 0 | 20.25 | 0.430 | 1.060 | 5.235 | 2.252 |
| 40 | 32.20 | 0.684 | 1.110 | 3.447 | 2.359 |
| 60 | 29.10 | 0.618 | 1.210 | 4.158 | 2.571 |
| 120 | 25.37 | 0.539 | 0.950 | 3.745 | 2.019 |
| 180 | 22.63 | 0.481 | 1.150 | 5.082 | 2.444 |
| 240 | 30.67 | 0.652 | 1.510 | 4.923 | 3.209 |
| 247 | 32.17 | 0.684 | 1.100 | 3.419 | 2.337 |
| 300 | 27.20 | 0.578 | 1.360 | 5.000 | 2.890 |
| | | X= 2.50 | | R=1.800 | |
| 0 | 21.90 | 0.465 | 1.190 | 5.434 | 2.529 |
| 40 | 35.30 | 0.750 | 0.950 | 2.691 | 2.019 |
| 60 | 32.40 | 0.688 | 0.830 | 2.562 | 1.764 |
| 120 | 27.80 | 0.591 | 1.060 | 3.813 | 2.252 |
| 180 | 27.47 | 0.584 | 1.210 | 4.405 | 2.571 |
| 247 | 35.70 | 0.759 | 0.900 | 2.521 | 1.912 |
| 300 | 32.25 | 0.685 | 0.930 | 2.884 | 1.976 |
| | | X= 2.50 | | R=2.000 | |
| 0 | 25.30 | 0.538 | 1.670 | 6.601 | 3.549 |
| 35 | 37.70 | 0.801 | 1.270 | 3.369 | 2.699 |
| 60 | 34.70 | 0.737 | 0.820 | 2.363 | 1.742 |
| 120 | 31.10 | 0.661 | 1.040 | 3.344 | 2.210 |
| 180 | 31.75 | 0.675 | 1.030 | 3.244 | 2.189 |
| 240 | 38.22 | 0.812 | 0.760 | 1.988 | 1.615 |
| 273 | 38.90 | 0.827 | 0.970 | 2.494 | 2.061 |
| 300 | 34.45 | 0.732 | 0.820 | 2.380 | 1.742 |
| | | X= 2.50 | | R=2.200 | |
| 0 | 29.85 | 0.634 | 1.930 | 6.466 | 4.101 |
| 60 | 32.55 | 0.692 | 3.500 | 10.753 | 7.437 |
| 120 | 34.00 | 0.722 | 1.890 | 5.559 | 4.016 |
| 180 | 34.62 | 0.736 | 1.550 | 4.477 | 3.294 |
| 240 | 38.22 | 0.812 | 2.670 | 6.986 | 5.674 |
| 264 | 39.00 | 0.829 | 2.670 | 6.846 | 5.674 |
| 300 | 35.28 | 0.750 | 2.360 | 6.689 | 5.015 |

| ANGLE | SPEED | SPEED RATIO | RMS SPEED | LOCAL INT | TURB INT |
|---|---|---|---|---|---|
| | | X= 2.50 | | R=2.375 | |
| 0 | 20.10 | 0.427 | 4.210 | 20.945 | 8.946 |
| 45 | 14.22 | 0.302 | 4.590 | 32.278 | 9.754 |
| 60 | 17.05 | 0.362 | 4.500 | 26.393 | 9.562 |
| 120 | 21.22 | 0.451 | 4.290 | 20.217 | 9.116 |
| 180 | 21.75 | 0.462 | 4.240 | 19.494 | 9.010 |
| 195 | 22.60 | 0.480 | 4.380 | 19.381 | 9.307 |
| 240 | 21.70 | 0.461 | 4.520 | 20.829 | 9.605 |
| 270 | 22.68 | 0.482 | 4.680 | 20.635 | 9.945 |
| 300 | 20.22 | 0.430 | 4.540 | 22.453 | 9.647 |
| | | X= 2.50 | | R=2.420 | |
| 0 | 16.58 | 0.352 | 3.950 | 23.824 | 8.394 |
| 45 | 10.70 | 0.227 | 4.030 | 37.664 | 8.564 |
| 60 | 13.58 | 0.289 | 4.080 | 30.044 | 8.670 |
| 120 | 17.12 | 0.364 | 3.880 | 22.664 | 8.245 |
| 180 | 17.44 | 0.371 | 3.800 | 21.789 | 8.075 |
| 195 | 18.70 | 0.397 | 3.960 | 21.176 | 8.415 |
| 240 | 17.85 | 0.379 | 4.100 | 22.969 | 8.712 |
| 265 | 18.75 | 0.398 | 4.220 | 22.507 | 8.967 |
| 300 | 16.28 | 0.346 | 4.100 | 25.184 | 8.712 |
| | | X= 1.75 | | R=0.000 | |
| 0 | 1.56 | 0.033 | 0.960 | 61.538 | 2.040 |
| 60 | 1.70 | 0.036 | 1.010 | 59.412 | 2.146 |
| 120 | 1.49 | 0.032 | 0.920 | 61.745 | 1.955 |
| 180 | 1.55 | 0.033 | 0.980 | 63.226 | 2.082 |
| 240 | 1.70 | 0.036 | 1.010 | 59.412 | 2.146 |
| 300 | 1.48 | 0.031 | 0.940 | 63.514 | 1.997 |
| | | X= 1.75 | | R=0.200 | |
| 0 | 1.74 | 0.037 | 1.030 | 59.195 | 2.189 |
| 60 | 2.06 | 0.044 | 1.300 | 63.107 | 2.762 |
| 120 | 1.73 | 0.037 | 1.050 | 60.694 | 2.231 |
| 180 | 1.48 | 0.031 | 0.930 | 62.838 | 1.976 |
| 240 | 1.62 | 0.034 | 1.000 | 61.728 | 2.125 |
| 300 | 1.48 | 0.031 | 0.900 | 60.811 | 1.912 |
| | | X= 1.75 | | R=0.400 | |
| 0 | 2.01 | 0.043 | 0.980 | 48.756 | 2.082 |
| 60 | 4.13 | 0.088 | 1.200 | 29.056 | 2.550 |

| ANGLE | SPEED | SPEED RATIO | RMS SPEED | LOCAL INT | TURB INT |
|---|---|---|---|---|---|
| 120 | 2.52 | 0.054 | 1.150 | 45.635 | 2.444 |
| 180 | 1.50 | 0.032 | 0.940 | 62.667 | 1.997 |
| 240 | 1.62 | 0.034 | 0.980 | 60.494 | 2.082 |
| 300 | 1.56 | 0.033 | 0.900 | 57.692 | 1.912 |
| | | X= 1.75 | | R=0.600 | |
| 0 | 2.75 | 0.058 | 1.550 | 56.364 | 3.294 |
| 60 | 8.48 | 0.180 | 2.680 | 31.604 | 5.695 |
| 120 | 5.40 | 0.115 | 2.700 | 50.000 | 5.737 |
| 180 | 1.80 | 0.038 | 1.160 | 64.444 | 2.465 |
| 240 | 1.70 | 0.036 | 1.060 | 62.353 | 2.252 |
| 300 | 1.86 | 0.040 | 1.180 | 63.441 | 2.507 |
| | | X= 1.75 | | R=0.800 | |
| 0 | 4.26 | 0.091 | 1.980 | 46.479 | 4.207 |
| 60 | 12.05 | 0.256 | 1.860 | 15.436 | 3.952 |
| 90 | 13.75 | 0.292 | 2.000 | 14.545 | 4.250 |
| 120 | 10.40 | 0.221 | 2.640 | 25.385 | 5.610 |
| 180 | 2.97 | 0.063 | 1.900 | 63.973 | 4.037 |
| 240 | 1.75 | 0.037 | 1.180 | 67.429 | 2.507 |
| 300 | 3.20 | 0.068 | 1.870 | 58.437 | 3.974 |
| | | X= 1.75 | | R=1.000 | |
| 0 | 6.85 | 0.146 | 2.260 | 32.993 | 4.802 |
| 60 | 12.00 | 0.255 | 1.820 | 15.167 | 3.867 |
| 90 | 15.55 | 0.330 | 1.180 | 7.588 | 2.507 |
| 120 | 13.90 | 0.295 | 1.640 | 11.799 | 3.485 |
| 180 | 6.05 | 0.129 | 2.560 | 42.314 | 5.440 |
| 240 | 2.20 | 0.047 | 1.540 | 70.000 | 3.272 |
| 300 | 6.30 | 0.134 | 2.470 | 39.206 | 5.249 |
| | | X= 1.75 | | R=1.200 | |
| 0 | 10.00 | 0.212 | 1.970 | 19.700 | 4.186 |
| 60 | 11.75 | 0.250 | 1.630 | 13.872 | 3.464 |
| 90 | 16.00 | 0.340 | 1.070 | 6.687 | 2.274 |
| 120 | 16.25 | 0.345 | 1.150 | 7.077 | 2.444 |
| 140 | 16.85 | 0.358 | 1.480 | 8.783 | 3.145 |
| 180 | 10.20 | 0.217 | 2.280 | 22.353 | 4.845 |
| 240 | 3.55 | 0.075 | 2.010 | 56.620 | 4.271 |
| 300 | 10.70 | 0.227 | 2.080 | 19.439 | 4.420 |

| ANGLE | SPEED | SPEED RATIO | RMS SPEED | LOCAL INT | TURB INT |
|---|---|---|---|---|---|
| | | X= 1.75 | | R=1.300 | |
| 0 | 11.30 | 0.240 | 1.820 | 16.106 | 3.867 |
| 60 | 13.00 | 0.276 | 1.830 | 14.077 | 3.889 |
| 120 | 17.00 | 0.361 | 1.120 | 6.588 | 2.380 |
| 140 | 18.85 | 0.401 | 1.300 | 6.897 | 2.762 |
| 180 | 11.65 | 0.248 | 1.950 | 16.738 | 4.144 |
| 240 | 4.50 | 0.096 | 2.170 | 48.222 | 4.611 |
| 300 | 12.10 | 0.257 | 1.630 | 13.471 | 3.464 |
| | | X= 1.75 | | R=1.400 | |
| 0 | 12.10 | 0.257 | 1.760 | 14.545 | 3.740 |
| 60 | 15.37 | 0.327 | 1.660 | 10.800 | 3.527 |
| 120 | 19.77 | 0.420 | 1.120 | 5.665 | 2.380 |
| 132 | 22.19 | 0.472 | 1.140 | 5.137 | 2.422 |
| 180 | 13.55 | 0.288 | 1.660 | 12.251 | 3.527 |
| 222 | 4.73 | 0.101 | 2.200 | 46.512 | 4.675 |
| 240 | 6.40 | 0.136 | 2.550 | 39.844 | 5.419 |
| 300 | 14.05 | 0.299 | 1.380 | 9.822 | 2.932 |
| | | X= 1.75 | | R=1.600 | |
| 0 | 13.85 | 0.294 | 1.550 | 11.191 | 3.294 |
| 60 | 20.20 | 0.429 | 1.840 | 9.109 | 3.910 |
| 120 | 21.10 | 0.448 | 1.080 | 5.118 | 2.295 |
| 132 | 24.70 | 0.525 | 0.960 | 3.887 | 2.040 |
| 180 | 13.95 | 0.296 | 1.350 | 9.677 | 2.869 |
| 222 | 10.15 | 0.216 | 2.370 | 23.350 | 5.036 |
| 240 | 13.50 | 0.287 | 2.870 | 21.259 | 6.099 |
| 300 | 16.95 | 0.360 | 1.400 | 8.260 | 2.975 |
| | | X= 1.75 | | R=1.800 | |
| 0 | 16.20 | 0.344 | 1.250 | 7.716 | 2.656 |
| 50 | 29.18 | 0.620 | 1.400 | 4.798 | 2.975 |
| 60 | 25.90 | 0.550 | 1.480 | 5.714 | 3.145 |
| 120 | 21.70 | 0.461 | 1.080 | 4.977 | 2.295 |
| 180 | 17.15 | 0.364 | 1.300 | 7.580 | 2.762 |
| 240 | 23.70 | 0.504 | 2.440 | 10.295 | 5.185 |
| 255 | 27.55 | 0.585 | 1.660 | 6.025 | 3.527 |
| 300 | 21.73 | 0.462 | 1.620 | 7.455 | 3.442 |

| ANGLE | SPEED | SPEED RATIO | RMS SPEED | LOCAL INT | TURB INT |
|---|---|---|---|---|---|
| | | X= 1.75 | | R=2.000 | |
| 0 | 17.82 | 0.379 | 1.220 | 6.846 | 2.592 |
| 5 | 16.82 | 0.357 | 1.250 | 7.432 | 2.656 |
| 40 | 32.75 | 0.696 | 1.140 | 3.481 | 2.422 |
| 60 | 29.00 | 0.616 | 1.040 | 3.586 | 2.210 |
| 120 | 23.27 | 0.494 | 1.160 | 4.985 | 2.465 |
| 180 | 21.72 | 0.462 | 1.510 | 6.952 | 3.209 |
| 240 | 31.00 | 0.659 | 1.610 | 5.194 | 3.421 |
| 245 | 32.27 | 0.686 | 1.150 | 3.564 | 2.444 |
| 300 | 27.12 | 0.576 | 1.550 | 5.715 | 3.294 |
| | | X= 1.75 | | R=2.200 | |
| 0 | 20.00 | 0.425 | 1.520 | 7.600 | 3.230 |
| 5 | 19.70 | 0.419 | 1.660 | 8.426 | 3.527 |
| 40 | 35.05 | 0.745 | 1.140 | 3.252 | 2.422 |
| 60 | 31.72 | 0.674 | 0.920 | 2.900 | 1.955 |
| 120 | 26.75 | 0.568 | 1.200 | 4.486 | 2.550 |
| 180 | 27.25 | 0.579 | 1.350 | 4.954 | 2.869 |
| 240 | 35.30 | 0.750 | 0.890 | 2.521 | 1.891 |
| 300 | 33.12 | 0.704 | 0.790 | 2.385 | 1.679 |
| | | X= 1.75 | | R=2.400 | |
| 0 | 24.77 | 0.526 | 2.070 | 8.357 | 4.399 |
| 30 | 32.30 | 0.686 | 3.070 | 9.505 | 6.524 |
| 60 | 31.57 | 0.671 | 2.810 | 8.901 | 5.971 |
| 120 | 30.27 | 0.643 | 1.500 | 4.955 | 3.187 |
| 180 | 31.54 | 0.670 | 1.250 | 3.963 | 2.656 |
| 240 | 36.80 | 0.782 | 1.600 | 4.348 | 3.400 |
| 270 | 37.50 | 0.797 | 1.870 | 4.987 | 3.974 |
| 300 | 33.10 | 0.703 | 1.530 | 4.622 | 3.251 |
| | | X= 1.75 | | R=2.483 | |
| 0 | 26.25 | 0.558 | 2.200 | 8.381 | 4.675 |
| 38 | 21.90 | 0.465 | 5.010 | 22.877 | 10.646 |
| 60 | 25.50 | 0.542 | 4.500 | 17.647 | 9.562 |
| 120 | 29.50 | 0.627 | 2.750 | 9.322 | 5.844 |
| 180 | 31.50 | 0.669 | 2.230 | 7.079 | 4.739 |
| 240 | 33.05 | 0.702 | 3.700 | 11.195 | 7.862 |
| 265 | 33.25 | 0.707 | 3.800 | 11.429 | 8.075 |
| 300 | 30.27 | 0.643 | 3.400 | 11.232 | 7.225 |

| ANGLE | SPEED | SPEED RATIO | RMS SPEED | LOCAL INT | TURB INT |
|---|---|---|---|---|---|
| | | X= 1.75 | | R=2.652 | |
| 0 | 18.33 | 0.390 | 3.790 | 20.676 | 8.054 |
| 45 | 10.77 | 0.229 | 4.180 | 38.812 | 8.882 |
| 60 | 13.55 | 0.288 | 4.210 | 31.070 | 8.946 |
| 120 | 18.33 | 0.390 | 3.930 | 21.440 | 8.351 |
| 180 | 20.27 | 0.431 | 3.900 | 19.240 | 8.287 |
| 195 | 21.60 | 0.459 | 4.090 | 18.935 | 8.691 |
| 240 | 19.73 | 0.419 | 4.300 | 21.794 | 9.137 |
| 300 | 17.77 | 0.378 | 4.300 | 24.198 | 9.137 |
| | | X= 1.75 | | R=2.690 | |
| 0 | 15.25 | 0.324 | 3.490 | 22.885 | 7.416 |
| 50 | 8.00 | 0.170 | 3.490 | 43.625 | 7.416 |
| 60 | 10.50 | 0.223 | 3.580 | 34.095 | 7.607 |
| 120 | 14.57 | 0.310 | 3.490 | 23.953 | 7.416 |
| 180 | 16.54 | 0.351 | 3.500 | 21.161 | 7.437 |
| 210 | 17.40 | 0.370 | 3.580 | 20.575 | 7.607 |
| 240 | 16.00 | 0.340 | 3.720 | 23.250 | 7.905 |
| 300 | 14.28 | 0.303 | 3.750 | 26.260 | 7.969 |
| | | X= 1.00 | | R=0.000 | |
| 0 | 2.03 | 0.043 | 1.290 | 63.547 | 2.741 |
| 60 | 2.01 | 0.043 | 1.300 | 64.677 | 2.762 |
| 120 | 2.01 | 0.043 | 1.270 | 63.184 | 2.699 |
| 180 | 2.12 | 0.045 | 1.310 | 61.792 | 2.784 |
| 240 | 2.02 | 0.043 | 1.280 | 63.366 | 2.720 |
| 300 | 2.00 | 0.042 | 1.260 | 63.000 | 2.677 |
| | | X= 1.00 | | R=0.200 | |
| 0 | 1.93 | 0.041 | 1.320 | 68.394 | 2.805 |
| 60 | 1.90 | 0.040 | 1.280 | 67.368 | 2.720 |
| 120 | 2.05 | 0.044 | 1.320 | 64.390 | 2.805 |
| 180 | 2.20 | 0.047 | 1.310 | 59.545 | 2.784 |
| 240 | 2.20 | 0.047 | 1.280 | 58.182 | 2.720 |
| 300 | 1.98 | 0.042 | 1.240 | 62.626 | 2.635 |
| | | X= 1.00 | | R=0.400 | |
| 0 | 1.82 | 0.039 | 1.280 | 70.330 | 2.720 |
| 60 | 1.99 | 0.042 | 1.310 | 65.829 | 2.784 |
| 120 | 2.18 | 0.046 | 1.330 | 61.009 | 2.826 |
| 180 | 2.25 | 0.048 | 1.350 | 60.000 | 2.869 |

| ANGLE | SPEED | SPEED RATIO | RMS SPEED | LOCAL INT | TURB INT |
|---|---|---|---|---|---|
| 240 | 2.25 | 0.048 | 1.320 | 58.667 | 2.805 |
| 300 | 2.02 | 0.043 | 1.240 | 61.386 | 2.635 |
| | | X= 1.00 | | R=0.600 | |
| 0 | 1.80 | 0.038 | 1.220 | 67.778 | 2.592 |
| 60 | 2.50 | 0.053 | 1.580 | 63.200 | 3.357 |
| 90 | 2.56 | 0.054 | 1.680 | 65.625 | 3.570 |
| 120 | 2.25 | 0.048 | 1.430 | 63.556 | 3.039 |
| 180 | 2.23 | 0.047 | 1.450 | 65.022 | 3.081 |
| 240 | 2.28 | 0.048 | 1.340 | 58.772 | 2.847 |
| 300 | 2.19 | 0.047 | 1.310 | 59.817 | 2.784 |
| | | X= 1.00 | | R=0.800 | |
| 0 | 1.87 | 0.040 | 1.220 | 65.241 | 2.592 |
| 60 | 4.29 | 0.091 | 2.250 | 52.448 | 4.781 |
| 90 | 4.50 | 0.096 | 2.450 | 54.444 | 5.206 |
| 120 | 2.80 | 0.059 | 1.780 | 63.571 | 3.782 |
| 180 | 2.18 | 0.046 | 1.430 | 65.596 | 3.039 |
| 240 | 2.22 | 0.047 | 1.360 | 61.261 | 2.890 |
| 300 | 2.27 | 0.048 | 1.390 | 61.233 | 2.954 |
| | | X= 1.00 | | R=1.000 | |
| 0 | 2.21 | 0.047 | 1.310 | 59.276 | 2.784 |
| 60 | 7.50 | 0.159 | 2.800 | 37.333 | 5.950 |
| 90 | 8.24 | 0.175 | 3.250 | 39.442 | 6.906 |
| 120 | 4.61 | 0.098 | 2.580 | 55.965 | 5.482 |
| 180 | 2.23 | 0.047 | 1.440 | 64.574 | 3.060 |
| 240 | 2.17 | 0.046 | 1.380 | 63.594 | 2.932 |
| 300 | 2.37 | 0.050 | 1.440 | 60.759 | 3.060 |
| | | X= 1.00 | | R=1.200 | |
| 0 | 3.09 | 0.066 | 1.680 | 54.369 | 3.570 |
| 60 | 9.98 | 0.212 | 2.470 | 24.749 | 5.249 |
| 90 | 12.48 | 0.265 | 2.530 | 20.272 | 5.376 |
| 120 | 8.80 | 0.187 | 2.980 | 33.864 | 6.332 |
| 180 | 2.82 | 0.060 | 1.620 | 57.447 | 3.442 |
| 240 | 2.10 | 0.045 | 1.380 | 65.714 | 2.932 |
| 300 | 3.11 | 0.066 | 1.870 | 60.129 | 3.974 |

| ANGLE | SPEED | SPEED RATIO | RMS SPEED | LOCAL INT | TURB INT |
|---|---|---|---|---|---|
| | | X= 1.00 | | R=1.300 | |
| 0 | 3.77 | 0.080 | 2.020 | 53.581 | 4.292 |
| 60 | 10.41 | 0.221 | 2.440 | 23.439 | 5.185 |
| 90 | 14.07 | 0.299 | 1.900 | 13.504 | 4.037 |
| 120 | 11.30 | 0.240 | 2.720 | 24.071 | 5.780 |
| 180 | 3.75 | 0.080 | 1.980 | 52.800 | 4.207 |
| 225 | 1.83 | 0.039 | 1.270 | 69.399 | 2.699 |
| 240 | 2.09 | 0.044 | 1.380 | 66.029 | 2.932 |
| 300 | 4.13 | 0.088 | 2.360 | 57.143 | 5.015 |
| | | X= 1.00 | | R=1.400 | |
| 0 | 6.00 | 0.127 | 2.270 | 37.833 | 4.824 |
| 60 | 11.90 | 0.253 | 1.980 | 16.639 | 4.207 |
| 90 | 15.62 | 0.332 | 1.360 | 8.707 | 2.890 |
| 120 | 14.72 | 0.313 | 1.980 | 13.451 | 4.207 |
| 180 | 5.60 | 0.119 | 2.320 | 41.429 | 4.930 |
| 225 | 2.45 | 0.052 | 1.050 | 42.857 | 2.231 |
| 240 | 2.58 | 0.055 | 1.120 | 43.411 | 2.380 |
| 300 | 6.50 | 0.138 | 2.520 | 38.769 | 5.355 |
| | | X= 1.00 | | R=1.600 | |
| 0 | 9.25 | 0.197 | 2.230 | 24.108 | 4.739 |
| 60 | 13.45 | 0.286 | 1.690 | 12.565 | 3.591 |
| 90 | 16.26 | 0.346 | 1.100 | 6.765 | 2.337 |
| 120 | 18.00 | 0.382 | 1.310 | 7.278 | 2.784 |
| 135 | 20.25 | 0.430 | 1.380 | 6.815 | 2.932 |
| 180 | 9.30 | 0.198 | 2.470 | 26.559 | 5.249 |
| 225 | 2.90 | 0.062 | 1.270 | 43.793 | 2.699 |
| 240 | 3.50 | 0.074 | 1.720 | 49.143 | 3.655 |
| 300 | 10.90 | 0.232 | 2.250 | 20.642 | 4.781 |
| | | X= 1.00 | | R=1.800 | |
| 0 | 11.77 | 0.250 | 1.820 | 15.463 | 3.867 |
| 60 | 18.50 | 0.393 | 1.960 | 10.595 | 4.165 |
| 120 | 19.25 | 0.409 | 1.090 | 5.662 | 2.316 |
| 135 | 23.22 | 0.493 | 0.920 | 3.962 | 1.955 |
| 180 | 12.45 | 0.265 | 1.830 | 14.699 | 3.889 |
| 225 | 5.38 | 0.114 | 2.200 | 40.892 | 4.675 |
| 240 | 7.64 | 0.162 | 3.000 | 39.267 | 6.375 |
| 300 | 14.62 | 0.311 | 1.640 | 11.218 | 3.485 |

| ANGLE | SPEED | SPEED RATIO | RMS SPEED | LOCAL INT | TURB INT |
|---|---|---|---|---|---|
| | | X= 1.00 | | R=2.000 | |
| 0 | 13.55 | 0.288 | 1.420 | 10.480 | 3.017 |
| 60 | 23.25 | 0.494 | 1.640 | 7.054 | 3.485 |
| 120 | 19.65 | 0.418 | 1.030 | 5.242 | 2.189 |
| 135 | 24.75 | 0.526 | 0.710 | 2.869 | 1.509 |
| 180 | 14.27 | 0.303 | 1.440 | 10.091 | 3.060 |
| 225 | 13.07 | 0.278 | 2.930 | 22.418 | 6.226 |
| 240 | 17.55 | 0.373 | 3.320 | 18.917 | 7.055 |
| 300 | 18.40 | 0.391 | 1.600 | 8.696 | 3.400 |
| | | X= 1.00 | | R=2.200 | |
| 0 | 15.50 | 0.329 | 1.140 | 7.355 | 2.422 |
| 40 | 31.00 | 0.659 | 1.170 | 3.774 | 2.486 |
| 60 | 27.30 | 0.580 | 1.040 | 3.810 | 2.210 |
| 120 | 20.78 | 0.442 | 1.010 | 4.860 | 2.146 |
| 135 | 25.80 | 0.548 | 0.830 | 3.217 | 1.764 |
| 180 | 18.40 | 0.391 | 1.440 | 7.826 | 3.060 |
| 225 | 23.20 | 0.493 | 2.560 | 11.034 | 5.440 |
| 240 | 27.12 | 0.576 | 2.280 | 8.407 | 4.845 |
| 270 | 29.05 | 0.617 | 1.100 | 3.787 | 2.337 |
| 300 | 24.10 | 0.512 | 1.640 | 6.805 | 3.485 |
| | | X= 1.00 | | R=2.400 | |
| 0 | 17.55 | 0.373 | 1.290 | 7.350 | 2.741 |
| 40 | 33.40 | 0.710 | 1.340 | 4.012 | 2.847 |
| 60 | 30.00 | 0.637 | 0.950 | 3.167 | 2.019 |
| 120 | 24.50 | 0.521 | 1.120 | 4.571 | 2.380 |
| 180 | 24.87 | 0.528 | 1.380 | 5.549 | 2.932 |
| 240 | 33.72 | 0.717 | 0.910 | 2.699 | 1.934 |
| 300 | 29.52 | 0.627 | 0.850 | 2.879 | 1.806 |
| | | X= 1.00 | | R=2.658 | |
| 0 | 23.50 | 0.499 | 2.050 | 8.723 | 4.356 |
| 40 | 21.70 | 0.461 | 4.860 | 22.396 | 10.327 |
| 60 | 24.10 | 0.512 | 4.270 | 17.718 | 9.074 |
| 120 | 27.15 | 0.577 | 2.460 | 9.061 | 5.227 |
| 180 | 29.62 | 0.629 | 1.840 | 6.212 | 3.910 |
| 240 | 31.77 | 0.675 | 3.340 | 10.513 | 7.097 |
| 300 | 28.37 | 0.603 | 3.140 | 11.068 | 6.672 |

| ANGLE | SPEED | SPEED RATIO | RMS SPEED | LOCAL INT | TURB INT |
|---|---|---|---|---|---|
| | | X= 1.00 | | R=2.843 | |
| 0 | 17.97 | 0.382 | 3.410 | 18.976 | 7.246 |
| 45 | 10.50 | 0.223 | 3.950 | 37.619 | 8.394 |
| 60 | 13.17 | 0.280 | 4.050 | 30.752 | 8.606 |
| 120 | 17.53 | 0.373 | 3.650 | 20.821 | 7.756 |
| 180 | 20.58 | 0.437 | 3.610 | 17.541 | 7.671 |
| 195 | 21.73 | 0.462 | 3.810 | 17.533 | 8.096 |
| 240 | 19.77 | 0.420 | 4.170 | 21.093 | 8.861 |
| 300 | 17.51 | 0.372 | 4.070 | 23.244 | 8.649 |
| | | X= 0.00 | | R=0.000 | |
| 0 | 4.24 | 0.090 | 1.720 | 40.566 | 3.655 |
| 60 | 4.10 | 0.087 | 1.700 | 41.463 | 3.612 |
| 120 | 3.62 | 0.077 | 1.720 | 47.514 | 3.655 |
| 180 | 4.25 | 0.090 | 1.730 | 40.706 | 3.676 |
| 240 | 4.03 | 0.086 | 1.700 | 42.184 | 3.612 |
| 300 | 3.66 | 0.078 | 1.730 | 47.268 | 3.676 |
| | | X= 0.00 | | R=0.200 | |
| 0 | 3.86 | 0.082 | 1.720 | 44.560 | 3.655 |
| 60 | 3.73 | 0.079 | 1.650 | 44.236 | 3.506 |
| 120 | 3.62 | 0.077 | 1.720 | 47.514 | 3.655 |
| 180 | 4.30 | 0.091 | 1.740 | 40.465 | 3.697 |
| 240 | 4.30 | 0.091 | 1.720 | 40.000 | 3.655 |
| 300 | 3.60 | 0.076 | 1.730 | 48.056 | 3.676 |
| | | X= 0.00 | | R=0.400 | |
| 0 | 3.52 | 0.075 | 1.670 | 47.443 | 3.549 |
| 60 | 3.16 | 0.067 | 1.620 | 51.266 | 3.442 |
| 120 | 3.38 | 0.072 | 1.720 | 50.888 | 3.655 |
| 180 | 4.21 | 0.089 | 1.790 | 42.518 | 3.804 |
| 240 | 4.26 | 0.091 | 1.800 | 42.254 | 3.825 |
| 300 | 3.58 | 0.076 | 1.750 | 48.883 | 3.719 |
| | | X= 0.00 | | R=0.600 | |
| 0 | 3.02 | 0.064 | 1.610 | 53.311 | 3.421 |
| 60 | 2.70 | 0.057 | 1.620 | 60.000 | 3.442 |
| 120 | 3.13 | 0.067 | 1.740 | 55.591 | 3.697 |
| 180 | 3.77 | 0.080 | 1.770 | 46.950 | 3.761 |
| 240 | 4.13 | 0.088 | 1.910 | 46.247 | 4.059 |
| 300 | 3.50 | 0.074 | 1.830 | 52.286 | 3.889 |

| ANGLE | SPEED | SPEED RATIO | RMS SPEED | LOCAL INT | TURB INT |
|---|---|---|---|---|---|
| | | X= 0.00 | | R=0.800 | |
| 0 | 2.69 | 0.057 | 1.520 | 56.506 | 3.230 |
| 60 | 2.71 | 0.058 | 1.820 | 67.159 | 3.867 |
| 120 | 2.76 | 0.059 | 1.700 | 61.594 | 3.612 |
| 180 | 3.24 | 0.069 | 1.740 | 53.704 | 3.697 |
| 240 | 3.75 | 0.080 | 1.930 | 51.467 | 4.101 |
| 300 | 3.46 | 0.074 | 1.790 | 51.734 | 3.804 |
| | | X= 0.00 | | R=1.000 | |
| 0 | 2.48 | 0.053 | 1.470 | 59.274 | 3.124 |
| 60 | 3.80 | 0.081 | 2.380 | 62.632 | 5.057 |
| 90 | 4.23 | 0.090 | 2.600 | 61.466 | 5.525 |
| 120 | 3.10 | 0.066 | 1.890 | 60.968 | 4.016 |
| 180 | 2.50 | 0.053 | 1.640 | 65.600 | 3.485 |
| 240 | 3.24 | 0.069 | 1.900 | 58.642 | 4.037 |
| 300 | 3.30 | 0.070 | 1.810 | 54.848 | 3.846 |
| | | X= 0.00 | | R=1.200 | |
| 0 | 2.75 | 0.058 | 1.690 | 61.455 | 3.591 |
| 60 | 6.10 | 0.130 | 2.650 | 43.443 | 5.631 |
| 90 | 7.38 | 0.157 | 3.170 | 42.954 | 6.736 |
| 120 | 5.00 | 0.106 | 2.630 | 52.600 | 5.589 |
| 180 | 2.56 | 0.054 | 1.640 | 64.063 | 3.485 |
| 225 | 2.31 | 0.049 | 1.590 | 68.831 | 3.379 |
| 240 | 2.78 | 0.059 | 1.830 | 65.827 | 3.889 |
| 300 | 3.07 | 0.065 | 1.850 | 60.261 | 3.931 |
| | | X= 0.00 | | R=1.300 | |
| 0 | 3.25 | 0.069 | 1.840 | 56.615 | 3.910 |
| 60 | 7.41 | 0.157 | 2.600 | 35.088 | 5.525 |
| 90 | 9.25 | 0.197 | 3.030 | 32.757 | 6.439 |
| 120 | 6.51 | 0.138 | 2.870 | 44.086 | 6.099 |
| 180 | 2.87 | 0.061 | 1.800 | 62.718 | 3.825 |
| 225 | 2.11 | 0.045 | 1.440 | 68.246 | 3.060 |
| 240 | 2.56 | 0.054 | 1.820 | 71.094 | 3.867 |
| 300 | 2.98 | 0.063 | 1.800 | 60.403 | 3.825 |
| | | X= 0.00 | | R=1.400 | |
| 0 | 4.62 | 0.098 | 1.990 | 43.074 | 4.229 |
| 60 | 8.45 | 0.180 | 2.480 | 29.349 | 5.270 |
| 90 | 11.22 | 0.238 | 2.600 | 23.173 | 5.525 |

| ANGLE | SPEED | SPEED RATIO | RMS SPEED | LOCAL INT | TURB INT |
|---|---|---|---|---|---|
| 120 | 8.77 | 0.186 | 2.790 | 31.813 | 5.929 |
| 180 | 4.05 | 0.086 | 1.930 | 47.654 | 4.101 |
| 225 | 2.77 | 0.059 | 1.460 | 52.708 | 3.102 |
| 240 | 3.10 | 0.066 | 1.590 | 51.290 | 3.379 |
| 300 | 3.68 | 0.078 | 1.800 | 48.913 | 3.825 |
| | | X= 0.00 | | R=1.600 | |
| 0 | 7.05 | 0.150 | 2.190 | 31.064 | 4.654 |
| 60 | 10.77 | 0.229 | 2.150 | 19.963 | 4.569 |
| 90 | 14.50 | 0.308 | 1.710 | 11.793 | 3.634 |
| 120 | 13.72 | 0.292 | 2.450 | 17.857 | 5.206 |
| 180 | 6.23 | 0.132 | 2.300 | 36.918 | 4.887 |
| 225 | 2.80 | 0.059 | 1.410 | 50.357 | 2.996 |
| 240 | 3.10 | 0.066 | 1.550 | 50.000 | 3.294 |
| 300 | 5.88 | 0.125 | 2.620 | 44.558 | 5.567 |
| | | X= 0.00 | | R=1.800 | |
| 0 | 9.86 | 0.210 | 2.070 | 20.994 | 4.399 |
| 60 | 13.75 | 0.292 | 2.050 | 14.909 | 4.356 |
| 90 | 15.37 | 0.327 | 1.470 | 9.564 | 3.124 |
| 120 | 17.38 | 0.369 | 1.670 | 9.609 | 3.549 |
| 135 | 19.23 | 0.409 | 2.160 | 11.232 | 4.590 |
| 180 | 9.27 | 0.197 | 2.220 | 23.948 | 4.717 |
| 225 | 3.90 | 0.083 | 1.880 | 48.205 | 3.995 |
| 240 | 4.52 | 0.096 | 2.340 | 51.770 | 4.972 |
| 300 | 10.25 | 0.218 | 2.720 | 26.537 | 5.780 |
| | | X= 0.00 | | R=2.000 | |
| 0 | 12.27 | 0.261 | 1.740 | 14.181 | 3.697 |
| 60 | 19.25 | 0.409 | 2.240 | 11.636 | 4.760 |
| 120 | 18.55 | 0.394 | 1.430 | 7.709 | 3.039 |
| 135 | 23.00 | 0.489 | 1.200 | 5.217 | 2.550 |
| 180 | 11.55 | 0.245 | 2.060 | 17.835 | 4.377 |
| 225 | 7.50 | 0.159 | 2.850 | 38.000 | 6.056 |
| 240 | 9.62 | 0.204 | 3.550 | 36.902 | 7.544 |
| 300 | 14.82 | 0.315 | 2.060 | 13.900 | 4.377 |
| | | X= 0.00 | | R=2.200 | |
| 0 | 14.08 | 0.299 | 1.370 | 9.730 | 2.911 |
| 45 | 28.05 | 0.596 | 1.520 | 5.419 | 3.230 |
| 60 | 24.00 | 0.510 | 1.740 | 7.250 | 3.697 |
| 120 | 18.75 | 0.398 | 1.240 | 6.613 | 2.635 |

| ANGLE | SPEED | SPEED RATIO | RMS SPEED | LOCAL INT | TURB INT |
|---|---|---|---|---|---|
| 180 | 14.22 | 0.302 | 1.620 | 11.392 | 3.442 |
| 189 | 13.80 | 0.293 | 1.860 | 13.478 | 3.952 |
| 240 | 19.27 | 0.409 | 3.860 | 20.031 | 8.202 |
| 300 | 19.72 | 0.419 | 1.830 | 9.280 | 3.889 |
| | | X= 0.00 | | R=2.400 | |
| 0 | 15.80 | 0.336 | 1.280 | 8.101 | 2.720 |
| 45 | 31.00 | 0.659 | 1.360 | 4.387 | 2.890 |
| 60 | 27.55 | 0.585 | 1.180 | 4.283 | 2.507 |
| 120 | 21.25 | 0.452 | 1.230 | 5.788 | 2.614 |
| 180 | 20.20 | 0.429 | 1.710 | 8.465 | 3.634 |
| 240 | 29.60 | 0.629 | 2.320 | 7.838 | 4.930 |
| 300 | 26.04 | 0.553 | 1.700 | 6.528 | 3.612 |
| | | X= 0.00 | | R=2.745 | |
| 0 | 21.20 | 0.450 | 2.370 | 11.179 | 5.036 |
| 60 | 23.10 | 0.491 | 4.390 | 19.004 | 9.329 |
| 120 | 24.72 | 0.525 | 2.830 | 11.448 | 6.014 |
| 180 | 27.55 | 0.585 | 2.500 | 9.074 | 5.312 |
| 200 | 30.12 | 0.640 | 2.860 | 9.495 | 6.077 |
| 240 | 30.34 | 0.645 | 3.750 | 12.360 | 7.969 |
| 300 | 26.40 | 0.561 | 3.530 | 13.371 | 7.501 |
| | | X= 0.00 | | R=2.947 | |
| 0 | 17.78 | 0.378 | 2.720 | 15.298 | 5.780 |
| 45 | 12.28 | 0.261 | 3.720 | 30.293 | 7.905 |
| 60 | 14.60 | 0.310 | 3.810 | 26.096 | 8.096 |
| 120 | 17.88 | 0.380 | 3.280 | 18.344 | 6.970 |
| 180 | 21.07 | 0.448 | 3.310 | 15.710 | 7.034 |
| 195 | 22.50 | 0.478 | 3.530 | 15.689 | 7.501 |
| 240 | 21.27 | 0.452 | 4.010 | 18.853 | 8.521 |
| 300 | 18.36 | 0.390 | 3.740 | 20.370 | 7.947 |
| | | X= 0.00 | | R=3.000 | |
| 0 | 15.50 | 0.329 | 3.060 | 19.742 | 6.502 |
| 45 | 9.55 | 0.203 | 3.410 | 35.707 | 7.246 |
| 60 | 11.73 | 0.249 | 3.570 | 30.435 | 7.586 |
| 120 | 14.28 | 0.303 | 3.510 | 24.580 | 7.459 |
| 180 | 16.63 | 0.353 | 3.790 | 22.790 | 8.054 |
| 195 | 18.50 | 0.393 | 3.930 | 21.243 | 8.351 |
| 240 | 17.97 | 0.382 | 4.100 | 22.816 | 8.712 |
| 300 | 15.78 | 0.335 | 3.680 | 23.321 | 7.820 |

| ANGLE | SPEED | SPEED RATIO | RMS SPEED | LOCAL INT | TURB INT |
|---|---|---|---|---|---|
| | | X=-1.25 | | R=0.000 | |
| 0 | 3.69 | 0.078 | 2.130 | 57.724 | 4.526 |
| 60 | 3.50 | 0.074 | 1.990 | 56.857 | 4.229 |
| 120 | 3.21 | 0.068 | 1.900 | 59.190 | 4.037 |
| 180 | 3.71 | 0.079 | 2.140 | 57.682 | 4.547 |
| 240 | 3.55 | 0.075 | 2.040 | 57.465 | 4.335 |
| 300 | 3.21 | 0.068 | 1.680 | 58.567 | 3.995 |
| | | X=-1.25 | | R=0.200 | |
| 0 | 3.96 | 0.084 | 2.260 | 57.071 | 4.802 |
| 60 | 3.50 | 0.074 | 2.000 | 57.143 | 4.250 |
| 120 | 3.25 | 0.069 | 1.900 | 58.462 | 4.037 |
| 180 | 3.55 | 0.075 | 2.050 | 57.746 | 4.356 |
| 240 | 3.56 | 0.076 | 2.050 | 57.584 | 4.356 |
| 300 | 3.22 | 0.068 | 1.910 | 59.317 | 4.059 |
| | | X=-1.25 | | R=0.400 | |
| 0 | 4.30 | 0.091 | 2.360 | 54.884 | 5.015 |
| 60 | 3.57 | 0.076 | 2.080 | 58.263 | 4.420 |
| 120 | 3.30 | 0.070 | 2.030 | 61.515 | 4.314 |
| 180 | 3.66 | 0.078 | 2.080 | 56.831 | 4.420 |
| 240 | 3.54 | 0.075 | 2.050 | 57.910 | 4.356 |
| 300 | 3.25 | 0.069 | 1.940 | 59.692 | 4.122 |
| | | X=-1.25 | | R=0.600 | |
| 0 | 5.07 | 0.108 | 2.500 | 49.310 | 5.312 |
| 60 | 4.17 | 0.089 | 2.290 | 54.916 | 4.866 |
| 120 | 3.92 | 0.083 | 2.360 | 60.204 | 5.015 |
| 180 | 4.00 | 0.085 | 2.290 | 57.250 | 4.866 |
| 240 | 3.55 | 0.075 | 2.040 | 57.465 | 4.335 |
| 300 | 3.27 | 0.069 | 1.940 | 59.327 | 4.122 |
| | | X=-1.25 | | R=0.800 | |
| 0 | 6.05 | 0.129 | 2.520 | 41.653 | 5.355 |
| 60 | 5.20 | 0.110 | 2.460 | 47.308 | 5.227 |
| 90 | 5.95 | 0.126 | 2.850 | 47.899 | 6.056 |
| 120 | 5.25 | 0.112 | 2.740 | 52.190 | 5.822 |
| 180 | 4.67 | 0.099 | 2.430 | 52.034 | 5.164 |
| 240 | 3.68 | 0.078 | 2.060 | 55.978 | 4.377 |
| 300 | 3.26 | 0.069 | 1.940 | 59.509 | 4.122 |

| ANGLE | SPEED | SPEED RATIO | RMS SPEED | LOCAL INT | TURB INT |
|---|---|---|---|---|---|
| | | X=-1.25 | | R=1.000 | |
| 0 | 7.48 | 0.159 | 2.430 | 32.487 | 5.164 |
| 60 | 6.72 | 0.143 | 2.460 | 36.607 | 5.227 |
| 90 | 8.56 | 0.182 | 2.840 | 33.178 | 6.035 |
| 120 | 7.47 | 0.159 | 2.950 | 39.491 | 6.269 |
| 180 | 5.94 | 0.126 | 2.520 | 42.424 | 5.355 |
| 240 | 3.69 | 0.078 | 2.090 | 56.640 | 4.441 |
| 300 | 3.32 | 0.071 | 2.030 | 61.145 | 4.314 |
| | | X=-1.25 | | R=1.200 | |
| 0 | 9.00 | 0.191 | 2.260 | 25.111 | 4.802 |
| 60 | 8.56 | 0.182 | 2.260 | 26.402 | 4.802 |
| 90 | 11.55 | 0.245 | 2.340 | 20.260 | 4.972 |
| 120 | 10.30 | 0.219 | 2.740 | 26.602 | 5.822 |
| 180 | 7.55 | 0.160 | 2.450 | 32.450 | 5.206 |
| 240 | 3.92 | 0.083 | 2.310 | 58.929 | 4.909 |
| 300 | 4.23 | 0.090 | 2.510 | 59.338 | 5.334 |
| | | X=-1.25 | | R=1.300 | |
| 0 | 10.00 | 0.212 | 2.120 | 21.200 | 4.505 |
| 60 | 9.48 | 0.201 | 2.110 | 22.257 | 4.484 |
| 90 | 12.70 | 0.270 | 1.970 | 15.512 | 4.186 |
| 120 | 11.95 | 0.254 | 2.530 | 21.172 | 5.376 |
| 180 | 8.44 | 0.179 | 2.360 | 27.962 | 5.015 |
| 240 | 4.24 | 0.090 | 2.510 | 59.198 | 5.334 |
| 270 | 3.55 | 0.075 | 2.230 | 62.817 | 4.739 |
| 300 | 5.24 | 0.111 | 2.850 | 54.389 | 6.056 |
| | | X=-1.25 | | R=1.400 | |
| 0 | 11.73 | 0.249 | 1.650 | 14.066 | 3.506 |
| 60 | 11.70 | 0.249 | 1.790 | 15.299 | 3.804 |
| 90 | 13.88 | 0.295 | 1.630 | 11.744 | 3.464 |
| 120 | 13.54 | 0.288 | 2.170 | 16.027 | 4.611 |
| 180 | 8.78 | 0.187 | 2.030 | 23.121 | 4.314 |
| 240 | 4.77 | 0.101 | 2.510 | 52.621 | 5.334 |
| 300 | 7.00 | 0.149 | 2.810 | 40.143 | 5.971 |
| | | X=-1.25 | | R=1.600 | |
| 0 | 13.55 | 0.288 | 1.320 | 9.742 | 2.805 |
| 60 | 13.95 | 0.296 | 1.670 | 11.971 | 3.549 |
| 120 | 16.62 | 0.353 | 1.600 | 9.627 | 3.400 |

| ANGLE | SPEED | SPEED RATIO | RMS SPEED | LOCAL INT | TURB INT |
|---|---|---|---|---|---|
| 180 | 10.70 | 0.227 | 1.780 | 16.635 | 3.782 |
| 240 | 7.05 | 0.150 | 3.250 | 46.099 | 6.906 |
| 300 | 11.19 | 0.238 | 2.750 | 24.576 | 5.844 |
| | | X=-1.25 | | R=1.800 | |
| 0 | 15.20 | 0.323 | 1.170 | 7.697 | 2.486 |
| 60 | 18.00 | 0.382 | 1.900 | 10.556 | 4.037 |
| 120 | 18.38 | 0.391 | 1.280 | 6.964 | 2.720 |
| 135 | 20.26 | 0.431 | 1.560 | 7.700 | 3.315 |
| 180 | 12.75 | 0.271 | 1.520 | 11.922 | 3.230 |
| 195 | 11.73 | 0.249 | 1.960 | 16.709 | 4.165 |
| 240 | 12.03 | 0.256 | 3.760 | 31.255 | 7.990 |
| 300 | 16.20 | 0.344 | 2.300 | 14.198 | 4.887 |
| | | X=-1.25 | | R=2.000 | |
| 0 | 16.60 | 0.353 | 1.170 | 7.048 | 2.486 |
| 50 | 24.13 | 0.513 | 2.280 | 9.449 | 4.845 |
| 60 | 22.50 | 0.478 | 1.740 | 7.733 | 3.697 |
| 120 | 19.62 | 0.417 | 1.080 | 5.505 | 2.295 |
| 180 | 15.78 | 0.335 | 1.520 | 9.632 | 3.230 |
| 195 | 15.03 | 0.319 | 1.800 | 11.976 | 3.825 |
| 240 | 18.95 | 0.403 | 4.040 | 21.319 | 8.585 |
| 300 | 21.20 | 0.450 | 1.800 | 8.491 | 3.825 |
| | | X=-1.25 | | R=2.200 | |
| 0 | 18.50 | 0.393 | 1.450 | 7.838 | 3.081 |
| 50 | 29.23 | 0.621 | 1.570 | 5.371 | 3.336 |
| 60 | 26.57 | 0.565 | 1.370 | 5.156 | 2.911 |
| 120 | 22.21 | 0.472 | 1.090 | 4.908 | 2.316 |
| 180 | 20.77 | 0.441 | 1.580 | 7.607 | 3.357 |
| 240 | 27.95 | 0.594 | 3.000 | 10.733 | 6.375 |
| 250 | 29.03 | 0.617 | 2.360 | 8.130 | 5.015 |
| 300 | 26.53 | 0.564 | 1.530 | 5.767 | 3.251 |
| | | X=-1.25 | | R=2.400 | |
| 0 | 19.82 | 0.421 | 1.800 | 9.082 | 3.825 |
| 60 | 27.45 | 0.583 | 2.320 | 8.452 | 4.930 |
| 120 | 24.80 | 0.527 | 1.520 | 6.129 | 3.230 |
| 180 | 25.40 | 0.540 | 1.520 | 5.984 | 3.230 |
| 240 | 32.20 | 0.684 | 1.910 | 5.932 | 4.059 |
| 300 | 28.20 | 0.599 | 1.940 | 6.879 | 4.122 |

| ANGLE | SPEED | SPEED RATIO | RMS SPEED | LOCAL INT | TURB INT |
|---|---|---|---|---|---|
| | | X=-1.25 | | R=2.462 | |
| 0 | 19.85 | 0.422 | 1.920 | 9.673 | 4.080 |
| 60 | 26.52 | 0.564 | 2.900 | 10.935 | 6.162 |
| 120 | 24.80 | 0.527 | 1.850 | 7.460 | 3.931 |
| 180 | 26.00 | 0.552 | 1.760 | 6.769 | 3.740 |
| 240 | 31.73 | 0.674 | 2.480 | 7.816 | 5.270 |
| 300 | 27.70 | 0.589 | 2.460 | 8.881 | 5.227 |
| | | X=-1.25 | | R=2.600 | |
| 0 | 19.00 | 0.404 | 2.320 | 12.211 | 4.930 |
| 60 | 23.73 | 0.504 | 3.690 | 15.550 | 7.841 |
| 120 | 23.65 | 0.503 | 2.660 | 11.247 | 5.652 |
| 180 | 25.07 | 0.533 | 2.650 | 10.570 | 5.631 |
| 240 | 29.00 | 0.616 | 3.750 | 12.931 | 7.969 |
| 270 | 29.57 | 0.628 | 3.600 | 12.174 | 7.650 |
| 300 | 25.22 | 0.536 | 3.280 | 13.006 | 6.970 |
| | | X=-1.25 | | R=2.796 | |
| 0 | 15.38 | 0.327 | 3.020 | 19.636 | 6.417 |
| 60 | 19.30 | 0.410 | 3.380 | 17.513 | 7.182 |
| 120 | 20.27 | 0.431 | 2.680 | 13.222 | 5.695 |
| 180 | 21.68 | 0.461 | 2.820 | 13.007 | 5.992 |
| 240 | 24.00 | 0.510 | 3.650 | 15.208 | 7.756 |
| 270 | 24.30 | 0.516 | 3.670 | 15.103 | 7.799 |
| 300 | 21.50 | 0.457 | 3.200 | 14.884 | 6.800 |
| | | X=-1.25 | | R=2.845 | |
| 0 | 11.60 | 0.246 | 3.110 | 26.810 | 6.609 |
| 60 | 17.30 | 0.368 | 3.450 | 19.942 | 7.331 |
| 120 | 17.97 | 0.382 | 3.110 | 17.307 | 6.609 |
| 180 | 19.30 | 0.410 | 3.200 | 16.580 | 6.800 |
| 240 | 21.65 | 0.460 | 3.880 | 17.921 | 8.245 |
| 265 | 22.60 | 0.480 | 3.810 | 16.858 | 8.096 |
| 300 | 19.60 | 0.416 | 3.350 | 17.092 | 7.119 |
| | | X=-2.50 | | R=0.000 | |
| 0 | 11.86 | 0.252 | 2.510 | 21.164 | 5.334 |
| 60 | 11.72 | 0.249 | 2.410 | 20.563 | 5.121 |
| 120 | 11.62 | 0.247 | 2.320 | 19.966 | 4.930 |
| 180 | 11.84 | 0.252 | 2.530 | 21.368 | 5.376 |
| 240 | 11.62 | 0.247 | 2.430 | 20.912 | 5.164 |

| ANGLE | SPEED | SPEED RATIO | RMS SPEED | LOCAL INT | TURB INT |
|---|---|---|---|---|---|
| 300 | 11.60 | 0.246 | 2.290 | 19.741 | 4.866 |
| | | X=-2.50 | | R=0.200 | |
| 0 | 12.41 | 0.264 | 2.580 | 20.790 | 5.482 |
| 60 | 11.96 | 0.254 | 2.240 | 18.729 | 4.760 |
| 120 | 11.85 | 0.252 | 2.270 | 19.156 | 4.824 |
| 180 | 11.84 | 0.252 | 2.450 | 20.693 | 5.206 |
| 240 | 11.62 | 0.247 | 2.560 | 22.031 | 5.440 |
| 300 | 11.40 | 0.242 | 2.370 | 20.789 | 5.036 |
| | | X=-2.50 | | R=0.400 | |
| 0 | 13.52 | 0.287 | 2.620 | 19.379 | 5.567 |
| 60 | 12.40 | 0.263 | 2.110 | 17.016 | 4.484 |
| 120 | 12.41 | 0.264 | 2.300 | 18.533 | 4.887 |
| 180 | 12.42 | 0.264 | 2.420 | 19.485 | 5.142 |
| 240 | 11.87 | 0.252 | 2.660 | 22.409 | 5.652 |
| 300 | 11.62 | 0.247 | 2.380 | 20.482 | 5.057 |
| | | X=-2.50 | | R=0.600 | |
| 0 | 15.00 | 0.319 | 2.420 | 16.133 | 5.142 |
| 60 | 13.14 | 0.279 | 2.020 | 15.373 | 4.292 |
| 120 | 13.85 | 0.294 | 2.420 | 17.473 | 5.142 |
| 180 | 13.47 | 0.286 | 2.390 | 17.743 | 5.079 |
| 240 | 12.62 | 0.268 | 2.830 | 22.425 | 6.014 |
| 300 | 11.48 | 0.244 | 2.480 | 21.603 | 5.270 |
| | | X=-2.50 | | R=0.800 | |
| 0 | 16.67 | 0.354 | 2.150 | 12.897 | 4.569 |
| 60 | 14.45 | 0.307 | 1.960 | 13.564 | 4.165 |
| 90 | 16.00 | 0.340 | 2.040 | 12.750 | 4.335 |
| 120 | 15.62 | 0.332 | 2.370 | 15.173 | 5.036 |
| 180 | 14.77 | 0.314 | 2.270 | 15.369 | 4.824 |
| 240 | 13.50 | 0.287 | 3.150 | 23.333 | 6.694 |
| 270 | 11.58 | 0.246 | 2.640 | 22.798 | 5.610 |
| 300 | 11.97 | 0.254 | 2.670 | 22.306 | 5.674 |
| | | X=-2.50 | | R=1.000 | |
| 0 | 16.75 | 0.398 | 1.830 | 9.760 | 3.889 |
| 60 | 16.37 | 0.348 | 1.830 | 11.179 | 3.889 |
| 90 | 17.75 | 0.377 | 1.470 | 8.282 | 3.124 |

| ANGLE | SPEED | SPEED RATIO | RMS SPEED | LOCAL INT | TURB INT |
|---|---|---|---|---|---|
| 120 | 18.18 | 0.386 | 1.950 | 10.726 | 4.144 |
| 180 | 16.73 | 0.356 | 1.900 | 11.357 | 4.037 |
| 240 | 15.00 | 0.319 | 3.480 | 23.200 | 7.395 |
| 270 | 12.00 | 0.255 | 2.990 | 24.917 | 6.354 |
| 300 | 13.95 | 0.296 | 3.350 | 24.014 | 7.119 |
| | | X=-2.50 | | R=1.200 | |
| 0 | 20.32 | 0.432 | 1.530 | 7.530 | 3.251 |
| 40 | 16.23 | 0.345 | 2.150 | 13.247 | 4.569 |
| 60 | 18.75 | 0.398 | 1.910 | 10.187 | 4.059 |
| 90 | 19.23 | 0.409 | 1.130 | 5.876 | 2.401 |
| 120 | 20.25 | 0.430 | 1.300 | 6.420 | 2.762 |
| 180 | 18.74 | 0.398 | 1.670 | 8.911 | 3.549 |
| 240 | 17.26 | 0.367 | 3.950 | 22.885 | 8.394 |
| 270 | 14.73 | 0.313 | 3.770 | 25.594 | 8.011 |
| 300 | 17.72 | 0.377 | 3.610 | 20.372 | 7.671 |
| | | X=-2.50 | | R=1.300 | |
| 0 | 21.20 | 0.450 | 1.420 | 6.698 | 3.017 |
| 40 | 17.26 | 0.367 | 2.320 | 13.441 | 4.930 |
| 60 | 20.39 | 0.433 | 1.930 | 9.465 | 4.101 |
| 90 | 20.20 | 0.429 | 1.160 | 5.743 | 2.465 |
| 120 | 21.52 | 0.457 | 1.070 | 4.972 | 2.274 |
| 180 | 20.00 | 0.425 | 1.650 | 8.250 | 3.506 |
| 240 | 19.00 | 0.404 | 4.020 | 21.158 | 8.542 |
| 270 | 16.78 | 0.357 | 4.050 | 24.136 | 8.606 |
| 300 | 20.23 | 0.430 | 3.300 | 16.312 | 7.012 |
| | | X=-2.50 | | R=1.400 | |
| 0 | 22.10 | 0.470 | 1.250 | 5.656 | 2.656 |
| 33 | 19.30 | 0.410 | 2.360 | 12.228 | 5.015 |
| 60 | 23.10 | 0.491 | 1.630 | 7.056 | 3.464 |
| 120 | 22.72 | 0.483 | 0.980 | 4.313 | 2.082 |
| 180 | 20.60 | 0.438 | 1.610 | 7.816 | 3.421 |
| 240 | 20.28 | 0.431 | 4.080 | 20.118 | 8.670 |
| 300 | 23.07 | 0.490 | 2.640 | 11.443 | 5.610 |
| | | X=-2.50 | | R=1.600 | |
| 0 | 23.10 | 0.491 | 1.300 | 5.628 | 2.762 |
| 60 | 26.56 | 0.564 | 1.570 | 5.911 | 3.336 |
| 120 | 24.78 | 0.527 | 0.930 | 3.753 | 1.976 |
| 180 | 23.76 | 0.505 | 1.710 | 7.197 | 3.634 |

| ANGLE | SPEED | SPEED RATIO | RMS SPEED | LOCAL INT | TURB INT |
|---|---|---|---|---|---|
| 240 | 25.80 | 0.548 | 4.040 | 15.659 | 8.585 |
| 300 | 27.62 | 0.587 | 1.950 | 7.060 | 4.144 |
| | | X=-2.50 | | R=1.800 | |
| 0 | 23.25 | 0.494 | 1.460 | 6.280 | 3.102 |
| 60 | 29.75 | 0.632 | 1.480 | 4.975 | 3.145 |
| 120 | 27.26 | 0.579 | 1.130 | 4.145 | 2.401 |
| 180 | 27.10 | 0.576 | 1.450 | 5.351 | 3.081 |
| 240 | 31.70 | 0.674 | 2.700 | 8.517 | 5.737 |
| 300 | 30.38 | 0.646 | 1.560 | 5.135 | 3.315 |
| | | X=-2.50 | | R=2.000 | |
| 0 | 22.76 | 0.484 | 1.660 | 7.293 | 3.527 |
| 60 | 30.12 | 0.640 | 2.330 | 7.736 | 4.951 |
| 120 | 28.38 | 0.603 | 1.690 | 5.955 | 3.591 |
| 180 | 28.27 | 0.601 | 1.710 | 6.049 | 3.634 |
| 240 | 33.20 | 0.705 | 2.500 | 7.530 | 5.312 |
| 300 | 30.22 | 0.642 | 2.290 | 7.578 | 4.866 |
| | | X=-2.50 | | R=2.200 | |
| 0 | 21.70 | 0.461 | 1.810 | 8.341 | 3.846 |
| 60 | 28.00 | 0.595 | 2.850 | 10.179 | 6.056 |
| 120 | 27.07 | 0.575 | 2.080 | 7.684 | 4.420 |
| 180 | 27.07 | 0.575 | 2.130 | 7.868 | 4.526 |
| 240 | 31.12 | 0.661 | 3.160 | 10.154 | 6.715 |
| 270 | 32.20 | 0.684 | 2.930 | 9.099 | 6.226 |
| 300 | 28.38 | 0.603 | 2.580 | 9.091 | 5.482 |
| | | X=-2.50 | | R=2.377 | |
| 0 | 20.18 | 0.429 | 1.810 | 8.969 | 3.846 |
| 60 | 25.97 | 0.552 | 2.760 | 10.628 | 5.865 |
| 120 | 25.48 | 0.541 | 2.150 | 8.438 | 4.569 |
| 180 | 25.40 | 0.540 | 2.250 | 8.858 | 4.781 |
| 240 | 28.88 | 0.614 | 3.130 | 10.838 | 6.651 |
| 270 | 29.77 | 0.633 | 3.060 | 10.279 | 6.502 |
| 300 | 26.55 | 0.564 | 2.560 | 9.642 | 5.440 |
| | | X=-3.50 | | R=0.000 | |
| 0 | 25.69 | 0.546 | 2.440 | 9.498 | 5.185 |
| 60 | 25.63 | 0.545 | 2.350 | 9.169 | 4.994 |

| ANGLE | SPEED | SPEED RATIO | RMS SPEED | LOCAL INT | TURB INT |
|---|---|---|---|---|---|
| 120 | 25.46 | 0.541 | 2.320 | 9.112 | 4.930 |
| 180 | 25.63 | 0.545 | 2.420 | 9.442 | 5.142 |
| 240 | 25.46 | 0.541 | 2.410 | 9.466 | 5.121 |
| 300 | 25.46 | 0.541 | 2.270 | 8.916 | 4.824 |
| | | X=-3.50 | | R=0.200 | |
| 0 | 26.32 | 0.559 | 2.400 | 9.119 | 5.100 |
| 60 | 25.78 | 0.548 | 2.080 | 8.068 | 4.420 |
| 120 | 25.69 | 0.546 | 2.190 | 8.525 | 4.654 |
| 180 | 25.75 | 0.547 | 2.400 | 9.320 | 5.100 |
| 240 | 25.78 | 0.548 | 2.580 | 10.008 | 5.482 |
| 300 | 25.46 | 0.541 | 2.380 | 9.348 | 5.057 |
| | | X=-3.50 | | R=0.400 | |
| 0 | 27.30 | 0.580 | 2.270 | 8.315 | 4.824 |
| 60 | 26.00 | 0.552 | 1.830 | 7.038 | 3.889 |
| 120 | 26.00 | 0.552 | 2.030 | 7.808 | 4.314 |
| 180 | 26.52 | 0.564 | 2.270 | 8.560 | 4.824 |
| 240 | 26.60 | 0.565 | 2.730 | 10.263 | 5.801 |
| 300 | 25.69 | 0.546 | 2.470 | 9.615 | 5.249 |
| | | X=-3.50 | | R=0.600 | |
| 0 | 28.97 | 0.616 | 1.950 | 6.731 | 4.144 |
| 10 | 29.20 | 0.620 | 2.060 | 7.055 | 4.377 |
| 60 | 26.60 | 0.565 | 1.650 | 6.203 | 3.506 |
| 120 | 27.18 | 0.578 | 1.900 | 6.990 | 4.037 |
| 180 | 27.73 | 0.589 | 2.020 | 7.285 | 4.292 |
| 240 | 27.90 | 0.593 | 2.920 | 10.466 | 6.205 |
| 300 | 25.97 | 0.552 | 2.580 | 9.935 | 5.482 |
| | | X=-3.50 | | R=0.800 | |
| 0 | 30.75 | 0.653 | 1.700 | 5.528 | 3.612 |
| 10 | 31.45 | 0.668 | 1.800 | 5.723 | 3.825 |
| 60 | 28.37 | 0.603 | 1.750 | 6.168 | 3.719 |
| 120 | 29.25 | 0.622 | 1.710 | 5.846 | 3.634 |
| 180 | 29.87 | 0.635 | 1.820 | 6.093 | 3.867 |
| 240 | 29.74 | 0.632 | 3.180 | 10.693 | 6.757 |
| 280 | 26.60 | 0.565 | 2.710 | 10.188 | 5.759 |
| 300 | 27.70 | 0.589 | 2.940 | 10.614 | 6.247 |

| ANGLE | SPEED | SPEED RATIO | RMS SPEED | LOCAL INT | TURB INT |
|---|---|---|---|---|---|
| | | X=-3.50 | | R=1.000 | |
| 0 | 32.52 | 0.691 | 1.330 | 4.090 | 2.826 |
| 10 | 33.26 | 0.707 | 1.540 | 4.630 | 3.272 |
| 40 | 28.54 | 0.606 | 1.770 | 6.202 | 3.761 |
| 60 | 31.23 | 0.664 | 1.830 | 5.860 | 3.889 |
| 120 | 32.00 | 0.680 | 1.220 | 3.813 | 2.592 |
| 180 | 32.54 | 0.691 | 1.670 | 5.132 | 3.549 |
| 240 | 31.98 | 0.680 | 3.400 | 10.632 | 7.225 |
| 280 | 28.73 | 0.610 | 3.190 | 11.103 | 6.779 |
| 300 | 31.25 | 0.664 | 3.400 | 10.880 | 7.225 |
| | | X=-3.50 | | R=1.200 | |
| 0 | 33.40 | 0.710 | 1.230 | 3.683 | 2.614 |
| 35 | 30.75 | 0.653 | 2.220 | 7.220 | 4.717 |
| 60 | 34.20 | 0.727 | 1.830 | 5.351 | 3.889 |
| 120 | 34.98 | 0.743 | 1.120 | 3.202 | 2.380 |
| 150 | 32.40 | 0.688 | 1.270 | 3.920 | 2.699 |
| 180 | 35.03 | 0.744 | 1.500 | 4.282 | 3.187 |
| 240 | 35.10 | 0.746 | 3.440 | 9.801 | 7.310 |
| 280 | 32.95 | 0.700 | 3.280 | 9.954 | 6.970 |
| 300 | 35.95 | 0.764 | 2.630 | 7.316 | 5.589 |
| 330 | 32.38 | 0.688 | 1.940 | 5.991 | 4.122 |
| | | X=-3.50 | | R=1.300 | |
| 0 | 33.52 | 0.712 | 1.240 | 3.699 | 2.635 |
| 35 | 32.67 | 0.694 | 2.530 | 7.744 | 5.376 |
| 60 | 35.97 | 0.764 | 1.780 | 4.949 | 3.782 |
| 120 | 36.22 | 0.770 | 1.100 | 3.037 | 2.337 |
| 180 | 36.40 | 0.773 | 1.250 | 3.434 | 2.656 |
| 230 | 38.22 | 0.812 | 2.650 | 6.934 | 5.631 |
| 240 | 37.69 | 0.801 | 3.110 | 8.252 | 6.609 |
| 300 | 37.71 | 0.801 | 2.010 | 5.330 | 4.271 |
| | | X=-3.50 | | R=1.400 | |
| 0 | 33.18 | 0.705 | 1.330 | 4.008 | 2.826 |
| 60 | 37.75 | 0.802 | 1.340 | 3.550 | 2.847 |
| 120 | 36.45 | 0.775 | 1.010 | 2.771 | 2.146 |
| 180 | 36.55 | 0.777 | 1.290 | 3.529 | 2.741 |
| 230 | 39.27 | 0.834 | 2.530 | 6.443 | 5.376 |
| 240 | 39.12 | 0.831 | 2.940 | 7.515 | 6.247 |
| 300 | 38.52 | 0.819 | 1.520 | 3.946 | 3.230 |

| ANGLE | SPEED | SPEED RATIO | RMS SPEED | LOCAL INT | TURB INT |
|---|---|---|---|---|---|
| | | X=-3.50 | | R=1.600 | |
| 0 | 32.73 | 0.695 | 1.460 | 4.461 | 3.102 |
| 60 | 38.40 | 0.816 | 1.910 | 4.974 | 4.059 |
| 120 | 37.00 | 0.786 | 1.430 | 3.865 | 3.039 |
| 180 | 36.92 | 0.785 | 1.500 | 4.063 | 3.187 |
| 240 | 40.90 | 0.869 | 2.200 | 5.379 | 4.675 |
| 300 | 38.48 | 0.818 | 1.910 | 4.964 | 4.059 |
| | | X=-3.50 | | R=1.800 | |
| 0 | 31.77 | 0.675 | 1.510 | 4.753 | 3.209 |
| 60 | 37.47 | 0.796 | 2.250 | 6.005 | 4.781 |
| 120 | 36.45 | 0.775 | 1.680 | 4.609 | 3.570 |
| 180 | 36.10 | 0.767 | 1.690 | 4.681 | 3.591 |
| 240 | 39.80 | 0.846 | 2.510 | 6.307 | 5.334 |
| 270 | 40.72 | 0.865 | 2.330 | 5.722 | 4.951 |
| 300 | 37.50 | 0.797 | 2.070 | 5.520 | 4.399 |
| | | X=-3.50 | | R=2.000 | |
| 0 | 29.50 | 0.627 | 1.690 | 5.729 | 3.591 |
| 60 | 34.39 | 0.731 | 2.860 | 8.316 | 6.077 |
| 120 | 31.80 | 0.676 | 2.640 | 8.302 | 5.610 |
| 180 | 31.64 | 0.672 | 2.680 | 8.470 | 5.695 |
| 240 | 35.72 | 0.759 | 3.380 | 9.462 | 7.182 |
| 270 | 37.00 | 0.766 | 3.220 | 8.703 | 6.842 |
| 300 | 34.57 | 0.735 | 2.690 | 7.781 | 5.716 |
| | | X=-4.50 | | R=0.000 | |
| 0 | 42.95 | 0.913 | 2.470 | 5.751 | 5.249 |
| 60 | 42.90 | 0.912 | 2.460 | 5.734 | 5.227 |
| 120 | 42.68 | 0.907 | 2.400 | 5.623 | 5.100 |
| 180 | 42.91 | 0.912 | 2.500 | 5.826 | 5.312 |
| 240 | 42.82 | 0.910 | 2.460 | 5.745 | 5.227 |
| 300 | 42.80 | 0.909 | 2.360 | 5.514 | 5.015 |
| | | X=-4.50 | | R=0.200 | |
| 0 | 43.30 | 0.920 | 2.450 | 5.658 | 5.206 |
| 60 | 43.15 | 0.917 | 2.200 | 5.098 | 4.675 |
| 120 | 42.90 | 0.912 | 2.210 | 5.152 | 4.696 |
| 180 | 43.25 | 0.919 | 2.390 | 5.526 | 5.079 |
| 240 | 43.37 | 0.922 | 2.610 | 6.018 | 5.546 |
| 300 | 42.91 | 0.912 | 2.520 | 5.873 | 5.355 |

| ANGLE | SPEED | SPEED RATIO | RMS SPEED | LOCAL INT | TURB INT |
|---|---|---|---|---|---|
| | | X=-4.50 | | R=0.400 | |
| 0 | 44.75 | 0.951 | 2.140 | 4.782 | 4.547 |
| 60 | 43.28 | 0.920 | 1.880 | 4.344 | 3.995 |
| 120 | 43.26 | 0.919 | 1.980 | 4.577 | 4.207 |
| 180 | 44.04 | 0.936 | 2.040 | 4.632 | 4.335 |
| 225 | 45.00 | 0.956 | 2.580 | 5.733 | 5.482 |
| 240 | 44.95 | 0.955 | 2.720 | 6.051 | 5.780 |
| 300 | 43.28 | 0.920 | 2.610 | 6.030 | 5.546 |
| | | X=-4.50 | | R=0.600 | |
| 0 | 46.25 | 0.983 | 1.770 | 3.827 | 3.761 |
| 60 | 44.20 | 0.939 | 1.660 | 3.756 | 3.527 |
| 120 | 44.75 | 0.951 | 1.760 | 3.933 | 3.740 |
| 180 | 46.00 | 0.977 | 1.840 | 4.000 | 3.910 |
| 225 | 46.97 | 0.998 | 2.640 | 5.621 | 5.610 |
| 240 | 46.54 | 0.989 | 2.800 | 6.016 | 5.950 |
| 300 | 44.20 | 0.939 | 2.720 | 6.154 | 5.780 |
| | | X=-4.50 | | R=0.800 | |
| 0 | 48.03 | 1.021 | 1.290 | 2.686 | 2.741 |
| 45 | 45.25 | 0.962 | 1.590 | 3.514 | 3.379 |
| 60 | 46.77 | 0.994 | 1.770 | 3.784 | 3.761 |
| 120 | 47.60 | 1.011 | 1.470 | 3.088 | 3.124 |
| 180 | 49.00 | 1.041 | 1.560 | 3.184 | 3.315 |
| 225 | 49.42 | 1.050 | 2.650 | 5.362 | 5.631 |
| 240 | 48.55 | 1.032 | 2.930 | 6.035 | 6.226 |
| 300 | 46.83 | 0.995 | 3.000 | 6.406 | 6.375 |
| | | X=-4.50 | | R=1.000 | |
| 0 | 49.46 | 1.051 | 1.130 | 2.285 | 2.401 |
| 40 | 47.23 | 1.004 | 1.870 | 3.959 | 3.974 |
| 60 | 49.71 | 1.056 | 1.680 | 3.380 | 3.570 |
| 120 | 50.73 | 1.078 | 1.070 | 2.109 | 2.274 |
| 180 | 51.62 | 1.097 | 1.140 | 2.208 | 2.422 |
| 225 | 52.56 | 1.117 | 2.300 | 4.376 | 4.867 |
| 240 | 51.74 | 1.099 | 2.860 | 5.528 | 6.077 |
| 300 | 51.26 | 1.089 | 2.540 | 4.955 | 5.397 |
| | | X=-4.50 | | R=1.200 | |
| 0 | 50.25 | 1.068 | 1.320 | 2.627 | 2.805 |
| 60 | 53.25 | 1.132 | 1.490 | 2.798 | 3.166 |

| ANGLE | SPEED | SPEED RATIO | RMS SPEED | LOCAL INT | TURB INT |
|---|---|---|---|---|---|
| 120 | 52.75 | 1.121 | 1.080 | 2.047 | 2.295 |
| 180 | 52.90 | 1.124 | 1.100 | 2.079 | 2.337 |
| 240 | 55.50 | 1.179 | 1.860 | 3.351 | 3.952 |
| 300 | 53.82 | 1.144 | 1.600 | 2.973 | 3.400 |
| | | X=-4.50 | | R=1.300 | |
| 0 | 50.75 | 1.078 | 1.300 | 2.562 | 2.762 |
| 60 | 54.10 | 1.150 | 1.590 | 2.939 | 3.379 |
| 120 | 53.50 | 1.137 | 1.240 | 2.318 | 2.635 |
| 180 | 53.52 | 1.137 | 1.180 | 2.205 | 2.507 |
| 240 | 56.37 | 1.198 | 1.760 | 3.122 | 3.740 |
| 300 | 54.50 | 1.158 | 1.580 | 2.899 | 3.357 |
| | | X=-4.50 | | R=1.400 | |
| 0 | 51.60 | 1.096 | 1.450 | 2.810 | 3.081 |
| 60 | 55.40 | 1.177 | 1.770 | 3.195 | 3.761 |
| 120 | 54.60 | 1.160 | 1.340 | 2.454 | 2.847 |
| 180 | 54.63 | 1.161 | 1.350 | 2.471 | 2.869 |
| 240 | 57.32 | 1.218 | 1.990 | 3.472 | 4.229 |
| 270 | 57.75 | 1.227 | 1.790 | 3.100 | 3.804 |
| 300 | 55.50 | 1.179 | 1.710 | 3.081 | 3.634 |
| | | X=-4.50 | | R=1.550 | |
| 0 | 52.16 | 1.108 | 1.430 | 2.742 | 3.039 |
| 60 | 55.54 | 1.180 | 1.800 | 3.241 | 3.825 |
| 120 | 54.73 | 1.163 | 1.370 | 2.503 | 2.911 |
| 180 | 54.68 | 1.162 | 1.350 | 2.469 | 2.869 |
| 240 | 57.50 | 1.222 | 1.980 | 3.443 | 4.207 |
| 270 | 57.95 | 1.231 | 1.910 | 3.296 | 4.059 |
| 300 | 55.73 | 1.184 | 1.690 | 3.032 | 3.591 |
| | | X=-5.20 | | R=0.000 | |
| 0 | 51.50 | 1.094 | 2.600 | 5.049 | 5.525 |
| 60 | 51.50 | 1.094 | 2.590 | 5.029 | 5.504 |
| 120 | 51.22 | 1.088 | 2.530 | 4.939 | 5.376 |
| 180 | 51.30 | 1.090 | 2.580 | 5.029 | 5.482 |
| 240 | 51.25 | 1.089 | 2.580 | 5.034 | 5.482 |
| 300 | 51.23 | 1.089 | 2.530 | 4.939 | 5.376 |

| ANGLE | SPEED | SPEED RATIO | RMS SPEED | LOCAL INT | TURB INT |
|---|---|---|---|---|---|
| | | X=-5.20 | | R=0.200 | |
| 0 | 51.72 | 1.099 | 2.520 | 4.872 | 5.355 |
| 60 | 51.55 | 1.095 | 2.350 | 4.559 | 4.994 |
| 120 | 51.25 | 1.089 | 2.330 | 4.546 | 4.951 |
| 180 | 51.62 | 1.097 | 2.480 | 4.804 | 5.270 |
| 240 | 51.96 | 1.104 | 2.720 | 5.235 | 5.780 |
| 300 | 51.55 | 1.095 | 2.630 | 5.102 | 5.569 |
| | | X=-5.20 | | R=0.400 | |
| 0 | 52.76 | 1.121 | 2.160 | 4.094 | 4.590 |
| 60 | 51.72 | 1.099 | 1.960 | 3.790 | 4.165 |
| 120 | 51.70 | 1.099 | 2.080 | 4.023 | 4.420 |
| 180 | 52.66 | 1.119 | 2.060 | 3.912 | 4.377 |
| 240 | 53.50 | 1.137 | 2.760 | 5.159 | 5.865 |
| 300 | 51.75 | 1.100 | 2.780 | 5.372 | 5.907 |
| | | X=-5.20 | | R=0.600 | |
| 0 | 54.58 | 1.160 | 1.680 | 3.078 | 3.570 |
| 60 | 52.63 | 1.118 | 1.790 | 3.401 | 3.804 |
| 120 | 52.95 | 1.125 | 1.810 | 3.418 | 3.846 |
| 180 | 54.73 | 1.163 | 1.840 | 3.362 | 3.910 |
| 223 | 55.65 | 1.183 | 2.510 | 4.510 | 5.334 |
| 240 | 55.00 | 1.169 | 2.840 | 5.164 | 6.035 |
| 300 | 52.92 | 1.125 | 2.870 | 5.423 | 6.099 |
| | | X=-5.20 | | R=0.800 | |
| 0 | 56.00 | 1.190 | 1.200 | 2.143 | 2.550 |
| 45 | 53.75 | 1.142 | 1.650 | 3.070 | 3.506 |
| 60 | 55.32 | 1.176 | 1.740 | 3.145 | 3.697 |
| 120 | 56.02 | 1.190 | 1.470 | 2.624 | 3.124 |
| 150 | 54.25 | 1.153 | 1.460 | 2.691 | 3.102 |
| 180 | 57.77 | 1.228 | 1.320 | 2.285 | 2.805 |
| 223 | 57.95 | 1.231 | 2.390 | 4.124 | 5.079 |
| 240 | 57.20 | 1.215 | 2.790 | 4.878 | 5.929 |
| 280 | 54.62 | 1.161 | 2.870 | 5.254 | 6.099 |
| 300 | 55.70 | 1.184 | 2.940 | 5.278 | 6.247 |
| | | X=-5.20 | | R=1.000 | |
| 0 | 57.73 | 1.227 | 1.140 | 1.975 | 2.422 |
| 35 | 56.00 | 1.190 | 1.920 | 3.429 | 4.080 |
| 60 | 58.50 | 1.243 | 1.660 | 2.838 | 3.527 |

| ANGLE | SPEED | SPEED RATIO | RMS SPEED | LOCAL INT | TURB INT |
|---|---|---|---|---|---|
| 120 | 59.52 | 1.265 | 0.990 | 1.663 | 2.104 |
| 150 | 57.20 | 1.215 | 1.130 | 1.976 | 2.401 |
| 180 | 60.03 | 1.276 | 1.010 | 1.682 | 2.146 |
| 223 | 61.27 | 1.302 | 1.770 | 2.889 | 3.761 |
| 240 | 61.20 | 1.300 | 2.440 | 3.987 | 5.185 |
| 300 | 60.00 | 1.275 | 2.180 | 3.633 | 4.632 |
| | | X=-5.20 | | R=1.200 | |
| 0 | 58.90 | 1.252 | 1.230 | 2.088 | 2.614 |
| 60 | 61.77 | 1.313 | 1.530 | 2.477 | 3.251 |
| 120 | 61.50 | 1.307 | 1.160 | 1.886 | 2.465 |
| 180 | 62.00 | 1.317 | 1.110 | 1.790 | 2.359 |
| 223 | 63.70 | 1.354 | 1.500 | 2.355 | 3.187 |
| 240 | 64.52 | 1.371 | 1.670 | 2.588 | 3.549 |
| 300 | 62.40 | 1.326 | 1.570 | 2.516 | 3.336 |
| | | X=-5.20 | | R=1.300 | |
| 0 | 60.00 | 1.275 | 1.250 | 2.083 | 2.656 |
| 60 | 62.50 | 1.328 | 1.610 | 2.576 | 3.421 |
| 120 | 62.45 | 1.327 | 1.230 | 1.970 | 2.614 |
| 180 | 63.45 | 1.348 | 1.170 | 1.844 | 2.486 |
| 240 | 66.00 | 1.402 | 1.660 | 2.515 | 3.527 |
| 300 | 63.42 | 1.348 | 1.530 | 2.412 | 3.251 |
| | | X=-5.20 | | R=1.400 | |
| 0 | 63.90 | 1.358 | 1.200 | 1.878 | 2.550 |
| 60 | 66.77 | 1.419 | 1.310 | 1.962 | 2.784 |
| 120 | 66.45 | 1.412 | 1.060 | 1.595 | 2.252 |
| 180 | 66.75 | 1.418 | 1.060 | 1.588 | 2.252 |
| 240 | 69.00 | 1.466 | 1.370 | 1.986 | 2.911 |
| 300 | 66.77 | 1.419 | 1.260 | 1.887 | 2.677 |
| | | X=-5.20 | | R=1.475 | |
| 0 | 64.53 | 1.371 | 1.140 | 1.767 | 2.422 |
| 60 | 67.50 | 1.434 | 1.420 | 2.104 | 3.017 |
| 120 | 65.73 | 1.397 | 1.290 | 1.963 | 2.741 |
| 180 | 65.50 | 1.392 | 1.410 | 2.153 | 2.996 |
| 240 | 69.05 | 1.467 | 1.610 | 2.332 | 3.421 |
| 270 | 70.00 | 1.487 | 1.550 | 2.214 | 3.294 |
| 300 | 67.76 | 1.440 | 1.300 | 1.919 | 2.762 |

☆USGPO: 1976 — 758-187/09 Region 5-11